POLITECNICO
MILANO 1863

Master Thesis

Evaluation of Active Rear Steering through Multi-Body Simulation

Supervised by:
Volvo Cars: Max Boerboom, Hossein Abadikhah
KTH Royal Institute of Technology: Lars Drugge
Politecnico di Milano: Michele Vignati

Gabriele Bertoli
Matteo Rossi

Academic Year 2020/2021

Evaluation of Active Rear Steering through Multi-Body Simulation

Abstract

The goal of this thesis work is to evaluate and quantify the advantages and disadvantages of Active Rear Steer (ARS). The evaluation is carried out through Multi-Body System (MBS) simulations. An analytical model has been developed to better understand the basic dynamics of vehicles equipped with rear steering. In parallel, a high fidelity MBS model is developed in Simpack. This model includes suspension kinematics and compliance, allowing for detailed analyses of steering hardware performance.

Next, different control strategies aiming at improving manoeuvrability, stability and agility are implemented in Simulink. In order to assess their effectiveness, the high fidelity model is utilised by running co-simulation with Simulink. Manoeuvrability is assessed through constant steer, constant radius and ramp steer manoeuvres. Stability is assessed through transient manoeuvres such as step steer and sine with dwell. Agility is assessed through step steer and frequency response. Ultimately, also a subjective assessment is carried out by means of Volvo Cars' dynamic driving simulator. The conclusion from the assessment is that the drivers feel the all wheel steered vehicle much more stable during evasive manoeuvres.

It is concluded that for manoeuvrability the minimum turning radius is reduced by 19 % at low velocity; this implies that the steering angle request is reduced at low velocity, while it is increased at high velocity. A slightly higher steering angle request at high velocity might be beneficial since the driver would be able to control the vehicle in a wider range of steering wheel angles. For agility the results are contradicting: on the one hand, according to the step steer rise time difference between lateral acceleration and yaw rate, the controlled vehicles are performing worse than the passive vehicle; on the other hand, according to the frequency response analysis, both the delays between steering input and yaw rate and between lateral acceleration and yaw rate are reduced up to respectively 75 % and 46 % for the considered frequency range. Finally, for stability, the yaw rate overshoot from a step steer can be reduced up to 65 % at high velocity and the sideslip angle can always be reduced. The vehicle equipped with ARS outperforms the passive vehicle in the sine with dwell manoeuvre.

Evaluation of Active Rear Steering through Multi-Body Simulation

Sammanfattning

Målet med detta examensarbete är att utvärdera och kvantifiera fördelarna och nackdelarna med Active Rear Steer (ARS) för Volvo Cars. Utvärderingen utförs genom Multi-Body System (MBS) simuleringar. En analytisk modell har utvecklats för att bättre förstå den grundläggande dynamiken i fordon utrustade med bakhjulsstyrning. Parallelt utvecklades en MBS-modell med hög precision i Simpack. Denna modell inkluderar hjulupphängningens kinematik och komplians, vilket möjliggör detaljerade analyser av styrhårdvarans prestanda.

Därefter implementeras olika kontrollstrategier som syftar till att förbättra manövrerbarhet, stabilitet och agilitet i Simulink. För att bedöma deras effektivitet används MBS-modellen för att köra co-simulering med Simulink. Manövrerbarhet bedöms genom konstant styrning, konstant radie och rampstyrning. Stabilitet bedöms genom transienta manövrar som stegstyrning och sinus med uppehåll. Agilitet bedöms genom stegstyrning och frekvensrespons. I slutändan görs också en subjektiv bedömning med hjälp av Volvo Cars dynamiska körsimulator. Slutsatsen från bedömningen är att förarna anser att fordonet upplevs vara mycket stabilare under undvikande manövrer.

Vidare är slutsatsen att för manövrerbarhet minskar den minsta svängradien med 19 % vid mycket låg hastighet; detta innebär att styrvinkelbegäran reduceras vid låg hastighet, medan den ökar vid hög hastighet. En något högre styrvinkelförfrågan kan vara fördelaktig eftersom föraren skulle kunna styra fordonet i ett större rattvinkel spann. För agilitet är resultaten motsägelsefulla: å ena sidan, enligt stegstyrningstidsskillnaden mellan lateral acceleration och girhastighet, fungerar de kontrollerade fordonen sämre än det passiva fordonet; å andra sidan, enligt frekvensresponsanalysen, reduceras både förseningarna mellan girhastighet och styringång och mellan lateral acceleration och girhastighet upp till ungefär 30 %. Slutligen, för stabilitet, kan girhastighetens översläng från en stegstyrning minskas upp till 65 % vid hög hastighet och sidoslip kan alltid minskas. Fordonet som är utrustat med ARS överträffar det passiva fordonet i manövern sinus med uppehåll.

Evaluation of Active Rear Steering through Multi-Body Simulation

Sommario

L'obiettivo di questa tesi è di valutare e quantificare per Volvo Cars i vantaggi e gli svantaggi di introdurre lo sterzo attivo all'asse posteriore. La valutazione viene eseguita attraverso simulazioni multi-body. Inizialmente viene eseguita un'analisi basata su un modello monotraccia a due gradi di libertà, con gomme lineari e velocità longitudinale imposta, per studiare come vari la dinamica del veicolo quando viene introdotto lo sterzo posteriore. Contemporaneamente, un modello multi-body viene sviluppato in dettaglio in Simpack. Rispetto al modello analitico, quest'ultimo prende in considerazione la cinematica delle sospensioni e la deformazione introdotta dai cuscinetti, permettendo un'analisi dettagliata dell'attuazione dello sterzo.

Successivamente, delle logiche di controllo vengono implementate in Simulink con l'obiettivo di migliorare la manovrabilità a bassa velocità, la stabilità e l'agilità ad alta velocità. Per valutarne l'efficacia, vengono eseguite delle co-simulazioni tra Simulink e il modello multi-body. La manovrabilità viene valutata attraverso manovre di sterzo fisso, raggio costante e ramp steer. La stabilità viene valutata attraverso le manovre di colpo di sterzo e sine with dwell. L'agilità viene valutata attraverso manovre di colpo di sterzo e risposta in frequenza. Infine, viene condotta anche una valutazione soggettiva sfruttando il simulatore di guida dinamico di Volvo Cars. Da quest'ultima valutazione emerge che il veicolo con quattro ruote sterzanti risulta molto più stabile e sicuro da guidare in caso di manovre di emergenza.

In conclusione, per la manovrabilità, il minimo raggio di sterzo è ridotto del 19 % a bassa velocità; questo risultato implica che l'angolo di sterzo necessario ad affrontare una curva a bassa velocità viene ridotto rispetto ad un veicolo passivo; ad alta velocità è vero il contrario. Una richiesta di sterzo leggermente maggiore, ad alta velocità, potrebbe avere un effetto positivo sulla guida, poichè il guidatore avrebbe la possibilità di controllare il veicolo in un range di angoli di sterzo leggermente più ampio. Riguardo l'agilità, i risultati sono contrastanti: guardando il colpo di sterzo, la differenza del rise time tra accelerazione laterale e velocità di imbardata è maggiore per un veicolo attivo, che indica un maggiore ritardo nella risposta del veicolo; però, secondo la risposta in frequenza, sia il ritardo tra sterzo e velocità di imbardata, sia il ritardo tra accelerazione laterale e velocità di imbardata vengono ridotti, rispettivamente fino al 75 % e 46 % nell'intervallo di frequenze considerato. Infine, riguardo la stabilità, l'overshoot della velocità di imbardata è ridotto fino al 65 % ad alta velocità e l'angolo di assetto è sempre ridotto; dalla manovra di sine with dwell si conclude che un veicolo controllato con sterzo attivo all'asse posteriore riesce ad eseguire la manovra con un'ampiezza del volante pari a due volte quella di un veicolo passivo.

In conclusione, senza limitazioni software o hardware, lo sterzo attivo all'asse posteriore è in grado di migliorare la manovrabilità e la stabilità di un veicolo. Riguardo l'agilità è necessario approfondire lo studio.

Acknowledgments

Before thanking all the awesome people met during this thesis, our warmest thanks go to our families, who always supported us even from distance throughout our studies, allowing us to live this incredible experience and to be where we are.

We owe our most sincere gratitude to our supervisors from Volvo Cars, Max Boerboom and Hossein Abadikhah. They dedicated an incredible amount of time and effort to our thesis, providing us every tool to carry out the work at our best, from an introduction course to learn a new software to obtaining the driving license to test vehicles at the Volvo Cars proving ground, closely following our progress and sharing their knowledge. All their support allowed for a work not only interesting from an engineering point of view, but also pleasant to carry out.

Special thanks go to the supervisors from our universities, Prof. Lars Drugge from KTH Royal Institute of Technology and Ing. Michele Vignati from Politecnico di Milano. Thank you for following us throughout all the thesis and giving us precious feedback whenever we needed it and also for helping us to stay on the right track.

A special mention must be made of the Simpack team, especially of Avijit Chauhan who taught us how to use Simpack and helped us along all the work from implementing the MBS model to achieving the results. We would like to thank also Remco Mansvelders who helped us integrating the control logic in Simpack.

Last but least, we want to thank the manager of the Driving Dynamics Functions Team, Carl Sandberg for giving us this great opportunity; the Driving Dynamics Functions Team where we found a friendly environment and especially Mohit Hemant Asher and Jacob Gustafsson for providing us relevant information and advice. Finally, we would like to thank Ajay Daniel from the Volvo Hällered Proving Ground for the advice about the manoeuvres performed for vehicle testing.

Contents

List of Figures

List of Tables

Nomenclature

$(x, y, z); G$ vehicle local reference frame

α_i tyre slip angle

β sideslip angle

δ_i steer angle at the wheel

$(\mathbb{X}, \mathbb{Y}, \mathbb{Z}); \mathbb{O}$ vehicle global reference frame

$\mathbf{\Omega}$ angular velocity vector

$\mathbf{V}_G$ velocity vector at the center of gravity

$\mathbf{V}_i$ velocity vector at the i-th location

ψ yaw angle

$_i$ =1,2. 1 refers to the front, 2 refers to the rear

a front axle to center of gravity distance

b rear axle to center of gravity distance

C_i i-th axle cornering stiffness

F_{yi} tyre lateral force at the contact patch

J yaw moment of inertia

l wheelbase

m mass

r yaw rate

u longitudinal velocity at the center of gravity

v lateral velocity at the center of gravity

ARS Active Rear Steering

AWS All Wheel Steer

FRF Frequency Response Function

FWS Front Wheel Steer

GUI Graphical User Interface

K&C Kinematics & Compliance

MBS Multi-Body System

OEM Original Equipment Manufacturer

RWS Rear Wheel Steer

SUV Sport Utility Vehicle

Chapter 1

Introduction

Passive systems of vehicles have been studied for decades, reaching a development level close to its full potential [1]. This is the reason why, today, active systems are the priority to bring further improvements to the automotive field. In the last two decades, more and more OEMs in the premium segment are introducing Active Rear Steering (ARS) in their high-end models. As a matter of fact, rear steer is not a recent technology: already in the 1980s Nissan, Mazda and a few more companies introduced their four-wheel steering systems; but all these solutions never found a large share in the market.
There are two main reasons why active rear steering should be a winning investment today. First of all, technology has drastically improved since the 1980s, not only on the hardware side, allowing for superior actuators, but also in terms of computational power required to run sophisticated actuator control models. Secondly, the ongoing electrification of vehicles requires the use of heavy battery packs; moreover, the current trend of designing large SUVs with a long wheelbase, leads to a further increase of mass. Combining these two phenomena, the consequence is that the tyres have to increase in width to avoid deteriorating the handling of the vehicle. Increased tyre width and increased wheelbase lead to reduced steer-ability of the vehicle. A possible solution to preserve or even improve the steer-ability is to introduce rear steering, which would also bring other benefits; in fact, Takaaki et al. [2], Kreutz et al. [3], Bin et al.[4] well as others [5], [6], [7], [8] have already demonstrated that it can improve manoeuvrability, handling and stability. Chapter 2.1 presents an overview of the literature regarding active rear steering.

1.1 Scope of the thesis

The goal of this thesis is to evaluate and quantify what are the advantages and disadvantages of introducing active rear steering, on the vehicle dynamics attributes. In other words, this thesis was initiated with the intent to answer the question:

Why should an automotive company invest in active rear steering?

This thesis will find an answer by implementing different control logic and assessing the effects of ARS from the results obtained with an MBS model.

Contemporaneously, Volvo Cars is interested in benchmarking a new MBS simulation software, Simpack. For this reason, part of the thesis is spent building a Volvo

Cars specific MBS model from scratch.

1.2 Out of scope of the thesis

The following points are out of the scope of the thesis:

- to validate the MBS model towards an existing physical vehicle. The MBS model is built on the latest data available from Volvo, but it does not represent any currently produced model from Volvo Cars. The scope of this thesis is to make a comparison of the same vehicle model, with and without ARS;
- to investigate feedback control. Both due to the fail-safety concern of closed-loop control and the limited time of this thesis, it was decided to focus on feedforward control;
- the study is limited to front-wheel drive vehicles.
- to design a control logic that is robust when vehicle parameters change;
- to consider the software and hardware limitations of the rear steer.

1.3 Thesis outline

The thesis is composed of eight chapters. The current chapter describes the thesis scope together with the background that motivates the research question.

Chapter 2 begins by describing the theoretical framework surrounding the research question and continues with the explanation of the relevant theory utilised for this thesis. Linear single-track models of both Front-Wheel Steer (FWS) and All-Wheel Steer (AWS) vehicles are derived and the transfer functions from the steering input to the vehicle states are computed. Linear steady-state and transient tyres are implemented together with non-linear tyres. The state-space model is also presented.

Chapter 3 describes why it was decided to utilise a linear single-track model and how it is employed to carry out an effective comparison between a FWS and an AWS vehicle.

Chapter 4 elaborates why a multi-body model is built and what kind of additional information it can provide. It describes what components of the vehicle are modelled in detail, what type of components are utilised and what are the general parameters of the vehicle.

Chapter 5 focuses on the control objectives and describes the implementation of two feedforward control logics: the first controller is a simple velocity dependent gain scheduling that attempts to minimise the sideslip angle; the second controller is a more advanced feedforward that makes the AWS vehicle behave like a reference vehicle.

Chapter 6 motivates why certain manoeuvres are selected to carry out the simulations and evaluate the control objectives. For the sake of completeness, a brief description of each manoeuvre is reported.

In Chapter 7 the results from the simulations are discussed for each control objective, showing only the relevant outcomes needed to draw the conclusions. The workflow is shown in Figure 1.1 and consists of:

- defining and tuning the control logics in MATLAB;
- implementing the controllers in Simulink;
- running co-simulations between Simulink and the MBS model;
- assessing the results.

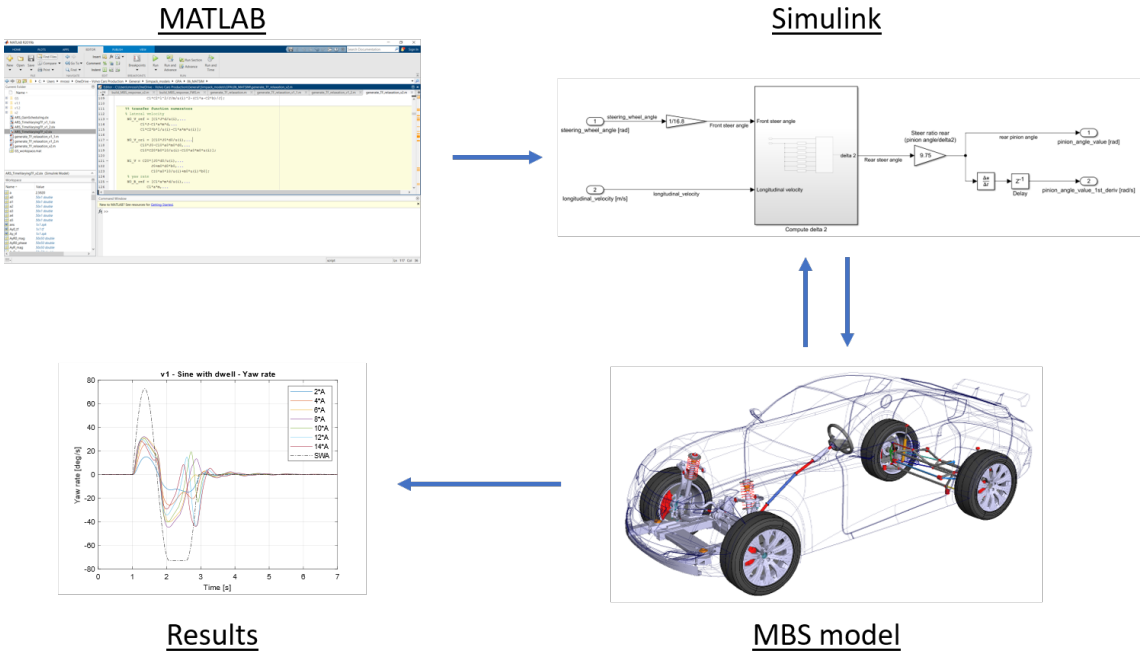

Figure 1.1: Workflow

In Chapter 8 the research question is answered, summarising all the benefits and drawbacks that active rear steering can bring, with the type of controllers implemented.

Chapter 2

Theory

Firstly, this chapter provides an overview of several previous studies related to active rear steering; secondly, it presents the theory used to carry out the linear analysis of the vehicle response. A single track model is derived and its state space model is shown. In addition to steady-state linear tyres, tyres with linear transient response and non-linear tyres are included.

2.1 Theoretical framework

Several studies have already been carried out regarding active rear steering, especially to improve stability at high speed. The majority of the studies found utilises feedback control to improve the vehicle response, compared to the studies that utilise a feedforward logic.

T. Eguchi et al. explain in [2] how the "Super Hicas" was developed. This is the rear steering system that Nissan adopted in the 1980s. The goal of the authors is to make the vehicle react as the driver wishes and, in order to do so, the sideslip angle of the vehicle is set to zero through a transfer function between front and rear steer angle.

M. Kreutz et al. in [3] presents two control strategies: the first one is a feedback controller that follows a yaw rate reference, but the authors explain that the choice of the reference model is not trivial. The second strategy avoids this issue and the controller is regarded as a virtual mass-spring-damper system; this allows a simple tuning and results comparable with the feedback control strategy, except for the μ-split test.

J. Ghosh in [8] designs a controller that utilises both feedforward and feedback logics. Feedforward is used in transient responses and feedback is used as fail-safe system in situations where the response is much different than expected. Since the vehicle is not linear, the controller parameters are scheduled for different velocities.

I. Besselink et al. in [5] implement a feedback controller that follows a yaw rate reference. Also, they implement a feedforward controller where the ratio between front and rear steer angle depends on the steering frequency. The feedforward controller is tuned to reach similar results in terms of yaw rate and lateral acceleration for a step steer. The sideslip angle is not reported.

M. Nagai et al., S. Yoo et al. and W. Jianyong et al. in [9], [10] and [11] respectively, explain that active rear steering alone improves the vehicle response, but only in the linear region; integrating direct yaw moment control to ARS allows

for improving the vehicle response in the non-linear region too.

2.2 Single track model

The single track model, also known as bicycle model, is probably the most famous and simplest model to study the vehicle lateral dynamics. It is often found in the studied publications because it can be simplified as a linear time invariant system. In this model the wheels of each axle are joined and represented by a single wheel as shown in Figure 2.1.

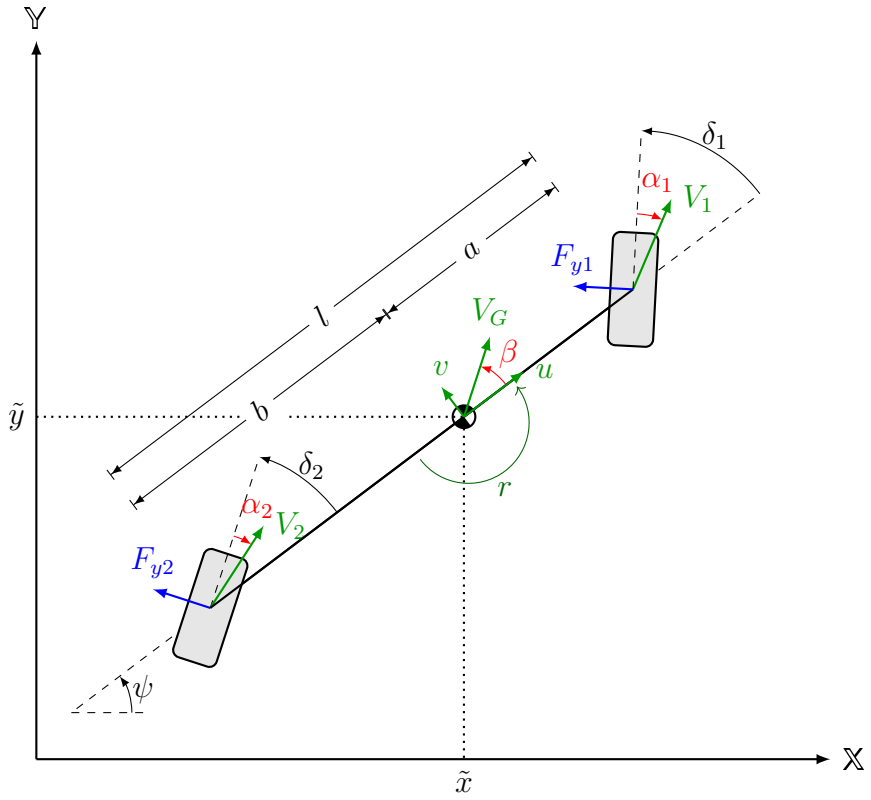

Figure 2.1: Single track model

In this section, the equations governing the lateral dynamics of a single track model with rear steer are derived. This model assumes that:

- the front and the rear tyres are represented as one single tyre on each axle. The imaginary tyre contact points, which the tyre forces are to act upon, lie along the center of the axle [12];
- the pneumatic trail and the aligning torque resulting from the slip angle of the tire is neglected [12];
- the road is flat and with uniform characteristics;
- the center of gravity is placed on the ground in the symmetry plane;
- the vehicle motion is planar;

- small steer angles;
- constant longitudinal velocity;
- the vehicle body is a single rigid body [13]. Suspensions and steering systems are rigid too;
- no aerodynamic effects.

Two reference systems are used: the first one is global ($\mathbb{X}, \mathbb{Y}, \mathbb{Z}; \mathbb{O}$) and can be considered as inertial, since the rotational effect of the earth can be neglected. The second reference system (x,y,z; G) with unit vectors ($\mathbf{i}$,$\mathbf{j}$,$\mathbf{k}$) is fixed to the center of mass of the vehicle body, with the x axis pointing forward, the y axis pointing leftwards and the z axis pointing upwards. Angles are defined positive according to the right-hand rule; please note that the slip angles α_i are positive in clockwise direction because they represent every normal driving scenario.

Kinematic equations

Kinematic equations are mathematical statements that relate position, velocity and acceleration of a body without considering inertias and forces that caused the motion. The motion of a vehicle, represented by a single-track model, can be described by knowing its velocity $\mathbf{V}_G$ at the center of mass and its angular velocity $\mathbf{\Omega}$. In the local reference system (x,y,z; G):

$$\mathbf{V}_G = u\,\mathbf{i} + v\,\mathbf{j} \tag{2.1}$$

and

$$\mathbf{\Omega} = r\,\mathbf{k} \tag{2.2}$$

where u is the longitudinal velocity, v the lateral velocity and r the yaw rate. For a given point $\mathbf{P} = (x_P, y_P, 0)$, on the vehicle body, its velocity $\mathbf{V}_P$ is given by:

$$\begin{aligned} \mathbf{V}_P &= \mathbf{V}_G + \mathbf{\Omega} \times \overline{GP} \\ &= (u\,\mathbf{i} + v\,\mathbf{j}) + r\,\mathbf{k} \times (x_P\,\mathbf{i} + y_P\,\mathbf{j}) \\ &= (u - r y_P)\mathbf{i} + (v + r x_P)\mathbf{j} \end{aligned} \tag{2.3}$$

Where $\overline{GP}$ is the vector going from G to $\mathbf{P}$. In the same way, the velocities at the front and rear axles, $\mathbf{V}_1$ and $\mathbf{V}_2$ respectively, can be expressed as:

$$\begin{aligned} \mathbf{V}_1 &= \mathbf{V}_G + \mathbf{\Omega} \times (a\mathbf{i} + 0\mathbf{j} + 0\mathbf{k}) \\ &= u\,\mathbf{i} + (v + ra)\,\mathbf{j} \end{aligned} \tag{2.4}$$

$$\begin{aligned} \mathbf{V}_2 &= \mathbf{V}_G + \mathbf{\Omega} \times (-b\mathbf{i} + 0\mathbf{j} + 0\mathbf{k}) \\ &= u\,\mathbf{i} + (v - rb)\,\mathbf{j} \end{aligned} \tag{2.5}$$

where a and b are the distance between the centre of mass and front and rear axles respectively.
The front and rear axles slip angles are defined as:

$$\alpha_1 \;=\; \delta_1 \;-\; \arctan\left(\frac{v \;+\; ra}{u}\right) \tag{2.6}$$

$$\alpha_2 \;=\; \delta_2 \;-\; \arctan\left(\frac{v \;-\; rb}{u}\right) \tag{2.7}$$

where δ_1 and δ_2 are the front and rear steer angles. For a vehicle with wheelbase $l = a + b$, under normal driving conditions, for $u \;>\; 0$:

$$u \;\gg\; |v| \qquad \text{and} \qquad u \;\gg\; |r|\, l$$

This allows for the small angles assumption leading to the following simplification:

$$\alpha_1 \;=\; \delta_1 \;-\; \frac{v \;+\; ra}{u} \tag{2.8}$$

$$\alpha_2 \;=\; \delta_2 \;-\; \frac{v \;-\; rb}{u} \tag{2.9}$$

The vehicle body acceleration, with respect to its own reference system (x,y,z; G), is expressed as:

$$\begin{aligned}
\mathbf{a}_G \;&=\; \dot{\mathbf{V}}_G \;+\; \boldsymbol{\Omega} \times \mathbf{V}_G \\
&=\; (\dot{u}\,\mathbf{i} \;+\; \dot{v}\,\mathbf{j}) \;+\; (-rv\,\mathbf{i} \;+\; ru\,\mathbf{j}) \\
&=\; (\dot{u} \;-\; rv)\,\mathbf{i} \;+\; (\dot{v} \;+\; ru)\,\mathbf{j} \\
&=\; a_x\,\mathbf{i} \;+\; a_y\,\mathbf{j}
\end{aligned} \tag{2.10}$$

The vehicle acceleration can be written as function of sideslip angle β instead of lateral velocity, since:

$$v \;=\; u \tan(\beta) \tag{2.11}$$

Assuming small angles it is possible to write:

$$\beta \;\simeq\; \frac{v}{u} \tag{2.12}$$

resulting in:

$$a_y \;=\; \left(\dot{\beta} \;+\; r\right) u \tag{2.13}$$

Equilibrium equations

The lateral and rotational equilibrium equations at the vehicle center of gravity are:

$$\begin{aligned} ma_y &= F \\ J\dot{r} &= M \end{aligned} \tag{2.14}$$

where m is the vehicle mass, J is the vehicle moment of inertia in z direction, F is the sum of lateral forces and M is the sum of moments in the z direction. Under the assumption of small steer angles and from equation 2.10, it is possible to rewrite the system of equations as:

$$\begin{aligned} m\left(\dot{v} + ru\right) &= Fy_1 + Fy_2 \\ J\dot{r} &= Fy_1 a - Fy_2 b \end{aligned} \tag{2.15}$$

where Fy_1 and Fy_2 are the lateral forces generated by the front and rear axles respectively.

Constitutive equations

Assuming linear axle characteristics, the lateral force generated by each axle is a linear function of the respective slip angle, as:

$$\begin{aligned} F_{y1} &= C_1\alpha_1 \\ F_{y2} &= C_2\alpha_2 \end{aligned} \tag{2.16}$$

where C_1 and C_2 are the front and rear axle cornering stiffness.

When tyres non-linear behaviour is considered, it is possible to use, among others, the Pacejcka MF-tyre model. The lateral force produced by each axle can be written as:

$$F_{yi} = D_i \sin\left(C_i \arctan\left(B_i\alpha_i - E_i\left(B_i\alpha_i - \arctan\left(B_i\alpha_i\right)\right)\right)\right) \tag{2.17}$$

where B, C, D and E are the Magic Formula tyre parameters.

Linear system

For linear axles characteristics, it is possible to write the following system of linear time-invariant differential equations:

$$\begin{aligned} m\left(\dot{v} + ur\right) &= C_1\left(\delta_1 - \frac{v + ra}{u}\right) + C_2\left(\delta_2 - \frac{v - rb}{u}\right) \\ J\dot{r} &= C_1\left(\delta_1 - \frac{v + ra}{u}\right)a - C_2\left(\delta_2 - \frac{v - rb}{u}\right)b \end{aligned} \tag{2.18}$$

The vehicle states are v and r and the inputs to the system are δ_1 and δ_2, in matrix form:

$$\begin{bmatrix} m & 0 \\ 0 & J \end{bmatrix} \begin{Bmatrix} \dot{v} \\ \dot{r} \end{Bmatrix} + \begin{bmatrix} \frac{C_1+C_2}{u} & \frac{C_1a-C_2b}{u} + mu \\ \frac{C_1a-C_2b}{u} & \frac{C_1a^2+C_2b^2}{u} \end{bmatrix} \begin{Bmatrix} v \\ r \end{Bmatrix} = \begin{bmatrix} C_1 \\ aC_1 \end{bmatrix} \delta_1 + \begin{bmatrix} C_2 \\ -bC_2 \end{bmatrix} \delta_2 \tag{2.19}$$

For steady-state conditions it is possible to find a simple relation between the vehicle states v, r (considering a_y too) and the inputs δ_1 and δ_2. The differences introduced by rear steering with respect to front steering are highlighted in red.

$$\frac{v}{\delta_1} = \frac{blC_1C_2 - aC_1mu^2}{l^2C_1C_2 + mu^2(bC_2 - aC_1)} \cdot u \tag{2.20}$$

$$\frac{v}{\delta_2} = \frac{alC_1C_2 + bC_2mu^2}{l^2C_1C_2 + mu^2(bC_2 - aC_1)} \cdot u \tag{2.21}$$

$$\frac{r}{\delta_1} = \frac{lC_1C_2}{l^2C_1C_2 + mu^2(bC_2 - aC_1)} \cdot u \tag{2.22}$$

$$\frac{r}{\delta_2} = \frac{-lC_1C_2}{l^2C_1C_2 + mu^2(bC_2 - aC_1)} \cdot u \tag{2.23}$$

$$\frac{a_y}{\delta_1} = \frac{lC_1C_2}{l^2C_1C_2 + mu^2(bC_2 - aC_1)} \cdot u^2 \tag{2.24}$$

$$\frac{a_y}{\delta_2} = \frac{-lC_1C_2}{l^2C_1C_2 + mu^2(bC_2 - aC_1)} \cdot u^2 \tag{2.25}$$

Shifting to Laplace domain it is possible to write:

$$\begin{aligned} v &\longrightarrow V & \dot{v} &\longrightarrow sV \\ r &\longrightarrow R & \dot{r} &\longrightarrow sR \\ \delta_1 &\longrightarrow \Delta_1 & \delta_2 &\longrightarrow \Delta_2 \end{aligned}$$

Thus, the system becomes:

$$\begin{bmatrix} \frac{C_1+C_2}{u} + ms & \frac{C_1a-C_2b}{u} + mu \\ \frac{C_1a-C_2b}{u} & \frac{C_1a^2+C_2b^2}{u} + Js \end{bmatrix} \begin{Bmatrix} V \\ R \end{Bmatrix} = \begin{bmatrix} C_1 \\ aC_1 \end{bmatrix} \Delta_1 + \begin{bmatrix} C_2 \\ -bC_2 \end{bmatrix} \Delta_2 \tag{2.26}$$

It is possible to write the following transfer functions from the inputs Δ_1 and Δ_2 to the states V and R. The differences introduced by rear steering with respect to front steering are highlighted in red.

$$\sigma = \frac{m(a^2C_1 + b^2C_2) + J(C_1 + C_2)}{2Jmu} \tag{2.27}$$

$$\omega_0^2 = \frac{mu^2(bC_2 - aC_1) + l^2C_1C_2}{Jmu^2} \tag{2.28}$$

$$G_{\frac{V}{\Delta_1}} = \frac{V}{\Delta_1} = \frac{C_1}{m} \cdot \frac{s - \frac{1}{Ju}(amu^2 - blC_2)}{s^2 + 2\sigma s + \omega_0^2} \tag{2.29}$$

$$G_{\frac{V}{\Delta_2}} = \frac{V}{\Delta_2} = \frac{C_2}{m} \cdot \frac{s - \frac{1}{Ju}(-bmu^2 - alC_1)}{s^2 + 2\sigma s + \omega_0^2} \tag{2.30}$$

$$G_{\frac{R}{\Delta_1}} = \frac{R}{\Delta_1} = \frac{aC_1}{J} \cdot \frac{s + \frac{lC_2}{amu}}{s^2 + 2\sigma s + \omega_0^2} \tag{2.31}$$

$$G_{\frac{R}{\Delta_2}} = \frac{R}{\Delta_2} = \frac{-bC_2}{J} \cdot \frac{s + \frac{lC_1}{bmu}}{s^2 + 2\sigma s + \omega_0^2} \tag{2.32}$$

The damping ratio is defined as:

$$\zeta = \frac{\sigma}{\sqrt{\omega_0^2}} = \frac{m(a^2C_1 + b^2C_2) + J(C_1 + C_2)}{2\sqrt{Jm\left[mu^2(bC_2 - aC_1) + l^2C_1C_2\right]}} \tag{2.33}$$

Knowing that the lateral acceleration is $A_Y = Vs + Ru$, it is possible to write the following transfer functions from Δ_1 and Δ_2 to A_Y:

$$G_{\frac{A_Y}{\Delta_1}} = \frac{A_Y}{\Delta_1} = \frac{V}{\Delta_1}s + \frac{R}{\Delta_1}u \tag{2.34}$$

$$G_{\frac{A_Y}{\Delta_2}} = \frac{A_Y}{\Delta_2} = \frac{V}{\Delta_2}s + \frac{R}{\Delta_2}u \tag{2.35}$$

Thus, obtaining:

$$G_{\frac{A_Y}{\Delta_1}} = \frac{A_Y}{\Delta_1} = \frac{C_1}{m} \cdot \frac{s^2 + \frac{blC_2}{Ju}s + \frac{lC_2}{J}}{s^2 + 2\sigma s + \omega_0^2} \tag{2.36}$$

$$G_{\frac{A_Y}{\Delta_2}} = \frac{A_Y}{\Delta_2} = \frac{C_2}{m} \cdot \frac{s^2 + \frac{alC_1}{Ju}s - \frac{lC_1}{J}}{s^2 + 2\sigma s + \omega_0^2} \tag{2.37}$$

While knowing that for the sideslip angle $B = \frac{V}{u}$, it is possible to write the transfer function from Δ_1 and Δ_2 to the sideslip angle B:

$$G_{\frac{B}{\Delta_1}} = \frac{V}{\Delta_1} \cdot \frac{1}{u} = \frac{C_1}{mu} \cdot \frac{s - \frac{1}{Ju}(amu^2 - blC_2)}{s^2 + 2\sigma s + \omega_0^2} \tag{2.38}$$

$$G_{\frac{B}{\Delta_2}} = \frac{V}{\Delta_2} \cdot \frac{1}{u} = \frac{C_2}{mu} \cdot \frac{s - \frac{1}{Ju}(-bmu^2 - alC_1)}{s^2 + 2\sigma s + \omega_0^2} \tag{2.39}$$

The transfer functions from the yaw rate R to the lateral acceleration A_Y for a front and rear steered vehicle are respectively:

$$\frac{A_{Y,\Delta_1}}{R_{\Delta_1}} = \frac{J}{ma} \cdot \frac{s^2 + \frac{blC_2}{Ju}s + \frac{lC_2}{J}}{s + \frac{C_2 l}{mau}} \tag{2.40}$$

$$\frac{A_{Y,\Delta_2}}{R_{\Delta_2}} = -\frac{J}{mb} \cdot \frac{s^2 + \frac{alC_1}{Ju}s - \frac{lC_1}{J}}{s + \frac{lC_1}{bmu}} \tag{2.41}$$

For an AWS vehicle:

$$B_{AWS} = G_{\frac{B}{\Delta_1}}\Delta_1 + G_{\frac{B}{\Delta_2}}\Delta_2 \tag{2.42}$$

$$R_{AWS} = G_{\frac{R}{\Delta_1}}\Delta_1 + G_{\frac{R}{\Delta_2}}\Delta_2 \tag{2.43}$$

$$A_{Y,AWS} = G_{\frac{A_Y}{\Delta_1}}\Delta_1 + G_{\frac{A_Y}{\Delta_2}}\Delta_2 \tag{2.44}$$

Considering a feedforward control where $\Delta_2 = \chi \cdot \Delta_1$, it is possible to write:

$$\frac{B_{AWS}}{\Delta_1} = G_{\frac{B}{\Delta_1}} + \chi \cdot G_{\frac{B}{\Delta_2}} \tag{2.45}$$

$$\frac{R_{AWS}}{\Delta_1} = G_{\frac{R}{\Delta_1}} + \chi \cdot G_{\frac{R}{\Delta_2}} \tag{2.46}$$

$$\frac{A_{Y,AWS}}{\Delta_1} = G_{\frac{A_Y}{\Delta_1}} + \chi \cdot G_{\frac{A_Y}{\Delta_2}} \tag{2.47}$$

2.2.1 State space model

The vehicle state space model is set up as:

$$\begin{aligned} \underline{\dot{\mathbf{x}}} &= [\mathbf{A}]\underline{\mathbf{x}} + [\mathbf{B}]\underline{\mathbf{u}} \\ \underline{\mathbf{y}} &= [\mathbf{C}]\underline{\mathbf{x}} + [\mathbf{D}]\underline{\mathbf{u}} \end{aligned} \tag{2.48}$$

where

$$\underline{\dot{\mathbf{x}}} = \begin{Bmatrix} \dot{v} \\ \dot{r} \end{Bmatrix} \qquad \underline{\mathbf{x}} = \begin{Bmatrix} v \\ r \end{Bmatrix} \qquad \underline{\mathbf{y}} = \begin{Bmatrix} \beta \\ r \\ a_y \end{Bmatrix} \qquad \underline{\mathbf{u}} = \begin{Bmatrix} \delta_1 \\ \delta_2 \end{Bmatrix} \tag{2.49}$$

and:

$$\begin{aligned}
\Big[\mathbf{A}\Big] &= \begin{bmatrix} -\frac{C_1+C_2}{mu} & -\frac{C_1a-C_2b}{mu} - u \\ -\frac{C_1a-C_2b}{Ju} & -\frac{C_1a^2+C_2b^2}{Ju} \end{bmatrix} \\
\Big[\mathbf{B}\Big] &= \begin{bmatrix} C_1 & C_2 \\ aC_1 & bC_2 \end{bmatrix} \\
\Big[\mathbf{C}\Big] &= \begin{bmatrix} \frac{1}{u} & 0 \\ 0 & 1 \\ -\frac{C_1+C_2}{mu} & -\frac{C_1a-C_2b}{mu} \end{bmatrix} \\
\Big[\mathbf{D}\Big] &= \begin{bmatrix} 0 & 0 \\ 0 & 0 \\ \frac{C_1}{m} & \frac{C_2}{m} \end{bmatrix}
\end{aligned} \tag{2.50}$$

2.2.2 Linear transient tyre model

This tyre model is implemented to understand why the vehicle exhibit high values of overshoot at low velocity.

Linear steady state tyres do not consider the delay to build up lateral force during transients. This can be taken into account introducing the relaxation length d; the effect of d decreases together with velocity, fading at around $50\,km/h$.

In this way, discontinuities in the slip angles do not produce discontinuities in the lateral force [13]. The constitutive equations 2.16 are changed to a first order differential equations as:

$$\begin{aligned} \frac{d}{u}\dot{F}_{y1} + F_{y1} &= C_1\alpha_1 \\ \frac{d}{u}\dot{F}_{y2} + F_{y2} &= C_2\alpha_2 \end{aligned} \tag{2.51}$$

This yields the following system of equations in the Laplace domain:

$$\begin{bmatrix} ms & mu & -1 & -1 \\ 0 & Js & -a & b \\ \frac{C_1}{u} & \frac{C_1 a}{u} & \frac{ds}{u}+1 & 0 \\ \frac{C_2}{u} & -\frac{C_2 b}{u} & 0 & \frac{ds}{u}+1 \end{bmatrix} \begin{Bmatrix} V \\ R \\ F_{Y1} \\ F_{Y2} \end{Bmatrix} = \begin{bmatrix} 0 \\ 0 \\ C_1 \\ 0 \end{bmatrix} \Delta_1 + \begin{bmatrix} 0 \\ 0 \\ 0 \\ C_2 \end{bmatrix} \Delta_2 \tag{2.52}$$

The transfer functions from front steer angle Δ_1 to lateral velocity V and yaw rate R are:

$$\begin{aligned} \frac{V}{\Delta_1} &= \frac{N_V}{D_0} \\ \frac{R}{\Delta_1} &= \frac{N_R}{D_0} \end{aligned} \tag{2.53}$$

where:

$$N_V = \frac{JC_1 d}{u}s^2 + \left(JC_1 - mC_1 ad\right)s + \frac{C_1 C_2 lb}{u} - mC_1 au \tag{2.54}$$

$$N_R = \frac{mC_1 ad}{u}s^2 + \left(J - mbd\right)s + \frac{C_1 al}{u} + mbu \tag{2.55}$$

$$\begin{aligned} D_0 = {} & \frac{Jmd^2}{u^2}s^4 + 2\frac{Jmd}{u}s^3 + \\ & + \left(Jm + md\frac{C_1 a^2 + C_2 b^2}{u^2} + Jd\frac{C_1 + C_2}{u^2}\right)s^2 + \\ & + \left(m\frac{C_1 a^2 + C_2 b^2}{u} + J\frac{C_1 + C_2}{u} - md\frac{C_1 a - C_2 b}{u}\right)s + \\ & + \frac{C_1 C_2 l^2}{u^2} - m\left(C_1 a - C_2 b\right) \end{aligned} \tag{2.56}$$

Chapter 3

How the vehicle linear response is analysed

A Graphical User Interface (GUI) is designed in MATLAB App Designer to carry out a linear vehicle response analysis exploiting a single-track model.

3.1 Why use a single track model

Before diving into a high fidelity and complex MBS model, it is fundamental to understand how the vehicle response changes when rear steering is introduced. A single track model is the simplest model to analyse the principal lateral dynamics of a vehicle. When linearised, it allows for analytically computing the transfer functions from the steering input to the vehicle states. It clearly shows what are the effects of the different vehicle parameters on the vehicle response and it is easy to implement; but it is valid for low lateral accelerations, up to $0.4\,g$ [14], or until the slip angle of the tyres does not exceed 2 deg, on dry tarmac conditions [13].
The linear single track model will also be the foundation of the control logics.

3.2 Vehicle linear response analysis tool

The goal of this initial analysis is to compare the response of a traditional Front Wheel Steer (FWS) vehicle with the response of the same vehicle equipped with also rear steering, i.e. an All Wheel Steer (AWS) vehicle.

The rear steer angle is here implemented as proportional to the front steer angle and the gain varies according to the longitudinal velocity. This method is called "gain scheduling" and it represents the simplest type of feedforward control.

In the frequency domain, the GUI shows the surface plots of the transfer functions of yaw rate, lateral acceleration and sideslip, with the front steer angle as input; in addition, it shows the transfer function between lateral acceleration and yaw rate. Furthermore, in the time domain, the GUI contains the vehicles responses to a step input; in the latter case, also non-linear tyres and linear tyres with relaxation length are implemented, to better understand the limitations of linear steady state tyres.

Moreover, the GUI shows where the zeros and poles of the transfer functions are located, how they change with longitudinal velocity and, finally, also how the

damping ratio of the vehicle changes with velocity.

Why making a GUI

The reason for designing this tool is that it allows to interactively set and change the vehicle parameters and immediately visualise how the transfer functions and the step response change. This ensures a quick and effective understanding of how the vehicle behaviour changes when parameters are varied. For instance, it is possible to visualise the effect of changing the wheelbase, mass or, for the step steer, the longitudinal velocity and the step amplitude. In addition, also the gain of the rear steer can be interactively varied: this allows to see how the AWS vehicle response changes for a different gain scheduling.

Figure 3.1 shows the GUI page that compares the transfer functions for a FWS (on the left) and an AWS (in the middle) vehicle; it also shows the poles and zeros location (top-right) and damping ratio (center-right). On the bottom left there are the vehicle parameters and on the bottom right there are the gain scheduling parameters.
Figure 3.2 shows the GUI page with the step response for a FWS (top-left) and an AWS (top-center) vehicle; Magic Formula parameters are shown on the top-right, overshoot values on the center-left, normalised axle characteristics on the center right and and bottom part is the same as in the transfer function page.

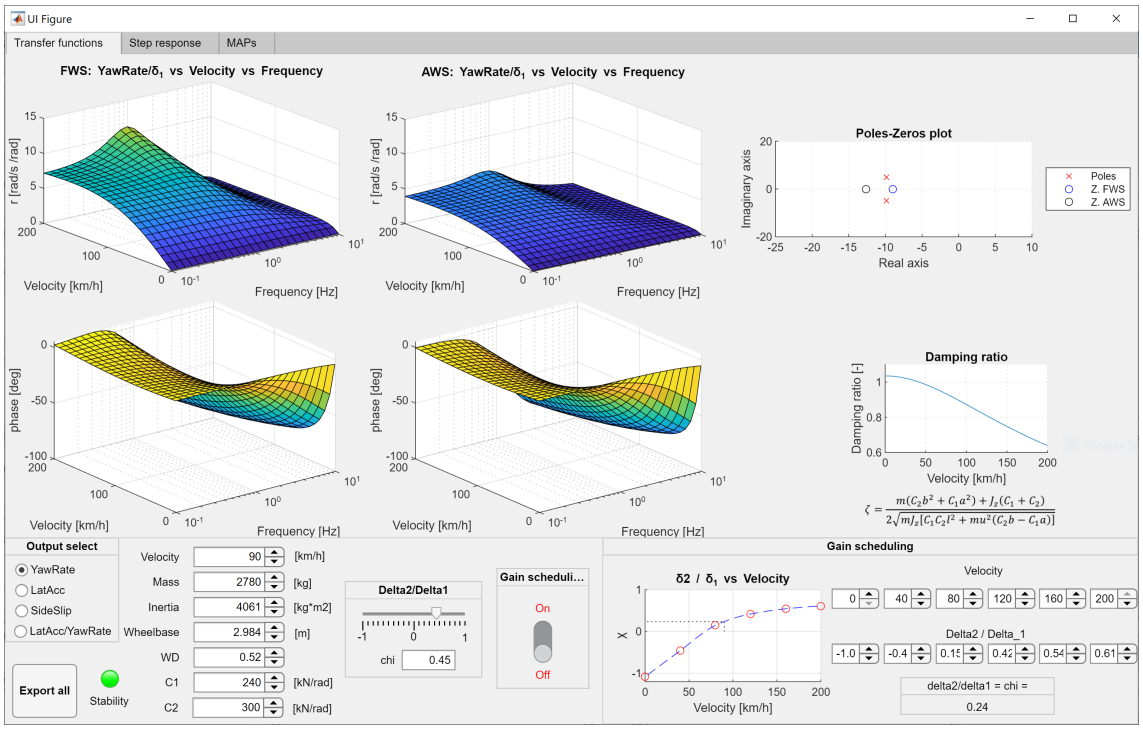

Figure 3.1: GUI page to compare transfer function of lateral acceleration, yaw rate and side-slip angle with front steer angle as input.

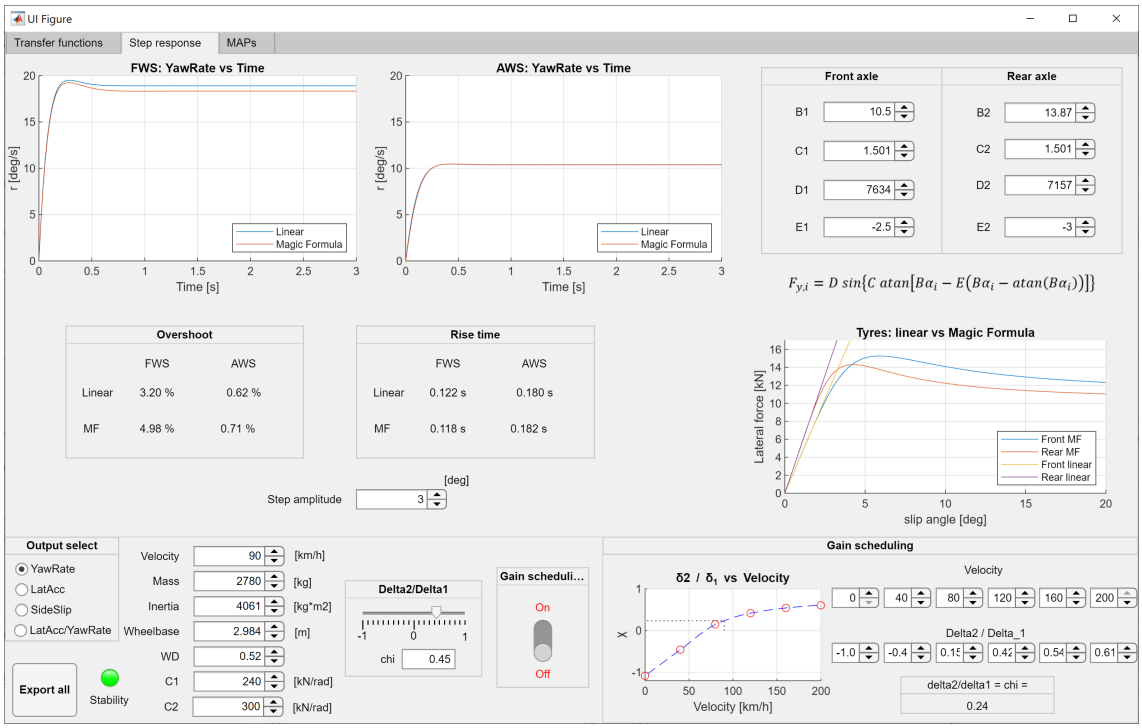

Figure 3.2: GUI page to study lateral acceleration, yaw rate and side-slip of a step response with front steer angle as input.

Chapter 4

Multi-body system model

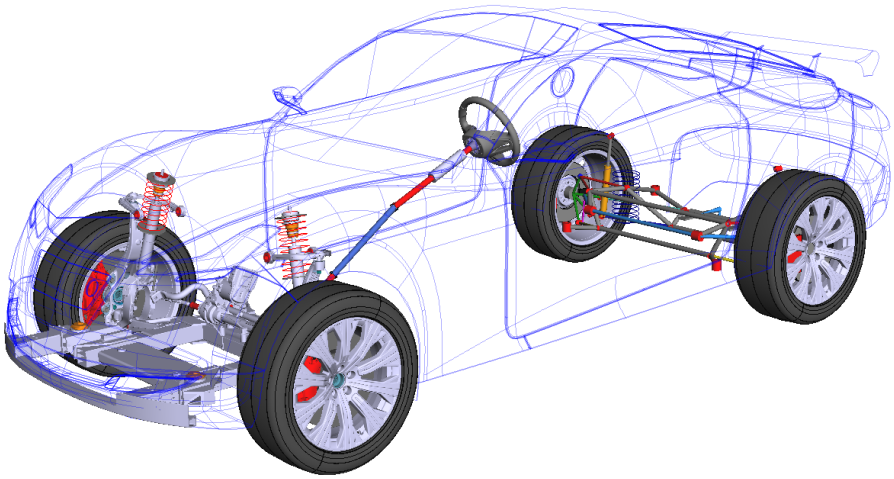

Figure 4.1: MBS model built in Simpack.

4.1 Why building an MBS model

A single track model is a great tool to carry out an initial vehicle response analysis, but an MBS model allows for a more detailed analysis.

Firstly, compared to a single track model, an MBS model can provide plenty of information, such as kinematics and dynamics of each single component. The price for such detailed results is that the information to input into the model must be detailed too. Indeed, it is necessary to know mass, inertia, position and mechanical properties of each component, and how they are interconnected.

Secondly, an MBS model considers the compliance and frictional effects of the elements in the system.

Finally, utilising an MBS model allows for investigating components requirements, for instance, to study what are the actuation requirements for the rear steer, in terms of range, torque, velocity and thus, power. This kind of information allows to give technical requirements to the suppliers, leading to a better result since the early development phase.

4.2 Why using Simpack

The MBS software utilised to build the model is Simpack, which is new to Volvo Cars vehicle dynamics department.

Volvo Cars is interested in evaluating Simpack for its ability to easily integrate control logics developed in Simulink and its real-time application in dynamic driving simulators. The real-time integration in the driving simulator is not part of this thesis but is a project that runs in parallel.

Consequently, some of time of the thesis is spent learning the new software together with the supervisors, building an MBS model from scratch.

4.3 The vehicle model

The model represents an SUV, similar to a Volvo XC90, despite Figure 4.1 shows a different body shape. The corresponding physical vehicle does not exist because the MBS model is a combination of an industrialized front suspension and a prototype rear suspension.

The front axle is taken from a Volvo XC90: it includes the subframe, the steering system, the anti-roll bar and the suspension, which is a double wishbone. On the other hand, the rear axle consists of subframe, steering system, anti-roll bar and a four link suspension. The rear axle is from a new platform, which is still in an early phase of development. This implies that the data available is less mature, compared to the front axle, and and likely to change since hard points are not fixed yet and packaging work is still ongoing.

The rear steering is a rack and pinion system. All bodies are rigid and compliance comes from bushings.

The driveline is not modeled, but torque is directly applied to the front wheels with the only purpose to reach or maintain a desired velocity. This type of driveline is considered as sufficient, since the focus of the thesis is to study the lateral dynamics. The tyre model used is a Magic Formula tyre model, with linear transient and turn-slip. The dimensions of the tyres are 275/35R22.

All simulations are carried out on a flat, dry road with constant friction coefficient $\mu = 1$. The vehicle parameters used are shown in Table 4.1.

Table 4.1: MBS and single-track model parameters.

Parameter	Value	Unit
Mass	2780	kg
Wheelbase	2.984	m
Weight distribution	52%	
Yaw inertia	4061	$kg \cdot m^2$
Front cornering stiffness	240	kN/rad
Rear cornering stiffness	300	kN/rad

4.3.1 Kinematics and compliance test rig

In addition to the full vehicle model, a kinematics and compliance (K&C) test rig is built in Simpack for the rear axle (Figure 4.2).

The K&C allows to study the kinematics of the suspension through simulations such as parallel wheel travel, opposite wheel travel and steer motion. Moreover, the compliance introduced by bushings can be investigated by applying a longitudinal force, a lateral force or a vertical moment at the wheel centre.

This K&C is used to check the correspondence between the MBS model in Simpack and the model built with Volvo Cars usual software. It was also used to tune some mechanical properties, such as the stiffness of the anti-roll bar, and to set the ratio between the pinion of the rear steering system and the angles at the rear wheels.

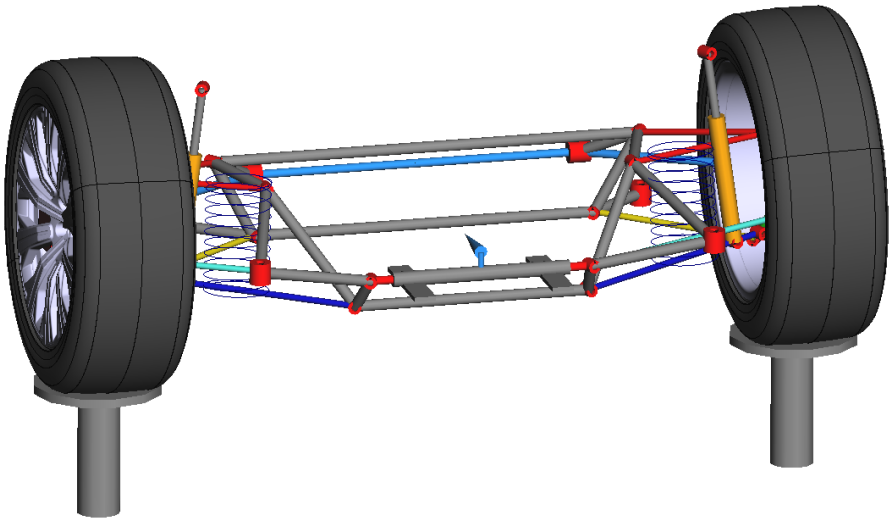

Figure 4.2: Kinematics and compliance test rig built in Simpack.

Chapter 5

Control implementation

All controls proposed here are idealised, meaning that there are no hardware and software limitations.

5.1 Control objectives

The argument for every added (active) system is that it needs to improve the vehicle capabilities.

Improved manoeuvrability

The first objective is to achieve better maneuverability at low velocity, which means to decrease the minimum turning radius, or, equivalently, to increase the yaw rate gain. Better manoeuvrability improves ease of parking and reduces the swept volume of the vehicle, which is useful in tight corners.

Improved stability

The second objective is to improve stability at high velocity. This requirement is bound to the yaw rate too, and, according to Kreutz, Horn and Zehetner [3], the response of the vehicle should exhibit a sufficiently small overshoot for a step steer manoeuvre: this allows the driver to better control the vehicle and to avoid fishtailing.

Improved agility

The third objective is to improve agility, which is related to the reactivity of the vehicle. According to J. Ghosh in [8], reactivity can be evaluated by the yaw rate rise time for a step steer input; but it can be seen also as the capability of the rear axle to rapidly build up lateral force. For a FWS vehicle, the negotiation of a turn occurs in the following way [1]:

1. the driver turns the steering wheel of a certain angle, generating a slip angle at the front wheels;
2. after a certain delay caused by the relaxation length of the front tyres, lateral force is built up at the front axle; this creates yaw rate and sideslip angle, thus, lateral acceleration;

3. the vehicle yaw generates a slip angle at the rear wheels;

4. after a certain delay caused by the relaxation length of the rear tyres, lateral force is built up at the rear axle and lateral acceleration increases.

This chain of events is responsible for the delay between the steering input and the lateral acceleration. On the contrary, the introduction of active rear steering allows to build up lateral force at the rear axle without waiting for the rise of the yaw rate. Since the lateral acceleration comes from the sum of the lateral forces at the front and rear axle, active rear steering allows to reduce this undesired delay. This also implies that the delay between lateral acceleration and yaw rate is reduced [8]. Indeed, T. Eguchi et al. [2] too agree on reducing the phase difference between lateral acceleration and yaw rate is beneficial.

Reduced sideslip angle

Furthermore, according to Guiggiani [13] it is good to keep the sideslip angle β small because *"vehicles behave in a better way if β spans a small range"*. An interpretation of this statement is that if $\beta = 0$ the vehicle is pointing in the same direction of its velocity vector (at its CoG); indeed, if $\beta > 0$ the vehicle has a "nose out" configuration and if $\beta < 0$ it has a "nose-in" configuration, as shown in Figure 5.1. Keeping β close to 0 would imply that if the driver is looking ahead, they are always pointing in the same direction of the velocity vector of the vehicle. Since the path is described by the heading angle (i.e. the yaw angle), which is what the driver controls, having a low side slip angle makes the vehicle follow the path that was intended by the driver.

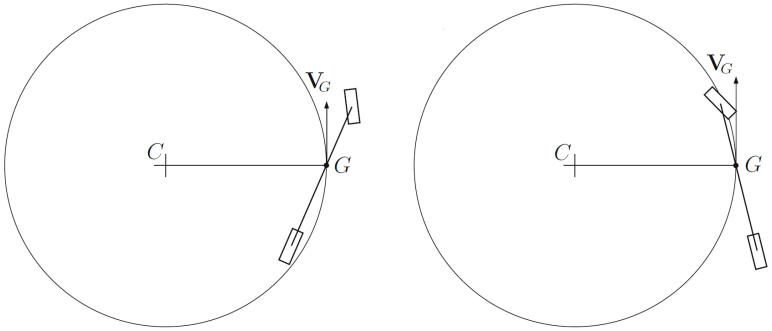

Figure 5.1: Nose out (on the left), nose-in (on the right) configuration of a vehicle, according to the positive or negative sign of the sideslip angle, respectively [13].

To summarise, the control logic should target the following improvements:

- increase yaw rate gain at low velocity;
- reduce yaw rate overshoot (increase yaw rate damping);
- reduce the yaw rate rise time and the phase delay between yaw rate and lateral acceleration;
- reduce the sideslip angle.

5.2 Gain scheduling

The first type of control implemented is the simple gain scheduling introduced in paragraph 3.2. It is a feedforward control that relates the rear steer angle δ_2 to the front steer angle δ_1, as $\delta_2 = \chi(u) \cdot \delta_1$; the gain $\chi(u) = \delta_2/\delta_1$ is function of longitudinal velocity u.
With this relation, it is possible to take equations 2.45, 2.46 and 2.47 and expand them as shown in equations 5.1, 5.2 and 5.3, respectively:

$$\frac{V_{AWS}}{\Delta_1} = \frac{1}{m} \cdot \frac{C_1[s - \frac{1}{Ju}(mu^2a - C_2lb)] + \chi C_2[s + \frac{1}{Ju}(mu^2b + C_1la)]}{s^2 + 2\sigma s + \omega_0^2} \tag{5.1}$$

$$\frac{R_{AWS}}{\Delta_1} = \frac{1}{J_z} \cdot \frac{aC_1(s + \frac{lC_2}{amu}) - \chi bC_2(s + \frac{C_1 l}{mub})}{s^2 + 2\sigma s + \omega_0^2} \tag{5.2}$$

$$\frac{A_{y\,AWS}}{\Delta_1} = \frac{1}{m} \cdot \frac{C_1(s^2 + s\frac{C_2lb}{J_z u} + \frac{C_2 l}{J_z}) + \chi C_2(s^2 + s\frac{C_1 la}{J_z u} - \frac{C_1 l}{J_z})}{s^2 + 2\sigma s + \omega_0^2} \tag{5.3}$$

Where the additional part introduced by rear steering, with respect to a FWS vehicle, is highlighted in red.

One interesting observation can be made from the poles of the transfer functions. Equations 2.31, 2.32 and 2.46, from chapter 2.2, represent the transfer functions of the yaw rate R with respect to the front steer input Δ_1, to the (only) rear steer input Δ_2, and to the front steer input for an AWS vehicle, respectively:

$$\frac{R}{\Delta_1} = \frac{aC_1}{J_z} \cdot \frac{s + \frac{lC_2}{amu}}{s^2 + 2\sigma s + \omega_0^2}$$

$$\frac{R}{\Delta_2} = \frac{-bC_2}{J_z} \cdot \frac{s + \frac{lC_1}{bmu}}{s^2 + 2\sigma s + \omega_0^2}$$

$$\frac{R_{AWS}}{\Delta_1} = \frac{1}{J_z} \cdot \frac{aC_1(s + \frac{lC_2}{amu}) - \chi bC_2(s + \frac{C_1 l}{mub})}{s^2 + 2\sigma s + \omega_0^2}$$

The denominators of the transfer functions, highlighted in blue, are always exactly the same. Thus, all the FWS, RWS and AWS vehicles have the same damping ratio and natural frequency. Therefore, according to the single track model, the introduction of the rear steer does not affect the properties of the system.

It is appropriate to highlight that this is true only if χ is a constant: if χ becomes a function of frequency too (as done in the control paragraph 5.3), the control of the rear steer can change the vehicle properties. The gain scheduling is only able to move the transfer function zeros, thus changing the response of the vehicle.

5.2.1 Mitigation of the sideslip angle

The first attempt to find χ is carried out calculating the χ values that set the sideslip angle to zero at all velocities and at steady state conditions.
To set the steady state sideslip angle to zero, the numerator of equation 5.1 is put equal to zero in steady-state conditions. This yields to the following function:

$$\chi(u) = -\frac{C_1}{C_2} \cdot \frac{C_2 lb - mu^2 a}{C_1 la + mu^2 b} \tag{5.4}$$

$\chi(u)$ is displayed in Figure 5.2: rear wheels will steer in opposite direction of the front wheels up to $\sim 65\,km/h$.

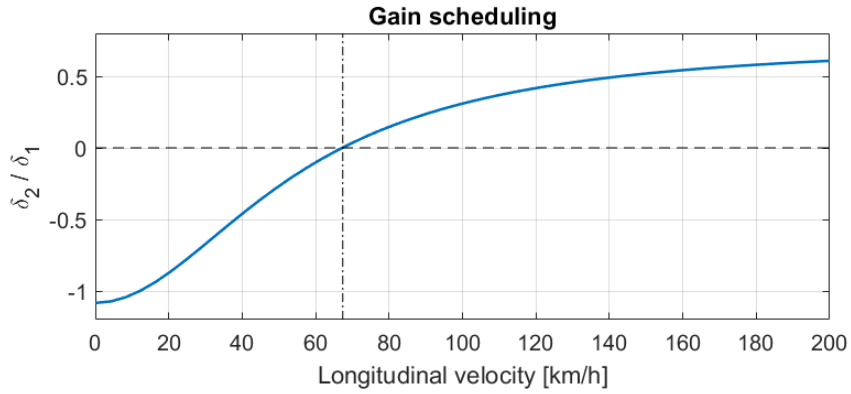

Figure 5.2: Gain scheduling that sets the sideslip angle to zero at all velocities.

Vehicle linear response analysis

Importing the gain scheduling curve of equation 5.4 in the GUI allows to quickly assess if this simple control logic meets the control objectives.
The sideslip angle, as desired, is set to zero for steady state conditions (Figure 5.3). At low velocity the sideslip angle is not exactly zero only because the gain scheduling entered into the GUI is implemented through an interpolation of only six points.

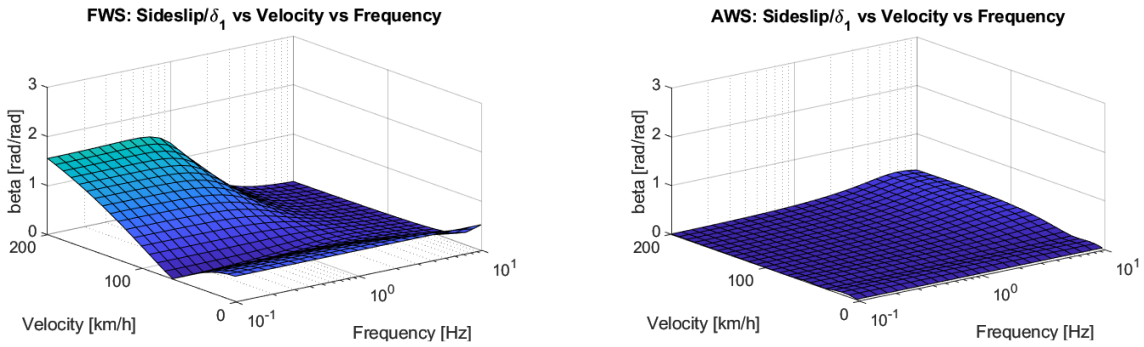

(a) FWS (b) AWS

Figure 5.3: Comparison of magnitude of the sideslip angle between a FWS and AWS vehicle with a simple gain scheduling. Figure A.1 shows also the phase.

Figure 5.4 shows the yaw rate transfer function:

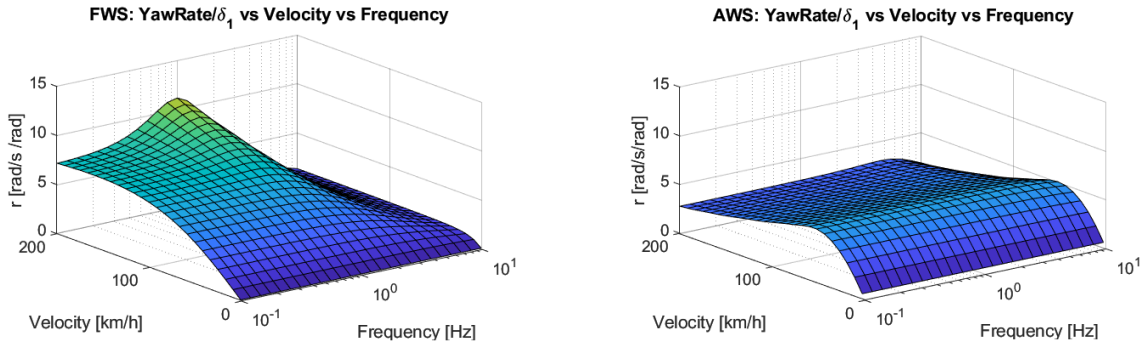

(a) FWS (b) AWS

Figure 5.4: Comparison of the yaw rate between a FWS and AWS vehicle with a simple gain scheduling. Figure A.2 shows also the phase.

The yaw rate magnitude of the AWS vehicle is initially increased at low velocities, which implies that manoeuvrability is improved. On the other hand, at high velocity the yaw rate is strongly decreased. To assess stability, Table 5.1 shows a comparison of the yaw rate overshoot to a step steer. To make the comparison fair, the FWS and AWS vehicle reach the same yaw rate value at steady state conditions. Moreover, the front steer angles are set to reach the maximum lateral acceleration of almost $0.4\,g$ allowed by the single-track model.

Table 5.1: Yaw rate overshoot and rise time comparison for a step steer.

Velocity: $90\,km/h$	FWS	AWS
Front steer angle	$1.1\,^\circ$	$1.44\,^\circ$
χ value	-	0.24
Rear steer angle	$0\,^\circ$	$0.35\,^\circ$
Overshoot	$3.24\,\%$	$1.79\,\%$
Rise time	$0.122\,s$	$0.144\,s$

Velocity: $130\,km/h$	FWS	AWS
Front steer angle	$0.85\,^\circ$	$1.56\,^\circ$
χ value	-	0.45
Rear steer angle	$0\,^\circ$	$0.7\,^\circ$
Overshoot	$12.59\,\%$	$5.02\,\%$
Rise time	$0.112\,s$	$0.169\,s$

It is possible to see the effect of the gain scheduling: at both velocities, the overshoot is decreased and the rise time has slightly increased. This behaviour can be explained looking at the transfer function 5.2: the introduction of rear steering, in blue, changes the position of the zero of the transfer function. As χ increases with velocity, the zero moves leftwards on the complex plane, compared to the zero of the FWS vehicle (Figure 5.5). According to control theory, this implies that the system will reduce its overshoot, but increasing the rise time, which is exactly the behaviour found in the GUI.

One more interesting plot is the phase between lateral acceleration and yaw rate (Figure 5.6). This plot shows that introducing the ARS with a simple gain scheduling eliminates the lag between yaw rate and lateral acceleration, which is a desired improvement: reducing the lag implies that the driver feels the vehicle as more reactive. Anyway, It has to be noted that this conclusion is limited to a single track model with an idealised actuator.

In conclusion, despite its easiness, this gain scheduling already brings some im-

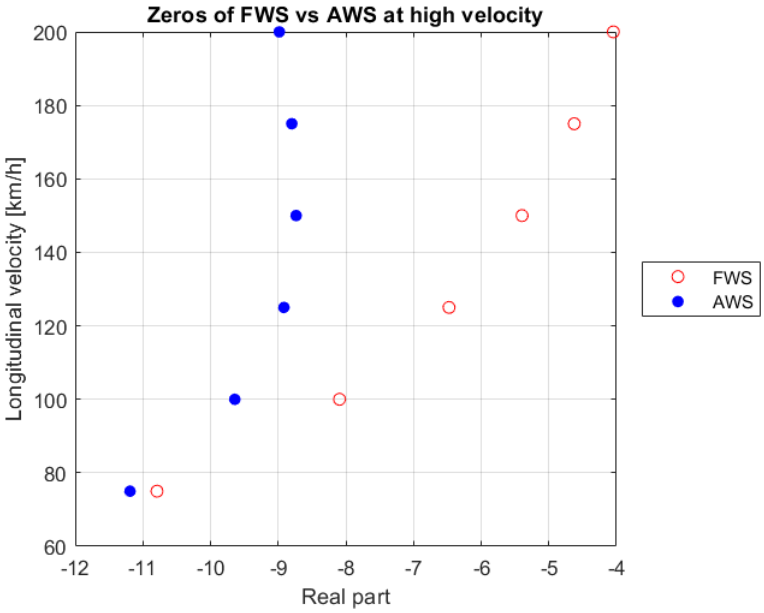

Figure 5.5: Zero of the yaw rate transfer function of an AWS vehicle, with a gain scheduling, moving leftwards compared to a FWS vehicle, when velocity is increased.

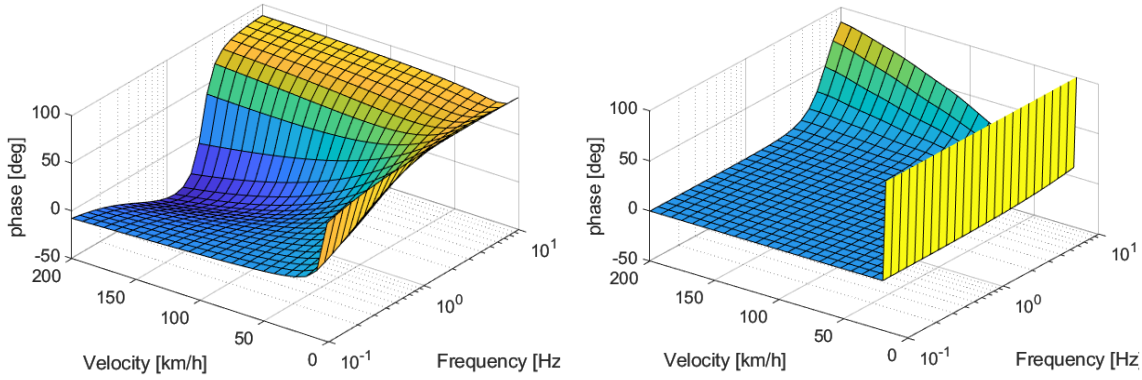

(a) FWS (b) AWS

Figure 5.6: Phase of lateral acceleration with respect to yaw rate. Figure A.3 shows also the magnitude.

provements to the vehicle response, especially for manoeuvrability at low velocity. However, it shows also two major drawbacks.

Firstly, the yaw rate is excessively reduced at high velocity: such low values cause the steering effort, in terms of angle request, to increase.
Applying a fixed steering wheel angle, with $\chi > 0$ the yaw rate decreases and the turning radius increases. This means that when comparing a FWS to an AWS vehicle, the latter one has to steer more to travel the same corner. To give a real example, a corner of a highway in Italy can be taken into account (Figure 5.7). This corner has a turning radius of approximately $100\,m$ and a speed limit of $80\,km/h$. At steady state the lateral acceleration reached is $0.5\,g$ and the required yaw rate is $12.73\,^\circ/s$. Table 5.2 shows the front steer angles δ_1 and the steering wheel angles δ_{sw} required to travel this corner, assuming $\chi = 0.15$ and a steer ratio of 16.8.
The steering wheel angle increases from $42\,^\circ$ for the FWS vehicle to $50\,^\circ$ for the AWS

Figure 5.7: A corner of the highway A7 in Italy. Screenshot from Google Maps.

Table 5.2: Steer angles required to negotiate a corner of $R \approx 100\,m$, at $80\,km/h$.

	Steer ratio	χ	δ_1	δ_{sw}
FWS	16.8	0	2.5 °	42 °
AWS	16.8	0.15	2.9 °	50 °

vehicle, which means that the driver should steer $\sim 20\,\%$ more to drive along the same corner.

Secondly, the value of the side-slip angle in normal driving conditions for a FWS is in the range of $\pm\ 1{-}2$ deg, which is already hardly noticeable by an average driver. Consequently, keeping a low sideslip angle is preferred, but setting it precisely to zero is unnecessary.

5.3 Feedforward following a reference response

A different approach is presented in this section: the objective is to design a feedforward control logic so that the AWS yaw rate response matches a reference yaw rate response defined from a FWS vehicle. In Laplace domain this is written as:

$$R_{AWS} = R_{ref} \tag{5.5}$$

where R_{AWS} is the yaw rate response of an AWS vehicle while R_{ref} is the desired yaw rate response.

The yaw rate response of an AWS vehicle, stated in equation 2.46, is:

$$R_{AWS} = G_{\frac{R}{\Delta_1}} \cdot \Delta_1(s) + G_{\frac{R}{\Delta_2}} \cdot \Delta_2(s)$$

where the yaw rate response is the sum of the contributions coming from the front and rear steer angles. $G_{\frac{R}{\Delta_1}}$ and $G_{\frac{R}{\Delta_2}}$ (derived in equations 2.31 and 2.32) are the yaw rate transfer functions from Δ_1 and Δ_2 respectively. Their value depends on the input frequency and the longitudinal velocity u.

The desired yaw rate response is derived from a reference single-track model of a FWS vehicle and it can be written as:

$$R_{ref} = G_{\frac{R_{ref}}{\Delta_1}} \cdot \Delta_1(s) \tag{5.6}$$

where $G_{\frac{R_{ref}}{\Delta_1}}$ is the transfer function that defines the desired yaw rate response.

According to the control objective defined in equation 5.5, it is finally possible to write:

$$G_{\frac{R}{\Delta_1}} \cdot \Delta_1(s) + G_{\frac{R}{\Delta_2}} \cdot \Delta_2(s) = G_{\frac{R_{ref}}{\Delta_1}} \cdot \Delta_1(s) \tag{5.7}$$

Dividing all the terms by Δ_1 and rearranging the above equation it is possible to compute the transfer function from Δ_1 to Δ_2 that allows the vehicle to behave likewise the reference:

$$\frac{\Delta_2(s)}{\Delta_1(s)} = \frac{G_{\frac{R_{ref}}{\Delta_1}} - G_{\frac{R}{\Delta_1}}}{G_{\frac{R}{\Delta_2}}} = X(u,s) \tag{5.8}$$

where $X(u,s)$ is the transfer function from Δ_1 to Δ_2 and it represents the feedforward control logic. Its value depends on the input frequency and on the longitudinal velocity u.

This results in the rear steer angle Δ_2 being function of front steer angle Δ_1, front steer angle frequency and longitudinal velocity u. In Laplace domain this is summarised as:

$$\Delta_2(s) = X(u,s) \cdot \Delta_1(s) \tag{5.9}$$

Finally, this brings to the the question: how to define the desired yaw rate response?

5.3.1 Definition of the yaw rate reference response

The reference yaw rate response is defined starting from a FWS linear single-track model which properties vary with longitudinal velocity.

Intuitively, a vehicle with a shorter wheelbase behaves better in an urban environment where reduced cornering radii and swept area play a major role. Conversely, at high velocity, vehicles stability benefits from a longer wheelbase: from equation 2.33, it is possible to understand that a longer wheelbase increases the damping ratio, thus having a positive effect on stability..

As a starting point, the reference yaw rate response is taken from a vehicle which wheelbase varies with respect to longitudinal velocity as reported in Figure 5.8.

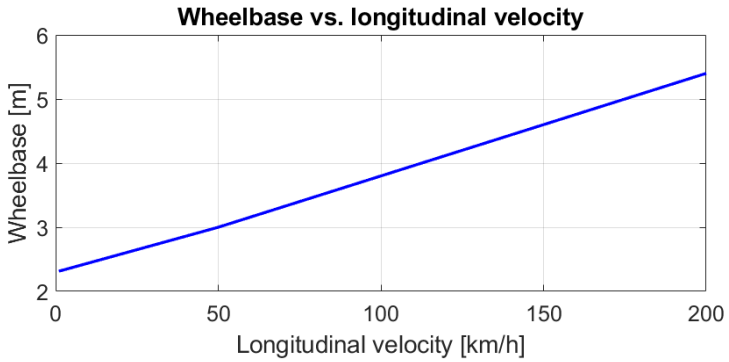

Figure 5.8: Reference vehicle wheelbase as function of longitudinal velocity.

According to the linear single-track model, this choice of wheelbase leads to the damping ratio and undamped natural frequency shown in Figure 5.9.

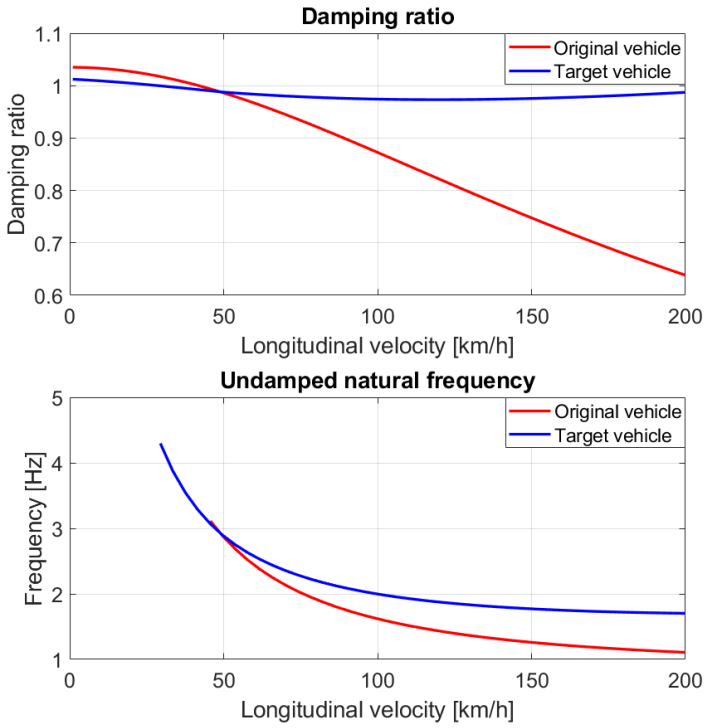

Figure 5.9: Damping ratio and undamped natural frequency, of a single track model, as function of longitudinal velocity. The original vehicle in red, the reference one in blue.

The reference vehicle damping ratio is almost constant with respect to longitudinal velocity and at velocities above $50\,km/h$ its value is much greater than the original FWS vehicle. This result suggests that, during transients, the vehicle exhibits less overshoot in its response.

Finally, Figure 5.10 shows the yaw rate transfer functions of the original compared to reference one, which wheelbase changes as previously shown in Figure 5.8.

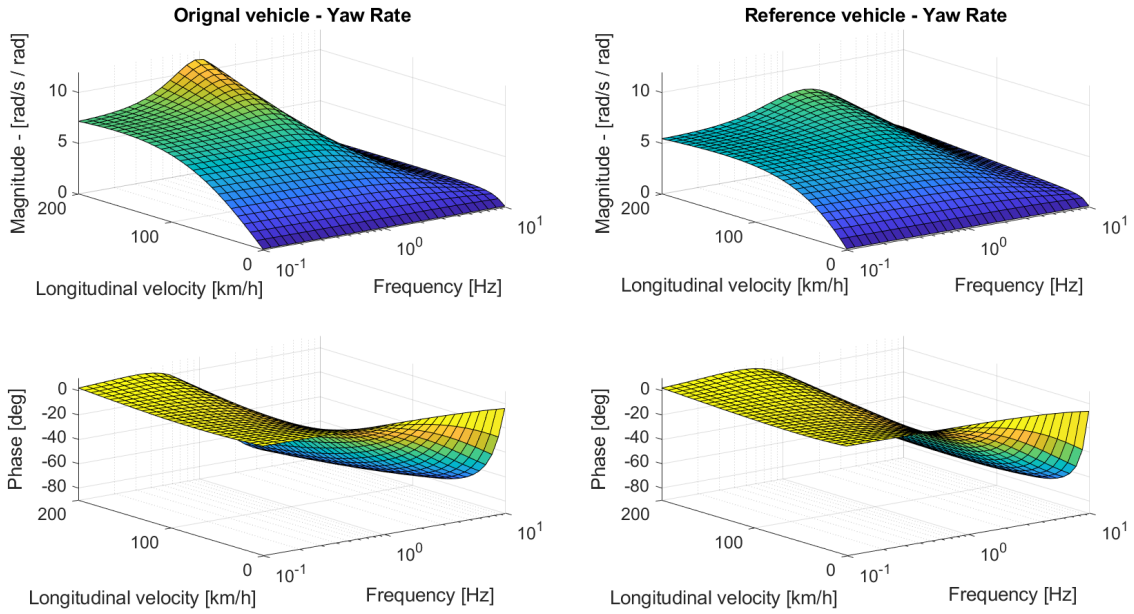

Figure 5.10: Yaw rate transfer functions of the original vehicle (left) and the desired one (right). Magnitude on the top, phase at the bottom.

At high velocity it noticeable how the peak is reduced and the phase is increased.

5.3.2 Control tuning

Following the procedure shown in section 5.3 and setting the reference vehicle as described in 5.3.1, it is possible to make the vehicle equipped with ARS to behave like the reference vehicle. The transfer function from Δ_1 to Δ_2 is in the form:

$$\frac{\Delta_2(s)}{\Delta_1(s)} = X(u,s) = g_{SS} \cdot \frac{s^3 + b_2 s^2 + b_1 s + b_0}{s^3 + a_2 s^2 + a_1 s + a_0} \tag{5.10}$$

where g_{SS} is the steady-state gain. It is important to notice that the coefficients b_i and a_i, including g_{SS}, are function of the longitudinal velocity u, meaning that the controller will use a different transfer function at each velocity. $X(u,s)$ looks like shown in Figure 5.11.

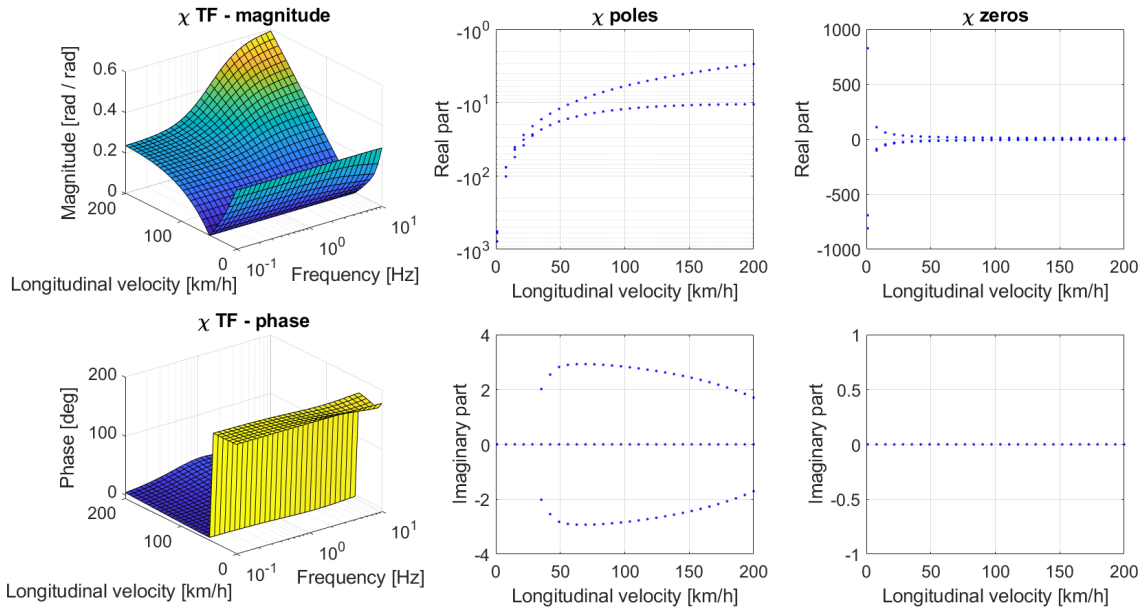

Figure 5.11: $X(u, s)$ transfer function. On the left column, magnitude and phase as function of frequency and longitudinal velocity. In the central and left column, the poles and zeros real and imaginary parts as function of longitudinal velocity.

From Figure 5.11 it is possible to notice that for longitudinal velocities lower than $30\,km/h$ all the poles are real, while above $30\,km/h$ one pole is real and two are complex conjugate. The zeros are always real. The $X(u, s)$ transfer function can be rewritten highlighting the poles and the zeros and for velocities lower than $30\,km/h$, $X(u, s)$ is:

$$X(u,s) = g_{SS} \cdot \frac{(s+z_1)(s+z_2)(s-z_3)}{(s+d_1)(s+d_2)(s+d_3)} \qquad z_i, d_i \in \mathbb{R} > 0 \tag{5.11}$$

Poles and zeros are real, with one zero being positive.

For $u > 30\,km/h$, $X(u, s)$ is:

$$X(u,s) = g_{SS} \cdot \frac{(s+z_1)(s+z_2)(s-z_3)}{(s+d_1)(s^2+d_2 s+d_3)} \qquad z_i, d_i \in \mathbb{R} > 0 \tag{5.12}$$

showing that $X(u, s)$ has a pair of complex conjugate poles.

The first problem to address is that the transfer function stated in equation 5.10 and shown in Figure 5.11 is not strictly proper: numerator and denominator are polynomials of the same order. This means that the transfer function amplitude does not approach zero when the input frequency approaches infinite. This is a drawback for noise filtering, hence the zero with highest frequency is removed, reducing $X(u, s)$ to a strictly proper transfer function with two zeros and three poles while keeping the same value of steady-state gain g_{SS}. This process is described in the following sections, where two tuning methods are presented.

The following tuning methods focus on improving the vehicle response from medium to high velocities ($u > 50\,km/h$) so the $X(u, s)$ transfer function a shown in equation 5.12 is studied.

Method 1 - "v1"

The goal of this method is to tune the $X(u,s)$ transfer function to reduce the yaw rate overshoot and the delay between yaw rate and lateral acceleration. The tuning is done for longitudinal velocities above $50\,km/h$.

The first step consists of making the $X(u,s)$ transfer function strictly proper. For this reason the positive zero z_3 is removed and the static gain is adjusted to be equal as the original one, leading to the following $X(u,s)$ expression:

$$X(u,s) = -z_3 \cdot g_{SS} \cdot \frac{(s+z_1)(s+z_2)}{(s+d_1)(s^2+d_2 s+d_3)} \qquad z_1 > z_2 \tag{5.13}$$

The proposed tuning method is then based on equation 5.13: the position of the largest zero z_1 is shifted on the real axis to reach the desired vehicle response. This is achieved by defining a factor $\lambda_1(u)$ that multiplies z_1 as shown in the following equation:

$$X(u,s) = -z_3 \cdot g_{SS} \cdot \frac{1}{\lambda_1} \cdot \frac{(s+\lambda_1 z_1)(s+z_2)}{(s+d_1)(s^2+d_2 s+d_3)} \tag{5.14}$$

In the complex plane, for $\lambda_1 < 1$, z_1 is shifted towards the imaginary axis, vice versa for $\lambda_1 > 1$. The value of $\lambda_1(u)$ is scheduled based on the longitudinal velocity u.

The effect of moving the largest zero closer or further from the imaginary axis can be visualized in the example shown in Figure 5.12. This example is based on a transfer function similar to the equation 5.14. The

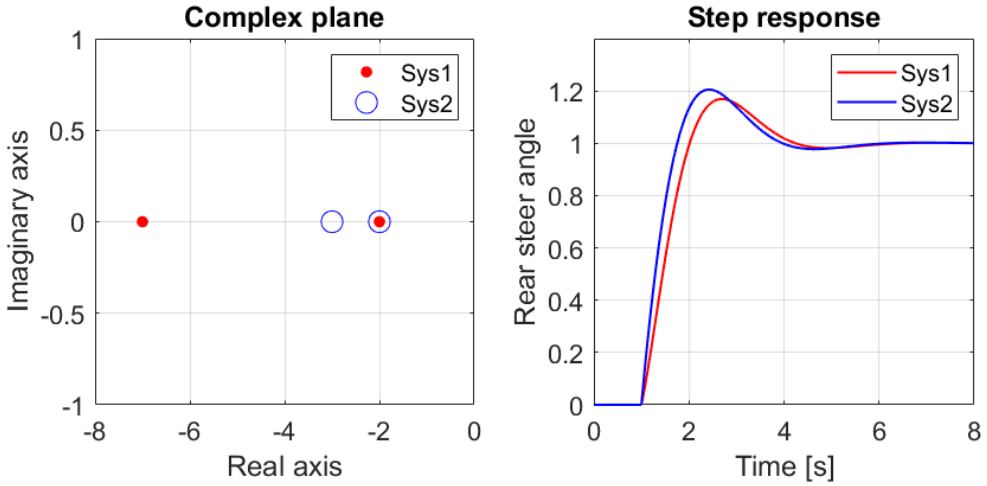

Figure 5.12: Example of the effect of the position of the zeros on the normalised rear steer angle for a step steer input.

The above picture shows how zeros closer to the imaginary axis are responsible for lower rise time and higher overshoot.

The tuning process is done at different longitudinal velocities in the range from $50\,km/h$ to $200\,km/h$ by simulating step steer manoeuvres. The factor λ_1 is adjusted with the aim to reduce both the yaw rate overshoot and the delay between lateral acceleration and yaw rate. The value of λ_1 depends on the longitudinal velocity u,

hence after the tuning process its value is interpolated to cover the whole velocity range.

According to this method, the resulting $X(u, s)$ transfer function is shown in Figure 5.13.

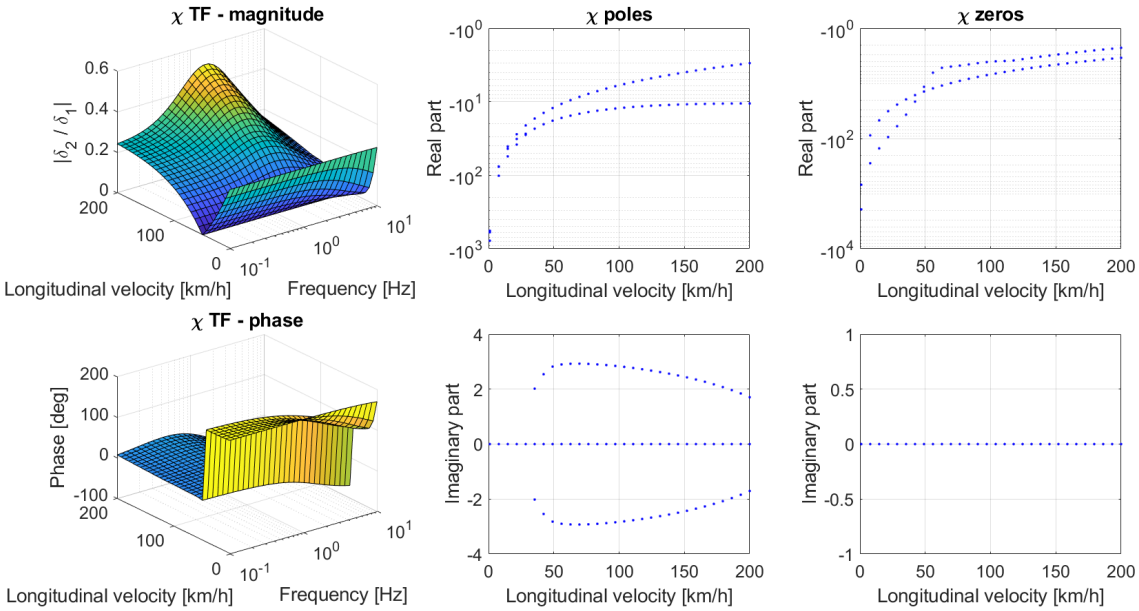

Figure 5.13: $X(u, s)$ transfer function after the tuning method $v1$. Left column: magnitude and phase as function of frequency and longitudinal velocity. Central and right columns: poles' and zeros' real and imaginary parts as function of longitudinal velocity.

Method 2 - "v2"

The goals of this method are similar to the one described in "Method 1": reduced yaw rate overshoot and reduced delay between yaw rate and lateral acceleration. In addition, this method pursues the reduction of yaw rate rise time too.

Firstly, this method differs from "Method 1" in how the $X(u, s)$ transfer function (see equation 5.12) is made strictly proper: the largest negative zero z_1 is removed while the positive zero z_3 is maintained. The steady state gain is kept equal as before, leading to the following expression for $u > 30km/h$:

$$X(u,s) = g_{SS} \cdot z_1 \cdot \frac{(s+z_2)(s-z_3)}{(s+d_1)(s^2+d_2 s+d_3)} \qquad z_i, d_i \in \mathbb{R} > 0 \tag{5.15}$$

Secondly, this method allows to individually tune the position of both zeros z_2 and z_3 and the real part of all the poles. For this purpose, the factors λ_2, λ_3 and λ_d are defined. Respectively, their value shift the position of z_2, z_3 and the real part of poles while keeping the same imaginary part. The steady-state gain is kept equal to the original. This is achieved as shown:

$$X(u,s) = \frac{g_{SS} z_1 \lambda_d}{\lambda_2 \lambda_3} \cdot \frac{d_3 + \frac{d_2^2}{4}(\lambda_d^2 - 1)}{d_3} \cdot \frac{(s+\lambda_2 z_2)(s-\lambda_3 z_3)}{(s+\lambda_d d_1)(s^2+\lambda_d d_2 s + d_3 + \frac{d_2^2}{4}(\lambda_d^2-1))} \tag{5.16}$$

The effect of λ_2, λ_3 and λ_d can be visualised in Figure 5.14, where an example of rear steer angle response to a step steer is reported.

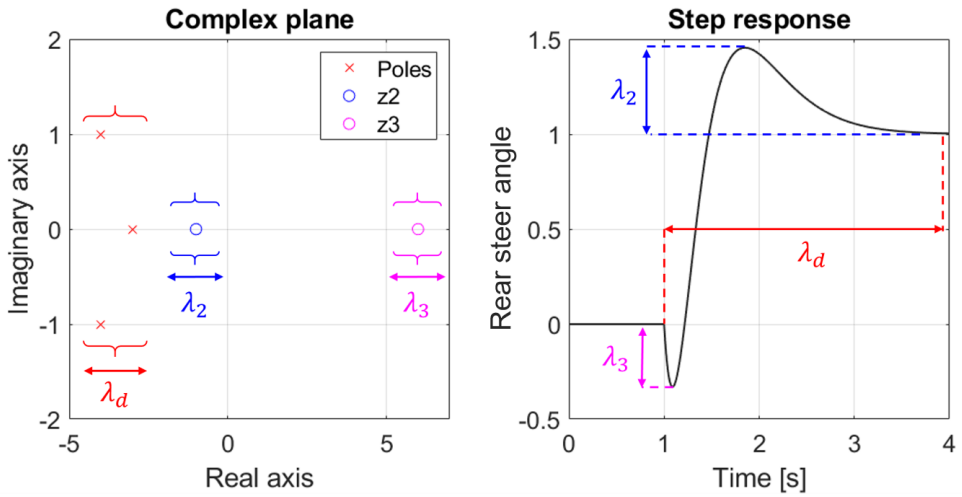

Figure 5.14: Example of the effect of λ_2, λ_3 and λ_d on the normalised rear steer angle for a step steer input.

It is important to underline that λ_2, λ_3 and λ_d have effect on the whole response, not exclusively on what is reported in Figure 5.14, but for the sake of this method their values are tuned according to the effect shown in the above picture. Namely:

- λ_2 mainly controls the overshoot of the rear steer angle. The overshoot means that the rear wheels turn in the same direction of the front wheels more than the steady-state value in a limited fraction of time. This effectively reduces the vehicle yaw rate overshoot while keeping low the steering effort in terms of steering angle request (i. e. the increased steering angle request depends on the rear steer angle steady-state value);

- λ_3 mainly controls the negative peak of the rear steer steer angle. The negative peak means that for sudden steering inputs, the rear wheels turn in the opposite direction to the front wheels, increasing the yaw rate gain and reducing the yaw rate rise time;

- λ_d mainly controls the transient time-span of the rear steer steer angle. This has a direct effect on how fast the rear wheels are turning. The λ_d value is chosen in conjunction to λ_2 and λ_3 to reduce both yaw rate overshoot and yaw rate rise time.

The tuning process is done at different longitudinal velocities in the range from $50\,km/h$ to $200\,km/h$ by simulating step steer manoeuvres. The factors λ_2, λ_3 and λ_d are adjusted with the aim to reduce both the yaw rate overshoot and the yaw rate rise time. The values of λ_2, λ_3 and λ_d depend on the longitudinal velocity u, hence after the tuning process their values are interpolated to cover the whole velocity range.

The main difference between method 1 and method 2 is in the effect of the parameters λ_3 and λ_d. As mentioned above, they control the amplitude of the negative peak and the transient duration.

The $X(u, s)$ transfer function resulting from this tuning method is shown in Figure 5.15.

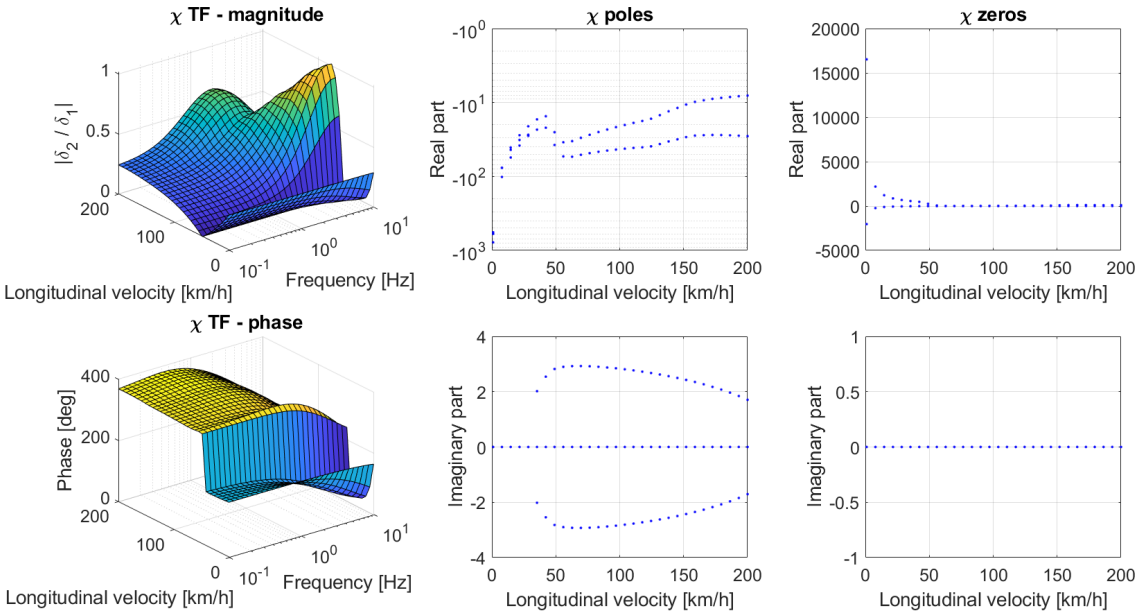

Figure 5.15: $X(u, s)$ transfer function after tuning method 2. Left column: magnitude and phase as function of frequency and longitudinal velocity. Central and right column: poles' and zeros' real and imaginary parts as function of longitudinal velocity.

Considerations

As a consequence of both tuning methods $v1$ and $v2$, the $X(u, s)$ transfer function is made strictly proper, meaning that its amplitude approaches zero for frequencies approaching infinite. This means that eventual high frequency noise content in the front steering signal is filtered out, having a minimal effect on the rear steer angle.

To assess the filtering behaviour, the response to a step step steer is simulated in Simulink and white noise is added to the front steer angle signal, input to the $X(u, s)$ transfer function. In Figure 5.16, the signals of front and rear steer angles are compared before and after adding the noise. In this example, the rear wheels are controlled by $v2$. As it is possible to notice, the high noise affecting the front steer angle is filtered out by the $X(u, s)$ transfer function, leading to a minimal effect on rear steer angle signal.

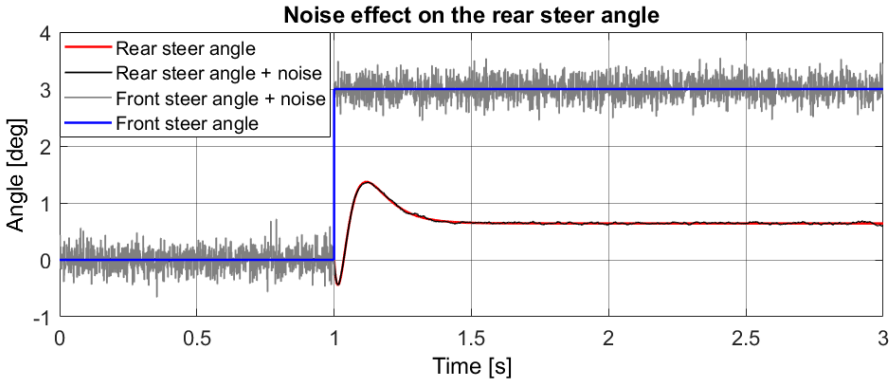

Figure 5.16: Effect of noise added to the front steer angle over the rear steer angle.

Chapter 6

Selection of driving scenarios

The driving scenarios selected to assess active rear steering with the proposed control logic are described in this chapter. The MBS full vehicle model is excited with different steering inputs at different longitudinal velocities, which allows to characterize the vehicle response with and without the effect of active rear steering. The differences between passive and active vehicles are quantified by means of the metrics reported in section 6.7 in Table 6.2.

6.1 Constant steer at low velocity

In this driving scenario a constant angle is applied at the steering wheel and the longitudinal velocity is kept constant. The intent of this test is to compare the minimum turning radii of the AWS and FWS vehicles at low longitudinal velocity; thus, the steering wheel angle is set to the maximum value of $540\,deg$. Reduced values of turning radius mean increased low speed manoeuvrability.

6.2 Constant radius at low velocity

The purpose of this driving scenario is to evaluate the difference in swept-area between the AWS and FWS vehicles. This is a closed loop manoeuvre, hence a driver model is selected in Simpack to perform the simulations. For this driving scenario, the driver follows a circular path with radius of $6\,m$ while keeping constant longitudinal velocity. Reduced swept area means increased low speed manoeuvrability.

6.3 Ramp steer

The ramp steer manoeuvre is useful for assessing the quasi-static response of the vehicle at every lateral acceleration condition. It allows to find the maximum lateral acceleration that a vehicle is able to withstand. Furthermore, the transition between linear and non-linear behaviour of a vehicle can be found, and the vehicle behaviour can be studied in the non-linear region.

A ramp steer manoeuvre is performed by increasing slowly and linearly the steering wheel input angle, starting from the on-center position and reaching a desired final value [15]. The longitudinal velocity is kept constant throughout the whole manoeuvre. An example of ramp steer is illustrated in Figure 6.1.

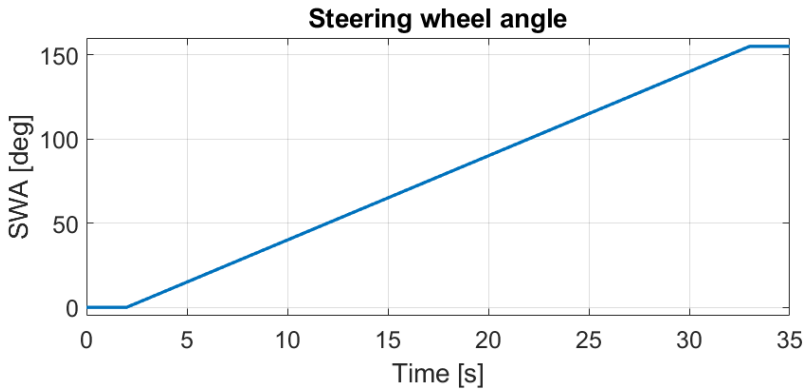

Figure 6.1: Example of steering wheel angle input for step steer.

A low steering rate is required for an adequate approximation of the vehicle steady-state behaviour. A steering wheel rate of $5\,deg/s$ is chosen.

6.4 Step steer

The step steer manoeuvre highlights the vehicle transient and steady-state response. In theory, a step signal goes from 0 to the steady-state value with infinite velocity. In practice, there are some hardware limitations; for instance, the steering robot used for field testing by Volvo Cars has a maximum steering rate of 500 deg/s. Field testing is not part of this thesis, but it is considered appropriate to include the hardware limitation when generating the steering signal for the MBS simulations. An example of steering wheel input signal is shown in Figure 6.2. The longitudinal velocity is kept constant until the step steer begins, then the throttle is released. The test is repeated at different longitudinal velocities and with different steering wheel angle steady-state values.

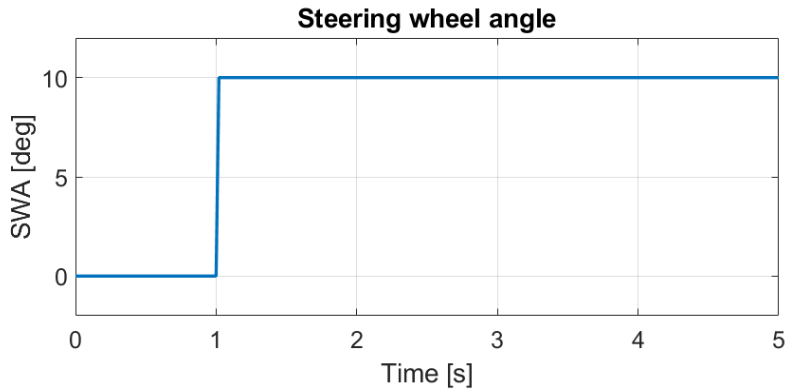

Figure 6.2: Example of steering wheel angle input for step steer.

6.5 Swept-Sine steering

The swept-sine steering manoeuvre tests the vehicle frequency response to sinusoidal steering inputs. It allows to reconstruct the transfer functions from the steering input to the vehicle states in the tested frequency range and to evaluate phase delays between states [16]. Figure 6.3 depicts an example of swept-sine steering signal.

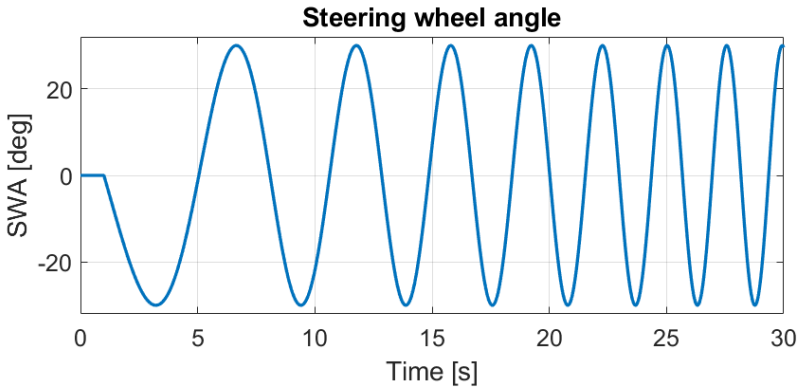

Figure 6.3: Example of steering wheel angle input for swept-sine steering.

The simulation is performed by keeping a constant longitudinal velocity and by linearly changing the steering angle frequency from $0.1\,Hz$ to $10\,Hz$ in $250\,s$. The sampling frequency is set to $30\,Hz$ allowing to correctly capture the maximum tested frequency of $10\,Hz$.

Various longitudinal velocities are tested. Since the system is non-linear, testing different steering amplitudes is necessary since the proportionality between input and output depends on the input value.

6.6 Sine with dwell

The sine with dwell test is used to determine the transient response behavior of the vehicle under conditions similar to lane change manoeuvres in real traffic.

A ramp steer manoeuvre at $80\,km/h$ needs to be performed before the sine with dwell. From the ramp steer test it is possible to calculate the steering wheel angle value at which the vehicle reaches $0.3\,g$ of lateral acceleration. This value is called A and it differs from FWS and AWS vehicles since the AWS vehicle is subjected to rear steering even at steady-state. These values are:

$$A_{FWS} = 22.0\,deg \qquad A_{AWS} = 24.8\,deg$$

The steering wheel input signal is a single sine of $0.7\,Hz$ with a dwell period of $0.50\,s$ at the second steering wheel angle peak. An example is reported in Figure 6.4.

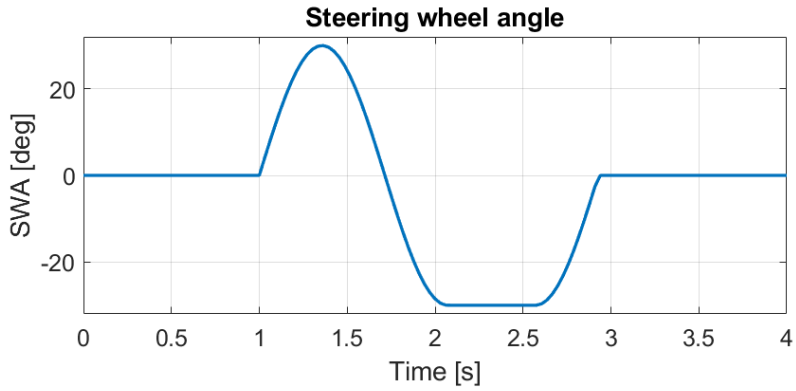

Figure 6.4: Example of steering wheel angle input for sine with dwell manoeuvre.

The longitudinal velocity is kept constant at $80\,km/h$ until the steering wheel input is applied; then, the throttle is released.

The sine with dwell test consists of multiple runs. On the first run, the steering wheel amplitude is set to $1.5 \cdot A_i$ and, if the run is successful, the amplitude for the next run is increased by an increment of $0.5 \cdot A_i$.

The success or failure of each run is determined by the vehicle state at three specific moments since the beginning of the steering signal:

- If the gain is 5.0 or greater, a lateral displacement check is made at $1.07\,s$ after the steering input beginning. For vehicles with mass up to $3500\,kg$, the lateral displacement of the vehicle center of mass must be $1.83\,m$ or greater relative

to the starting position of the test. If the displacement is less, the vehicle fails the test.

- A peak yaw rate is obtained for the test. The instantaneous yaw rate at $1.0\,s$ after the end of the steering signal must be 35 % of the peak value or less. If the instant yaw rate is higher than 35 % of the peak yaw rate, the vehicle fails the test.
- The instantaneous yaw rate at $1.75\,s$ after the end of the steering input must be 20 % of the peak value or less. If the instantaneous yaw rate is higher than 20 % of the peak yaw rate, the vehicle fails the test [17].

The performance is measured by how many runs the vehicle can succeed before failing. Yaw rate, sideslip angle lateral acceleration are evaluated to assess the vehicle stability.

6.7 Summary

In Table 6.1 the main parameters for each driving scenario are summarized.

Table 6.1: Driving scenarios parameters

Manoeuvre	Longitudinal velocity	Steering wheel	Used to assess
Step steer	$20 \div 200\,km/h$	$17 \div 170\,deg$	$stability, agility$
Constant steer	$5\,km/h$	$540\,deg$	$manoeuvrability$
Constant radius	$5\,km/h$	–	$manoeuvrability$
Ramp steer	$20 \div 200\,km/h$	$0 \div 170\,deg$	$understeer\,gradient$
Swept-sine steering	$10 \div 200\,km/h$	$17 \div 34\,deg$	$frequency\,response$
Sine with dwell	$80\,km/h$	$33 \div 308\,deg$	$stability$

Table 6.2: Metrics used to evaluate ARS.

Manoeuvre	**Manoeuvrability**	**Stability**	**Agility**
Step steer	–	yaw rate overshoot	yaw rate rise time & rise time difference between yaw rate and lat. acc.
Constant steer	turning radius	–	–
Constant radius	swept area	–	–
Ramp steer	–	–	understeer gradient
Swept-sine steer	–	–	steering to yaw rate delay & lat. acc. to yaw rate delay
Sine with dwell	–	yaw rate & sideslip angle	–

Chapter 7

Simulations results

This chapter presents all and only the relevant results extracted from the simulations, which are utilised to draw the conclusions of this thesis. The results are grouped to show a comparison between the control logics implemented and the FWS vehicle, in terms of manoeuvrability, stability and agility, which are the control objectives. In addition, the understeer gradient is evaluated. Finally, a subjective assessment of the different control strategies is carried out in the dynamic driving simulator of Volvo Cars.

For stability and agility the FWS vehicle is compared against three controlled vehicles with: gain scheduling (GS), $v1$ and $v2$ controllers. One comment needs to be made about the gain scheduling controller: it is not used the one that mitigates the sideslip angle reported in section 5.2.1. Instead, it is decided to utilise a gain scheduling based on the steady-state values of the $X(u, s)$ transfer function from tuning method 1. Figure 7.1 depicts the gain scheduling values utilised, highlighted in red.

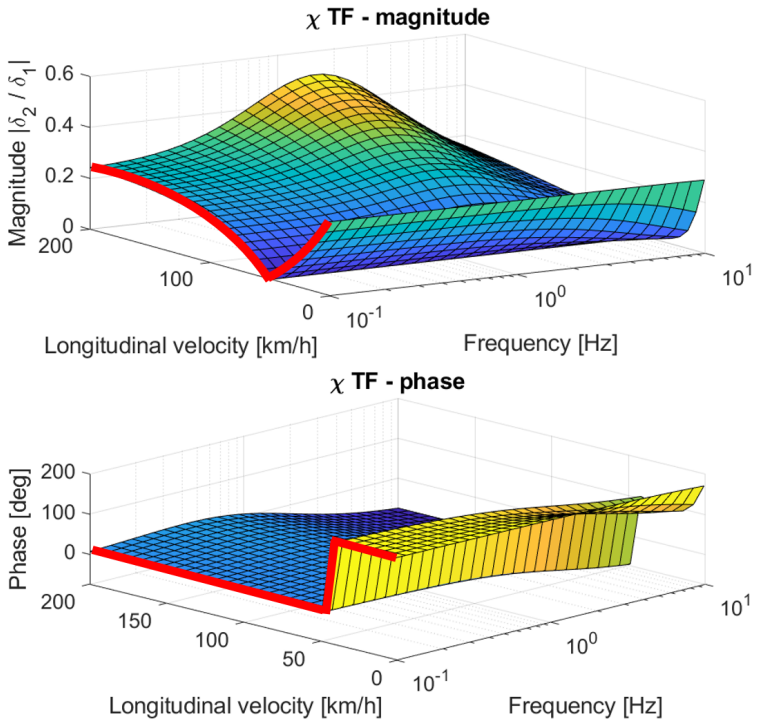

Figure 7.1: Gain scheduling values highlighted in red

7.1 Manoeuvrability

For manoeuvrability, the minimum turning radius, the steering effort and the swept area are assessed. The manoeuvres are performed in steady-state conditions, which means that there is no difference in choosing among the gain scheduling, $v1$ and $v2$ controllers.

7.1.1 Minimum turning radius

The minimum turning radius is a clear indicator of the vehicle low speed manoeuvrability: the lower the turning radius the higher the manoeuvrability.

To evaluate the minimum turning radius, a constant steer manoeuvre is simulated at low velocity. The steering wheel angle is set to its maximum value of 540 deg and the longitudinal velocity is kept constant at 5 km/h. The turning radius is measured at the vehicle center of mass. Figure 7.2 shows the result of the simulation.

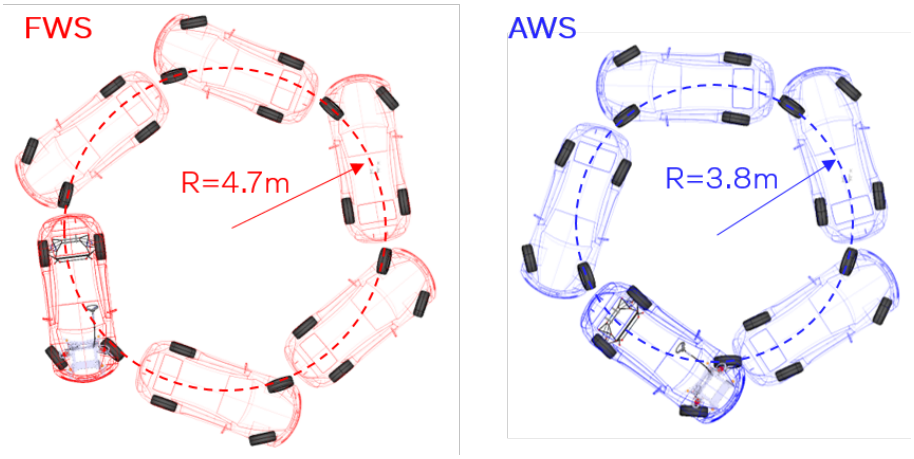

Figure 7.2: Turning radius comparison between FWS (red) and AWS (blue) vehicles. Constant steering wheel angle of 540 deg at 5 km/h.

As shown in the above picture, with the AWS vehicle it is possible to reduce the turning radius from 4.7 m to 3.8 m, meaning a reduction of almost 20 %. This result depends on the maximum steering angle allowed by the rear wheels; in this case, the rear steer angle is 9 deg.

7.1.2 Steering effort

In this thesis, the steering effort is associated with the steering angle request and not with the torque. The steering effort is a relative quantity, meaning that it is possible to define it when comparing different vehicles. A lower steering effort means that the driver is able to negotiate a corner applying a smaller steering wheel angle; vice versa for a higher steering effort. Figure 7.3 shows the relative steering effort of an AWS vehicle with respect to a FWS vehicle.

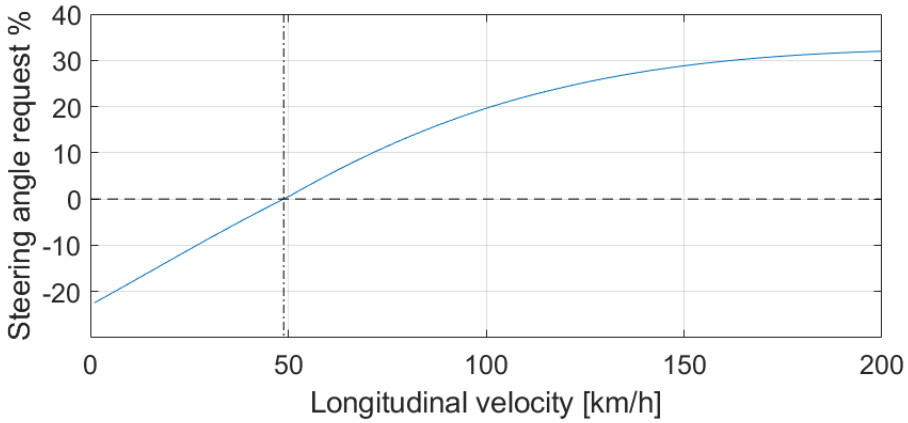

Figure 7.3: AWS vehicle steering angle request relative to a FWS vehicle.

The relative steering effort is calculated as follows:

$$\delta_{net_{FWS}} = \delta_{net_{AWS}}$$

$$\delta_{1_{FWS}} - \delta_{2_{FWS}} = \delta_{1_{AWS}} - \delta_{2_{AWS}} \qquad \delta_{2_{FWS}} = 0,\ \delta_{2_{AWS}} = \chi\delta_{1_{AWS}}$$

$$\delta_{1_{FWS}} = \delta_{1_{AWS}}(1-\chi)$$

$$\delta_{1_{AWS}} = \frac{\delta_{1_{FWS}}}{(1-\chi)}$$

$$Steering\,angle\,request = \frac{\delta_{1_{AWS}} - \delta_{1_{FWS}}}{\delta_{1_{FWS}}} \tag{7.1}$$

Where $\delta_{net_i} = \delta_{1_i} - \delta_{2_i}$ is the net steer angle.

For velocities below $\sim 50\,km/h$, steering the rear wheels in the opposite direction of the front wheels reduces the steering effort; this result is complementary to the reduction of the turning radius.

For longitudinal velocities above $\sim 50\,km/h$, the steering effort is increased since the rear wheels steer in the same direction of the front wheels, reducing the net steer angle.

7.1.3 Swept area

The swept area is the area required by a vehicle when driving along a path. A vehicle that requires less area can be manoeuvred in tighter environments, meaning better manoeuvrability.

To evaluate the swept area, a constant radius manoeuvre is simulated at low velocity. The manoeuvre is of closed-loop type, thus, the standard Simpack driver model is used. The turning radius is $6\,m$ and the longitudinal velocity is kept constant at $5\,km/h$. Figure 7.4 shows the result of the simulation.

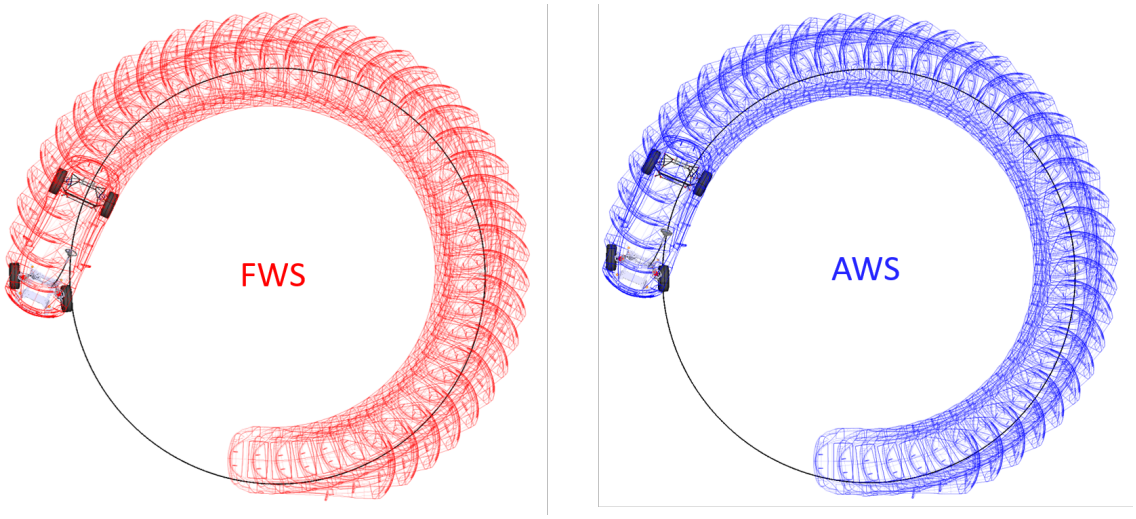

Figure 7.4: Swept area comparison between FWS and AWS vehicles when driving along a circular path with radius of 6 m.

From the above picture, it is possible to visualize how the AWS vehicle, compared to the FWS vehicle, requires less area when driving along the same path at the same longitudinal velocity. The reduction in swept area is justified by the lower sideslip angle of the AWS vehicle. Figure 7.5 shows the sideslip angle comparison between the AWS and FWS vehicles during the manoeuvre. At low velocity, minimising the sideslip angle would minimise the swept area.

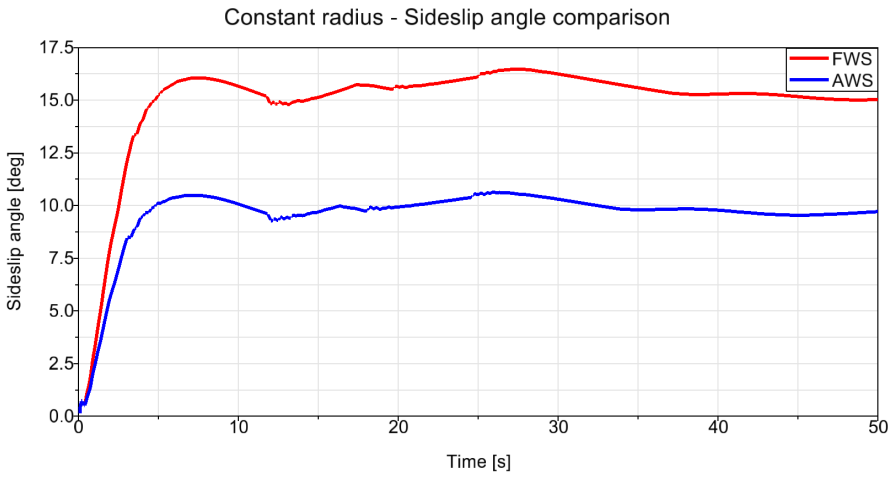

Figure 7.5: Sideslip angle comparison between FWS and AWS vehicles when driving along a circular path with radius of 6 m.

7.2 Understeer gradient

Depending on the chosen definition of the understeer gradient, it is possible to conclude that the vehicles with active rear steer have more, or the same, understeer as the FWS vehicle. On the one hand, according to Guiggiani [13], some popular and unclear definitions of understeer and oversteer are *"Understeer is what occurs when a car steers less than the amount commanded by the driver"* or *"Understeer is the tendency of an automobile to turn less sharply than the driver would expect"*. According to these popular definitions, the controlled vehicles would be classified as more understeering at high velocity, since the steering angle request is higher.

On the other hand, understeer/oversteer can be seen as a property of the vehicle, independently from the steering angle request: a vehicle is defined as understeered if the front axle is the first one to loose traction during a corner. According to this definition and taking into account the net steer angle $\delta_{net} = \delta_1 - \delta_2$ (instead of only the front steer angle) to calculate the understeer gradient, the AWS vehicle would exhibit the exact same understeer gradient as the FWS vehicle, as shown in Figure 7.6. Indeed, it would sound wrong to state that the vehicle is less understeered at low velocity just because the steering angle request is lower, as the first definition would suggest.

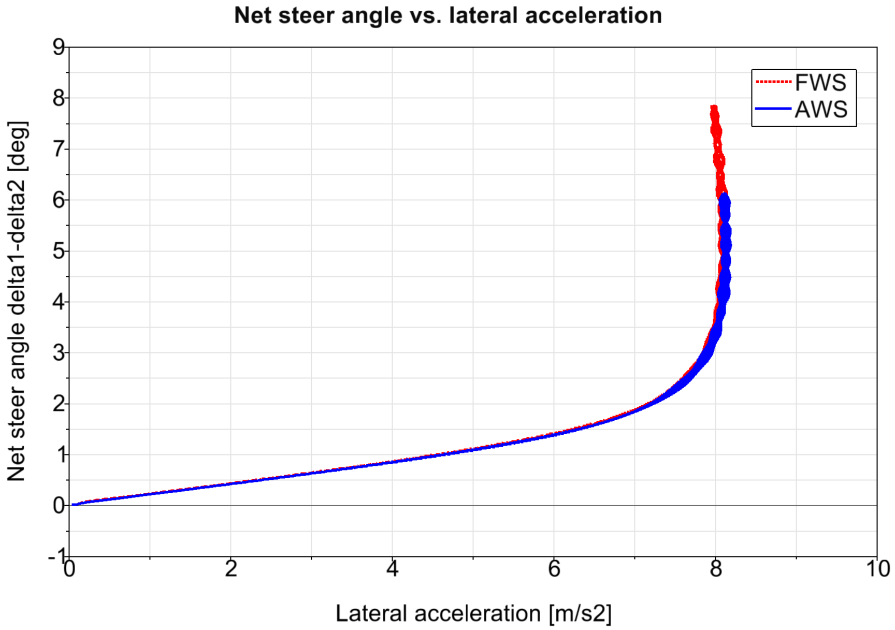

Figure 7.6: Comparison of the understeer gradient for a FWS and an AWS vehicle, considering the net steer angle.

7.3 Stability

Stability is assessed through transient manoeuvres, such as step steer and sine with dwell. The step steer is utilised to calculate the yaw rate overshoot; the sine with dwell, which is a manoeuvre close to real-life driving scenarios, is utilised to check what improvements the controlled vehicles achieve, in terms of yaw rate, sideslip angle and lateral acceleration.

7.3.1 Step steer: yaw rate overshoot

Figure 7.7 shows a comparison between FWS and AWS vehicles in terms of front and rear steer angles, sideslip angle, yaw rate and lateral acceleration, for a step steer manoeuvre at $100\,km/h$. Appendix section A.2 reports also the results for step steer manoeuvres at, respectively, $40\,km/h$, $70\,km/h$ and $130\,km/h$.

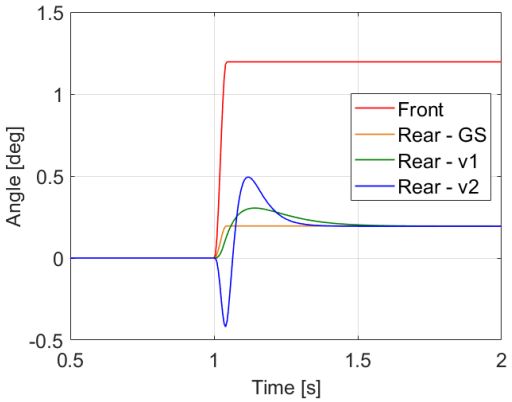

(a) Steer angles

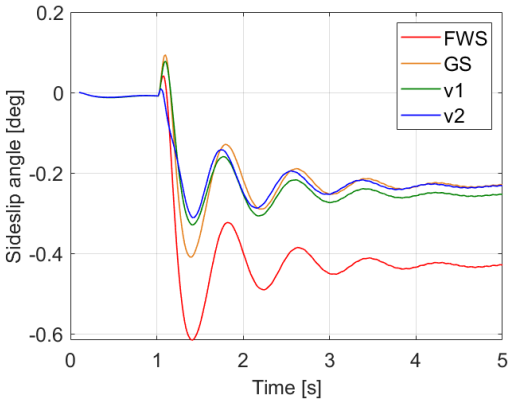

(b) Sideslip angle

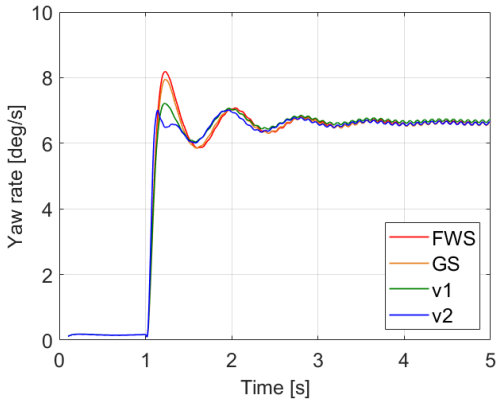

(c) Yaw rate

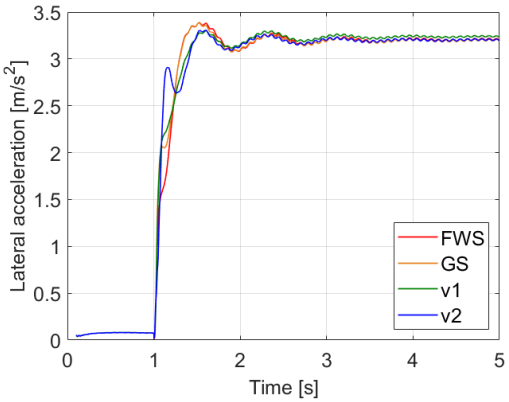

(d) Lateral acceleration

Figure 7.7: Step steer at $100\,km/h$. Comparison of the front and rear steer angles (a), sideslip angles (b), yaw rate (c) and lateral acceleration (d) between FWS, gain scheduling, v1 and v2 vehicles.

For the FWS vehicle, the manoeuvre is performed with $1\,deg$ of front steer angle. For the AWS vehicle, which is controlled by the gain scheduling (GS), $v1$ and $v2$ controllers, the front steer angle needs to be adjusted in order to reach the same yaw rate steady-state value. This is done setting the net steer angle of the AWS vehicle equal to the net steer angle of the FWS vehicle, according to equation 7.1 and using the steady-state values of $X(u, s)$, i.e. the gain scheduling.

From Figure 7.7a it is possible to appreciate the difference between $v1$ and $v2$ in controlling the rear steer angle. Figure 7.7b shows that the sideslip angle is reduced with all types of controllers. Figure 7.7c shows that the FWS vehicle has the highest yaw rate overshoot, the GS brings minor improvements, while $v1$ and $v2$ are able to drastically reduce the overshoot, which means increased stability.

Figure 7.8 gives a broader overview of how much the overshoot can be reduced. The yaw rate overshoot of the FWS and AWS vehicles is now compared by simulating the step steer manoeuvre every $10\,km/h$.

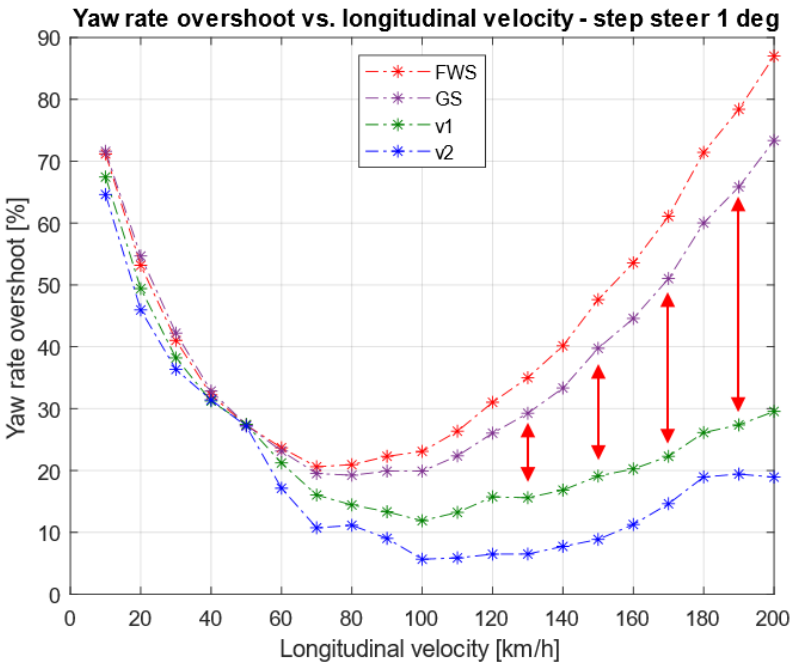

Figure 7.8: Yaw rate overshoot from a step steer of $1\,deg$ carried out every $10\,km/h$, for the FWS vehicle and the three AWS vehicles.

For velocities higher than $50\,km/h$ the FWS vehicle has the worst performance compared to the controlled vehicles: the vehicle controlled with gain scheduling brings minor improvements, while the vehicle controlled with $v1$ and $v2$ are performing better.

Comparing the difference of performance between the GS and the $v1$ and $v2$ controllers, which is highlighted by the red vertical arrows, it is possible to appreciate the benefits brought by controllers working in the frequency domain.

7.3.2 Sine with dwell

This section compares the yaw rate, the sideslip angle and the lateral acceleration between the FWS vehicle and the three controlled AWS vehicles. The manoeuvre is shown for different steering wheel angle amplitudes A (see 6.6). The black dashed line represent the pattern of the steering wheel angle, but not the absolute value.

Yaw rate

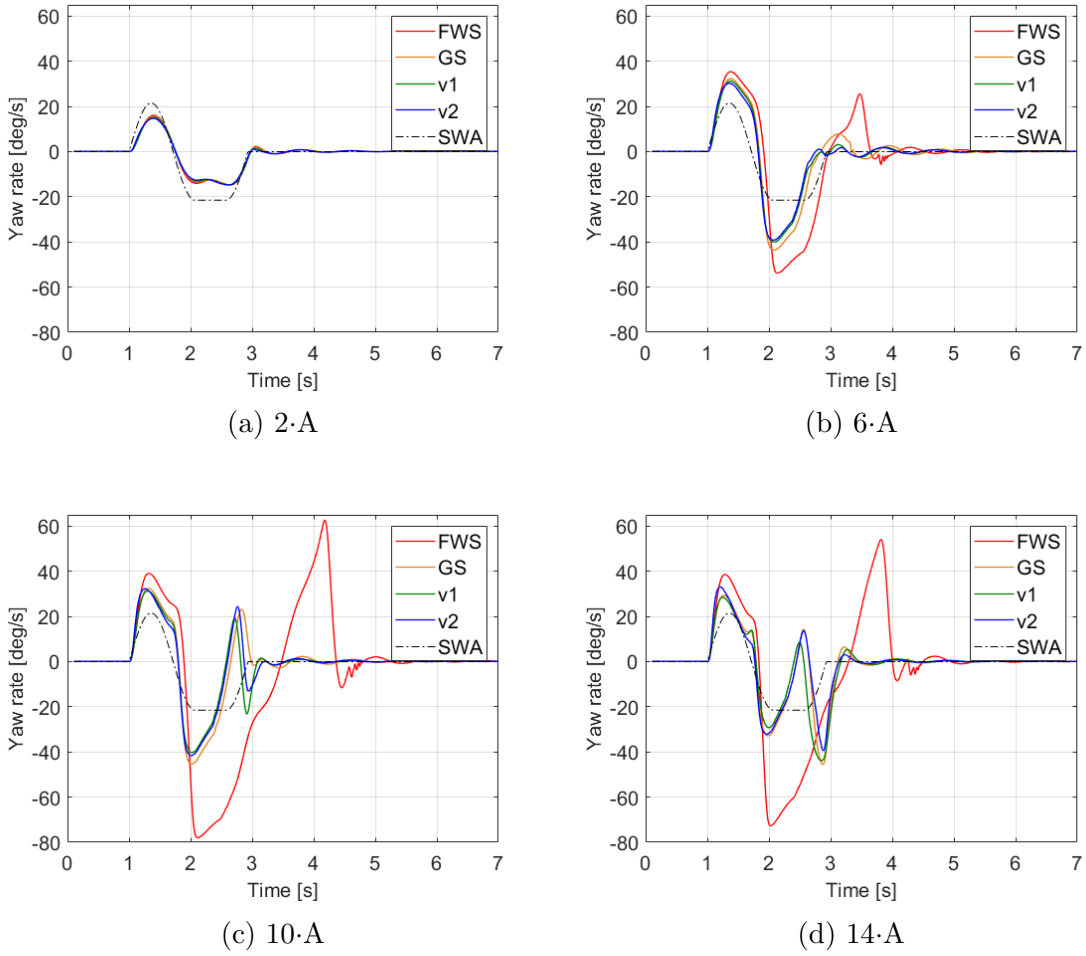

(a) 2·A (b) 6·A

(c) 10·A (d) 14·A

Figure 7.9: Comparison of the yaw rate between the four types of vehicles (FWS, GS, $v1$, $v2$) for a sine with dwell manoeuvre carried out at $2A$, $6A$, $10A$ and $14A$, where A is the amplitude of the steering wheel angle.

Figure 7.9a shows very few differences between the passive and the active vehicles. In Figure 7.9b the FWS vehicle exhibits some overshoot after the steering wheel angle goes back to zero, at around $3\,s$, but the vehicle is still able to meet the requirements of the manoeuvre. Figures 7.9c and 7.9d show a clear difference between the passive and the active vehicles. The high peaks at around $4\,s$ are the reason why the FWS vehicle fails to pass the manoeuvre at $8 \cdot A$, while the controlled vehicles are able to meet the requirements up to $14 \cdot A$, which is the maximum steering wheel angle amplitude prescribed by the manoeuvre ($300\,deg$). Overall, the reduction of the peaks values is due to the increased damping of the controlled vehicles and the

result is increased stability. It is interesting to notice that, opposed to the yaw rate overshoot results, in this case working in the frequency domain does not bring any major improvement since the GS control is as effective as $v1$ and $v2$.

Sideslip angle

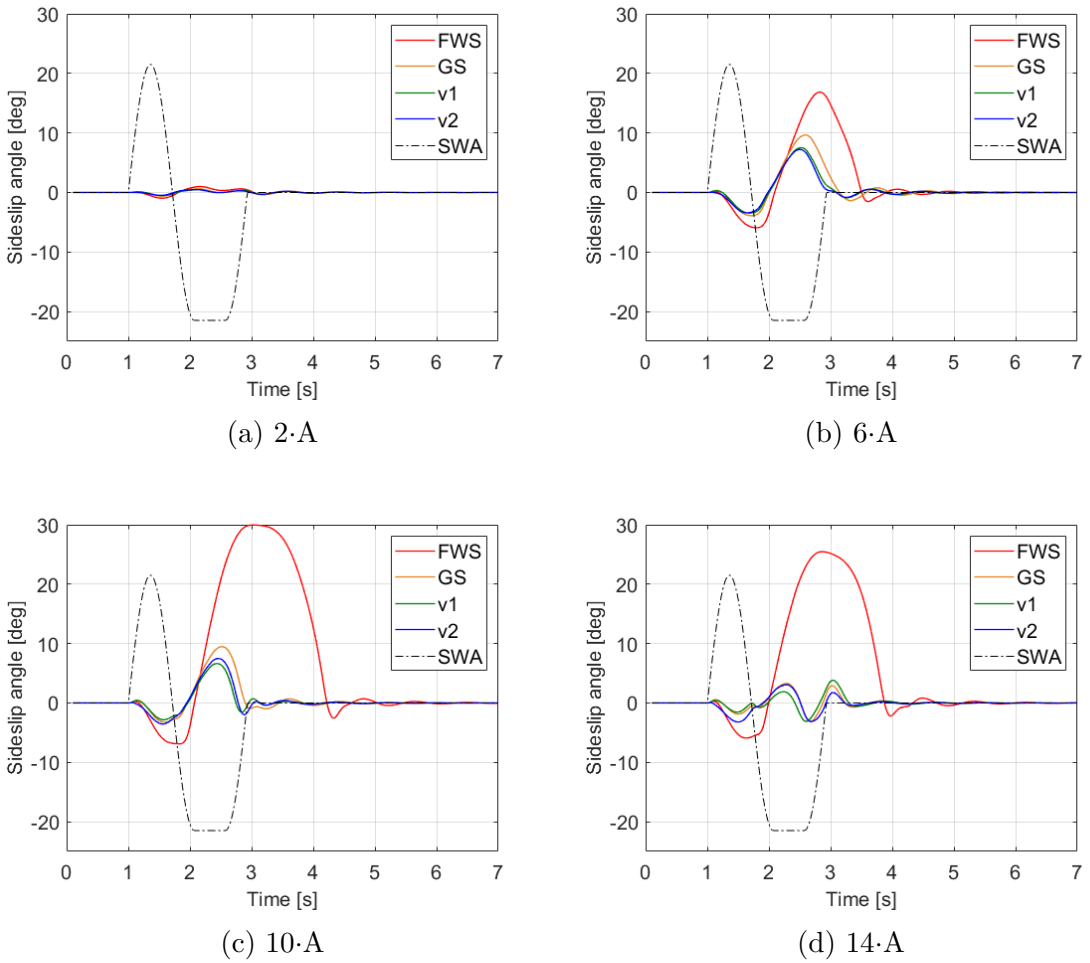

(a) 2·A (b) 6·A

(c) 10·A (d) 14·A

Figure 7.10: Comparison of the sideslip angle between the four types of vehicles (FWS, GS, $v1$, $v2$) for a sine with dwell manoeuvre carried out at $2A$, $6A$, $10A$ and $14A$, where A is the amplitude of the steering wheel angle.

As stated in Chapter 5.1, vehicles behave better if the sideslip angle is kept small. Figures 7.10b, 7.10c and 7.10d clearly show that the sideslip angle of the AWS vehicles spans in a narrower range compared to the passive vehicle. A smaller sideslip angle implies that it is easier for the driver to control and correct the trajectory of the vehicle. Similarly to the yaw rate, the performance of the GS controller is comparable to the performance of $v1$ and $v2$.

Lateral acceleration

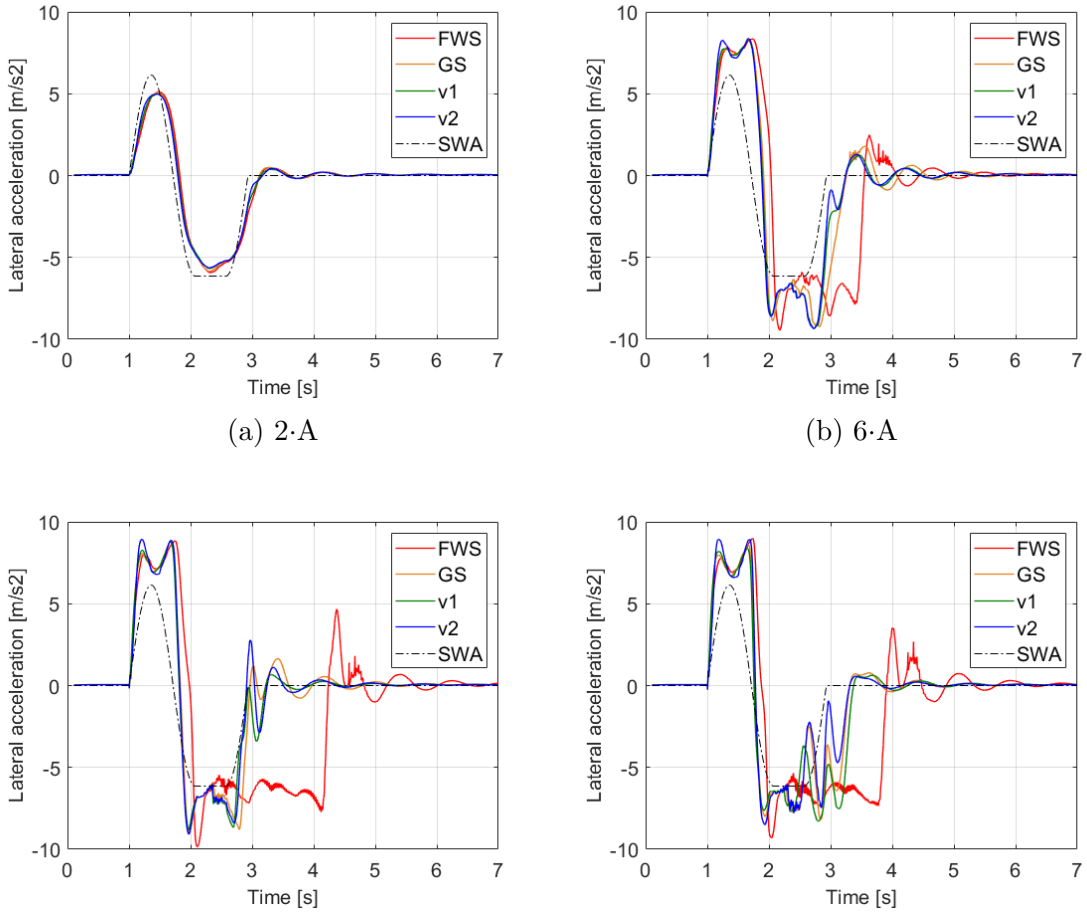

(a) 2·A (b) 6·A

(c) 10·A (d) 14·A

Figure 7.11: Comparison of the lateral acceleration between the four types of vehicles (FWS, GS, $v1$, $v2$) for a sine with dwell manoeuvre carried out at $2A$, $6A$, $10A$ and $14A$, where A is the amplitude of the steering wheel angle.

Looking at Figures 7.11b, 7.11c and 7.11d it is possible to say that:

- all the controlled vehicles are faster to reach the first negative peak, at $\sim 2\,s$, meaning that the delay between steering input and lateral acceleration is reduced;
- after $\sim 3\,s$, when the steering wheel angle goes to zero, the overshoot and the settling time are lower.

The first point indicates improved agility for the vehicles equipped with ARS, while the second point indicates improved stability.

7.4 Agility

Agility is assessed through step steer and swept-sine steer manoeuvres. The results are divided into "transient" and "frequency response" groups. In the first group, the yaw rate rise time and the rise time difference between lateral acceleration and yaw rate are assessed; In the second group, the phase delay from steering input to yaw rate and the phase delay from yaw rate to lateral acceleration are evaluated.

7.4.1 Transient

The transient behaviour of the vehicle is assessed through step steer manoeuvres performed every $10\,km/h$ with a steering amplitude of $1\,deg$ for the FWS vehicle and adjusting the value for the controlled vehicles as described in section 7.3.1.

Yaw rate rise time

The delay between yaw rate and steering input is measured with yaw rate rise time. A low yaw rate rise time means higher reactivity.

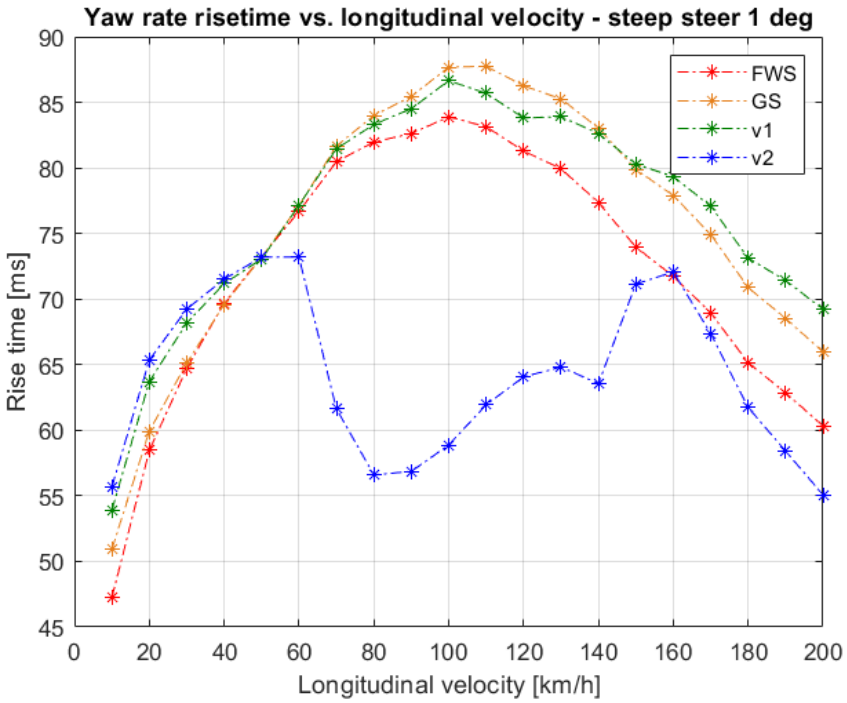

Figure 7.12: Yaw rate rise time for a step steer of $1\,deg$ carried out every $10\,km/h$, for the FWS vehicle and the three AWS vehicles.

According to Figure 7.12, $v2$ is the only controller that is able to reduce the yaw rate rise time, this is due to its tuning objectives. Nevertheless, the increase of rise time for the GS and $v1$ controllers is in the order of 5 to $10\,ms$, which would probably be barely noticeable by the driver.

Rise time difference between lateral acceleration and yaw rate

The delay between lateral acceleration and yaw rate is measured through the difference between lateral acceleration and yaw rate rise time.

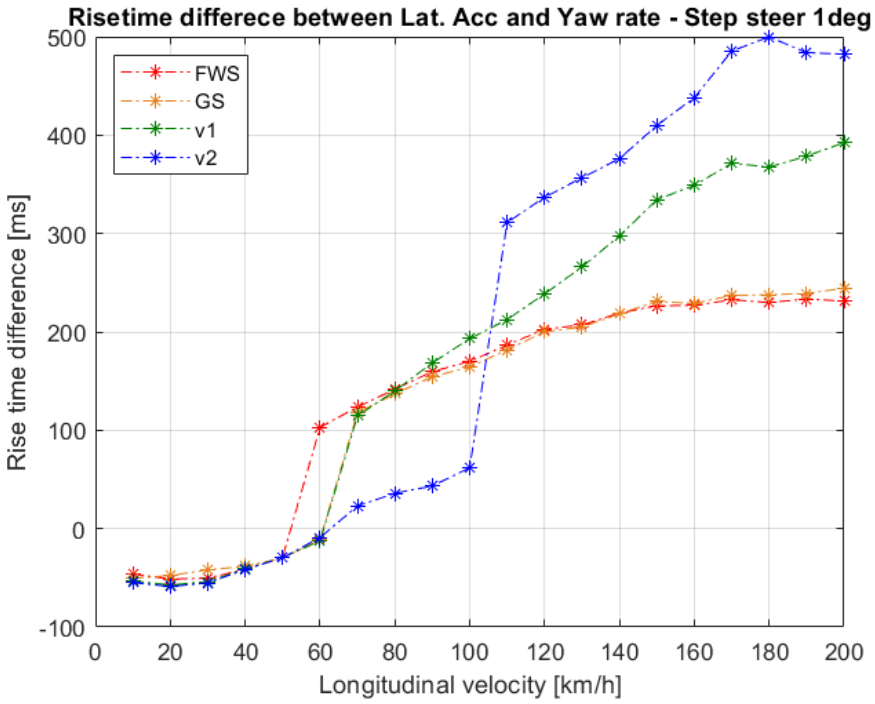

Figure 7.13: Difference between lateral acceleration and yaw rate rise time for a step steer of $1\,deg$ carried out every $10\,km/h$, for the FWS vehicle and the three AWS controlled vehicles.

According to Figure 7.13, at high velocity the controllers $v1$ and $v2$ are performing worse than the FWS vehicle. Actually, this result depends on how the rise time is computed; in this case, it is defined as the time-span required by the signal to go from 10 % to 90 % of its steady-state value. Indeed, the reason for this behaviour can be understood by looking at Figure 7.7 (other examples can be seen in Appendix section A.2) where it is possible to see how, by reducing the yaw rate overshoot, a "step" is created in the lateral acceleration response causing the increased difference in rise time shown in Figure 7.13. The reason is that the controllers $v1$ and $v2$ prevent the yaw rate to reach high values (i. e. reduced overshoot) while the sideslip angle keeps reducing its value ($\dot{\beta} < 0$). With the assumption of planar motion (Appendix section A.3 shows the validity of this assumption), the effect of yaw rate and sideslip angle on lateral acceleration is explained by equation 2.13 (reported here for convenience):

$$a_y = \left(r + \dot{\beta}\right) u$$

From the above equation, it is possible to understand that, if the yaw rate stops from increasing and the sideslip angle keeps decreasing, the value of lateral acceleration does not increase but creates a "step" in its response. In Figure 7.14 it is possible to visualize how the "step" of the lateral acceleration and the definition of rise time are responsible for the increased rise time difference.

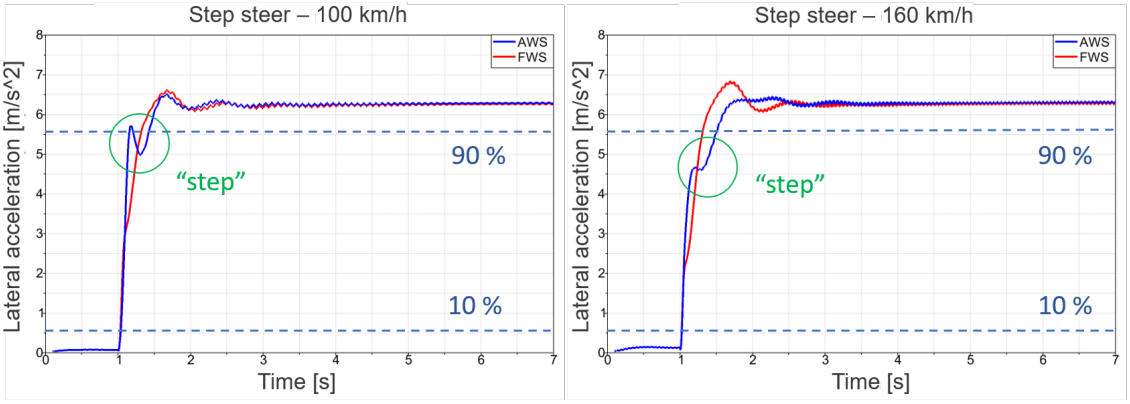

Figure 7.14: "Step" in the lateral acceleration responsible for the increase of the difference between lateral acceleration and yaw rate rise time at high velocity for controller $v2$.

When the "step" happens before the signal reaches 90 % of its steady-state value, the result is a higher rise time.

7.4.2 Frequency response

The frequency response of the vehicle is assessed with swept-sine manoeuvres performed every $20\,km/h$. The MBS model Frequency Response Functions (FRFs) from the steering input to the vehicle states are computed as the ratio between the spectra of the required signals. The spectra are computed using the Fast Fourier Transform (FFT) algorithm available in MATLAB.

Appendix A.4 shows all the transfer functions obtained from the MBS model, from front steer angle to yaw rate, sideslip angle and lateral acceleration, for the passive and all active vehicles.

The delay between yaw rate and steering input is evaluated looking at the phase of its frequency response function. The same for the delay between lateral acceleration and yaw rate.

Steering angle to yaw rate FRF phase

By looking at the surfaces in Figure 7.15, it is possible to notice how controller $v1$ (Figure 7.15c) and $v2$ (Figure 7.15d) provide a higher phase than the FWS and the GS vehicles (Figures 7.15a and 7.15b), especially at high velocity.

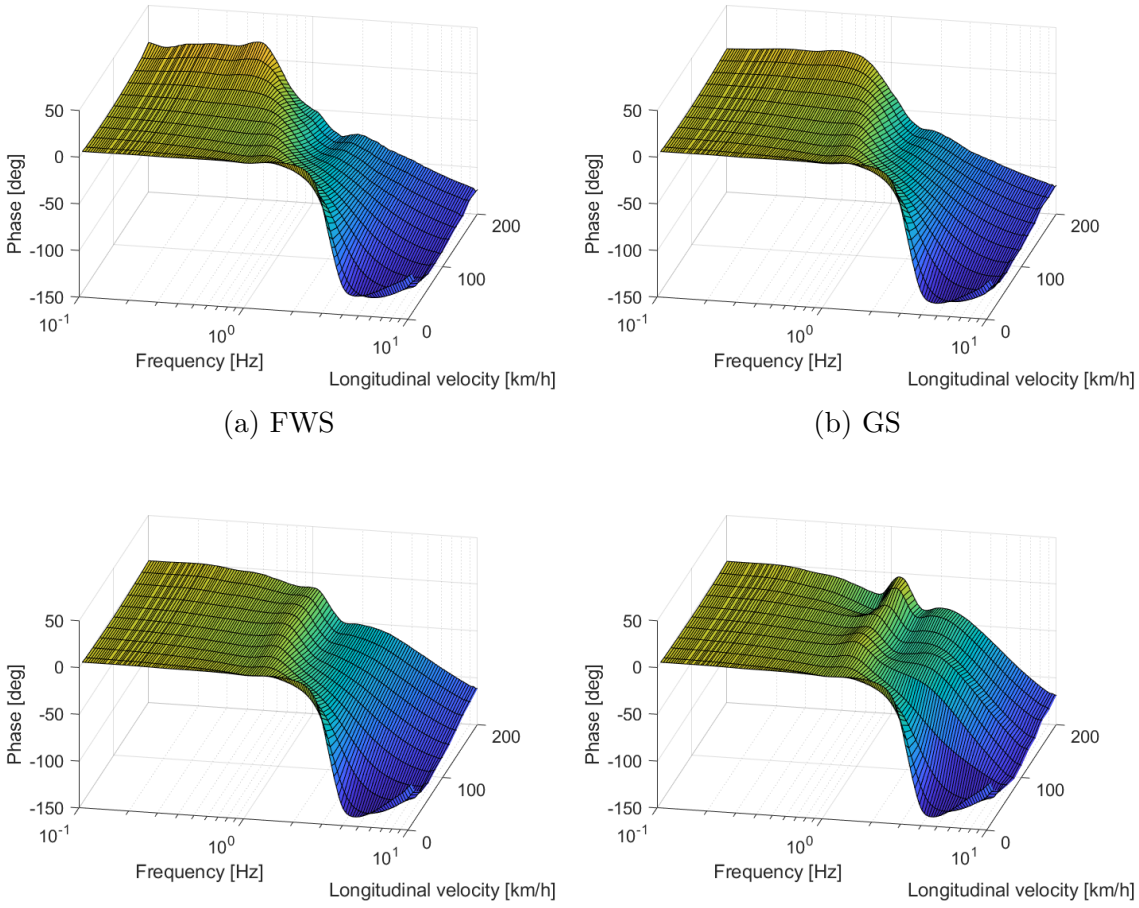

(a) FWS (b) GS

(c) v1 (d) v2

Figure 7.15: Comparison of the 3D phase of the FRF from front steer angle to yaw rate, for a FWS vehicle (a) and the three AWS vehicles controlled with a gain scheduling (b), v1 (c) and v2 (d) methods.

Looking at the 2D phase in Figure 7.16, for velocities above $80\,km/h$ and for frequencies around and above $1\,Hz$ the controllers $v1$ and $v2$ show a higher phase, meaning reduced delay between steering input and yaw rate, i.e. increased agility.

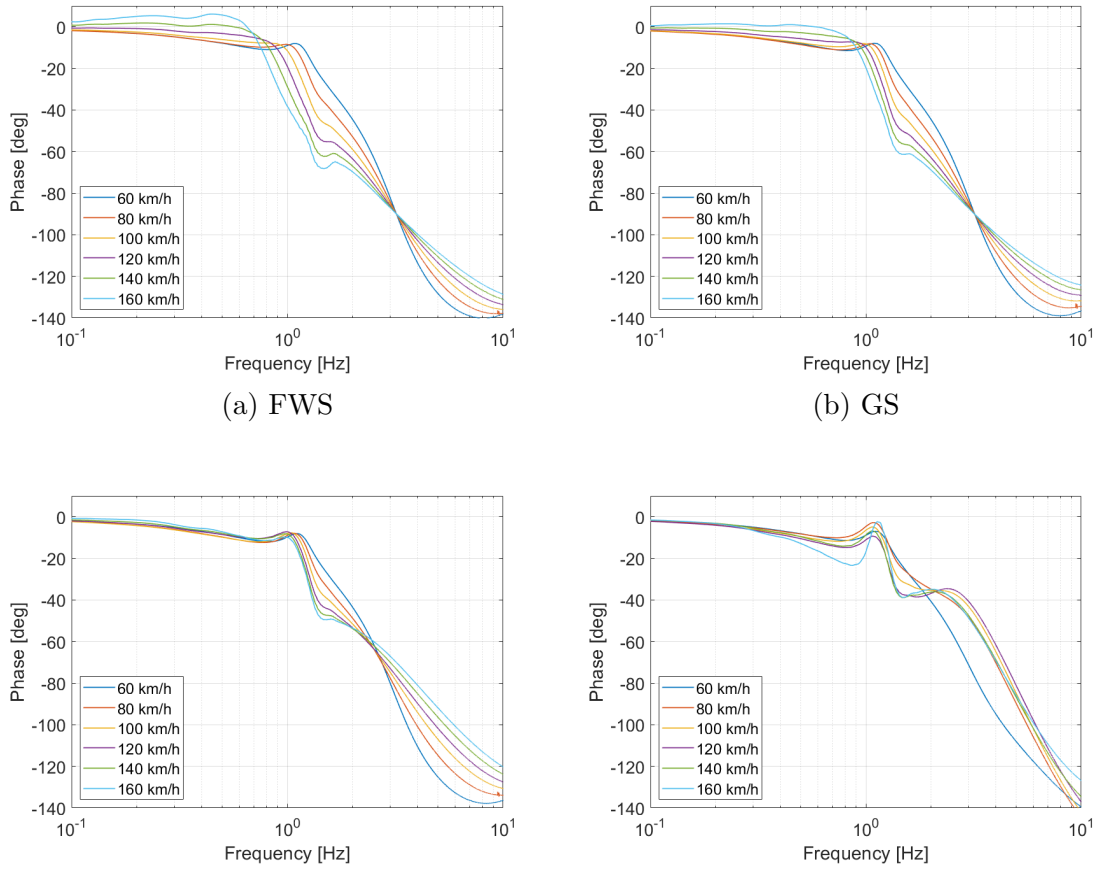

(a) FWS (b) GS

(c) v1 (d) v2

Figure 7.16: Comparison of the 2D phase of the FRF from front steer angle to yaw rate, for a FWS vehicle (a) and the three AWS vehicles controlled with a gain scheduling (b), v1 (c) and v2 (d) methods.

In particular, for a steering input of $1\,Hz$, the controllers $v1$ and $v2$ reduce the phase delay by up to 75%. With the gain scheduling the phase delay is reduced by up to 50%.

Figure 7.17 shows the phase difference between the AWS and the FWS vehicles. A positive phase difference means that the AWS vehicle exhibits less delay between steering input and yaw rate. The phase of the FWS vehicle is reported in Figure 7.17a for convenience.

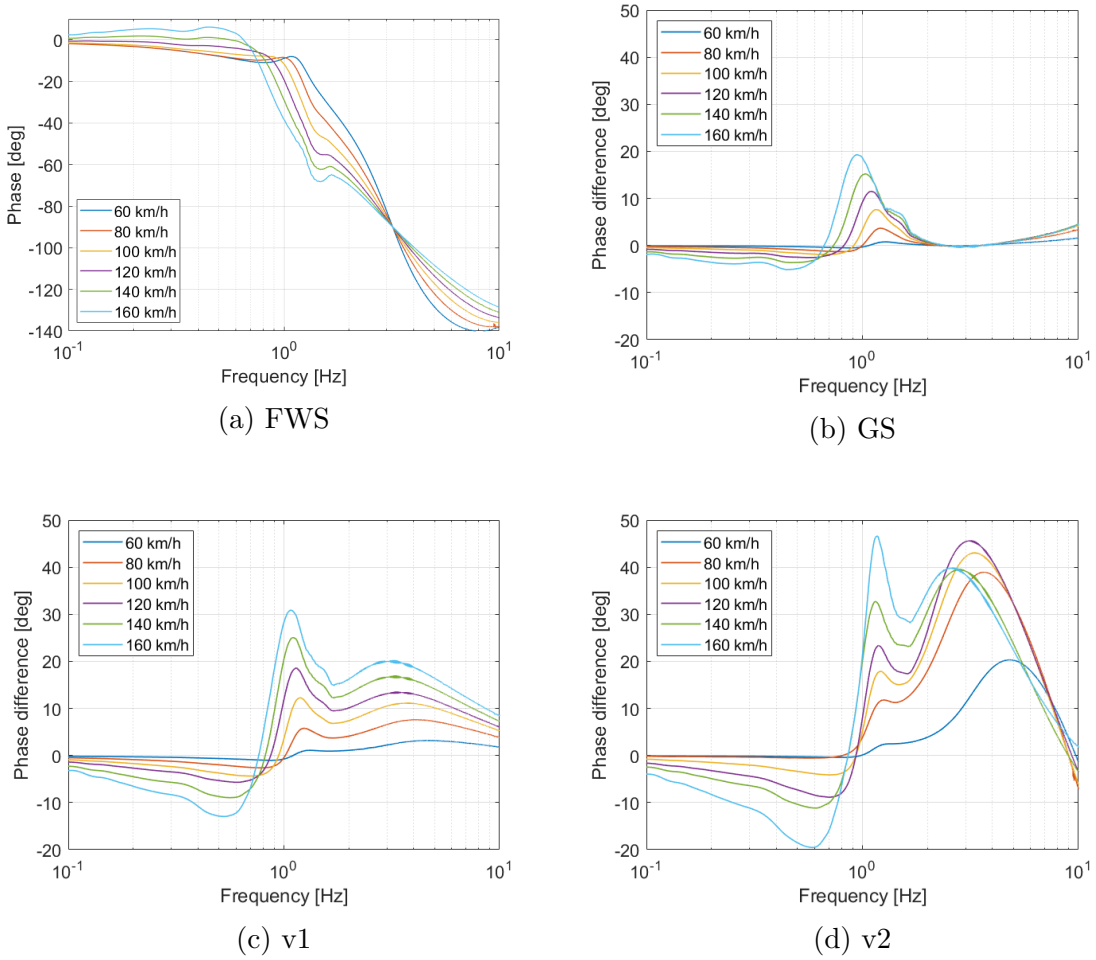

(a) FWS

(b) GS

(c) v1

(d) v2

Figure 7.17: Comparison of the phase differences between the FWS vehicle (a) and the AWS vehicles (controlled with a GS (b), v1 (c), v2 (d)) for the FRF from front steer angle to yaw rate.

Figure 7.17 shows how for frequencies above $1\,Hz$, the AWS vehicles controlled with $v1$ and $v2$ have a large positive phase difference, meaning that that for high frequency steering input the AWS vehicle reacts faster to the driver demand.

Yaw rate to lateral acceleration FRF phase

By looking at the surfaces in Figure 7.18, it is possible to notice how controller $v1$ (Figure 7.18c) and $v2$ (Figure 7.18d) provide a higher phase than the FWS and the GS vehicles (Figures 7.18a and 7.18b), especially at high velocity.

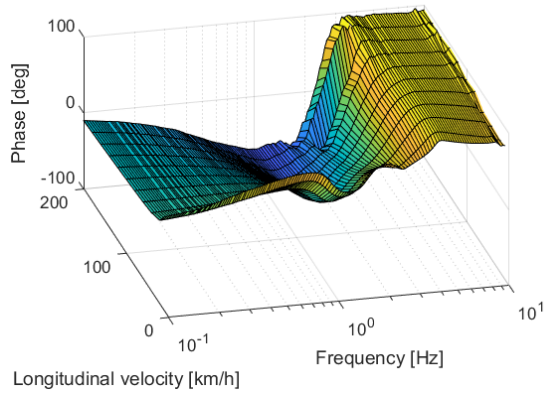

(a) FWS

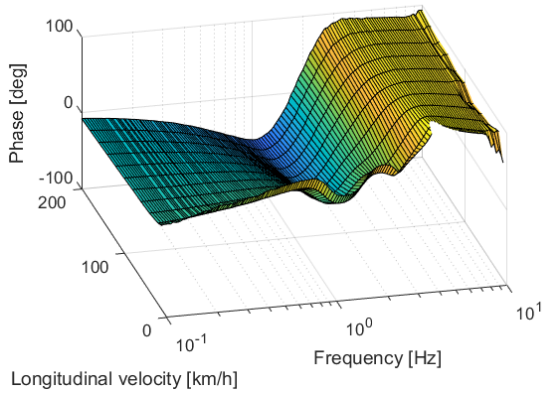

(b) GS

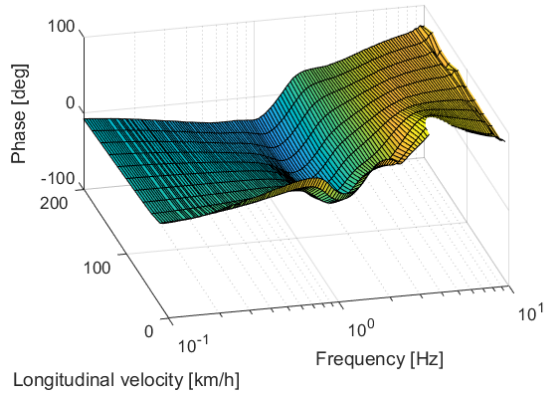

(c) v1

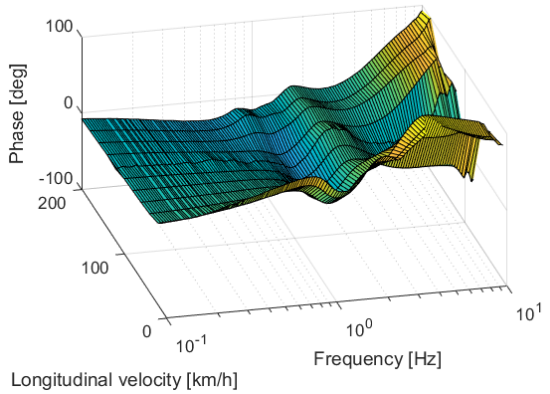

(d) v2

Figure 7.18: Comparison of the 3D phase of the FRF from yaw rate to lateral acceleration, for a FWS vehicle (a) and the three AWS vehicles controlled with a gain scheduling (b), v1 (c) and v2 (d) methods.

Looking at the 2D phase in Figure 7.19, for velocities above $80\,km/h$ and for frequencies around and slightly above $1\,Hz$ the controllers $v1$ and $v2$ show a higher phase, meaning reduced delay between yaw rate and lateral acceleration.

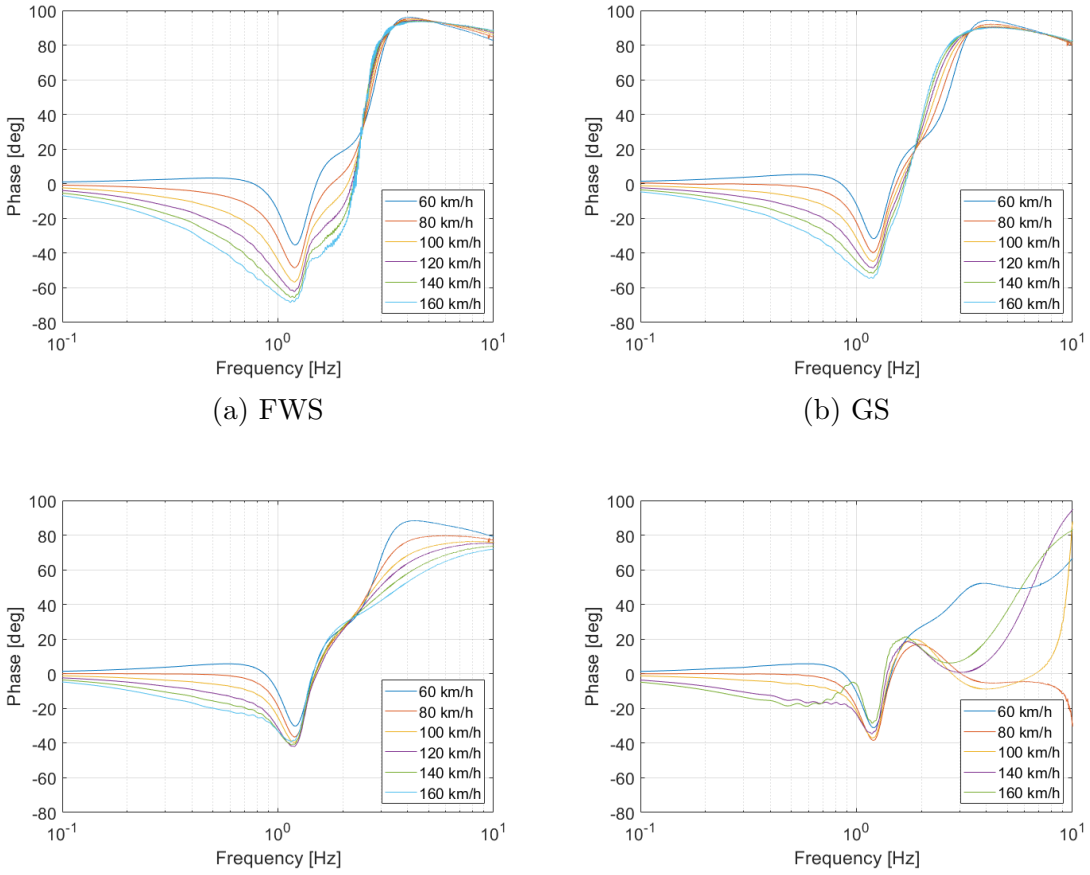

(a) FWS (b) GS

(c) v1 (d) v2

Figure 7.19: Comparison of the 2D phase of the FRF from yaw rate to the lateral acceleration, for a FWS vehicle (a) and the three AWS vehicles controlled with a gain scheduling (b), v1 (c) and v2 (d) methods.

In particular, for a steering input of $1\,Hz$, the controllers $v1$ and $v2$ reduce the phase delay by up to $46\,\%$. With the gain scheduling the phase delay is reduced up to $23\,\%$.

Figure 7.20 shows how for frequencies up to $2\,Hz$, the AWS vehicles controlled with $v1$ and $v2$ have a large positive phase difference, meaning that that for high frequency steering input the AWS vehicle exhibits less delay between lateral acceleration and yaw rate. The vehicle controlled with the gain scheduling reduces the delay mainly at the input frequency of $2\,Hz$.

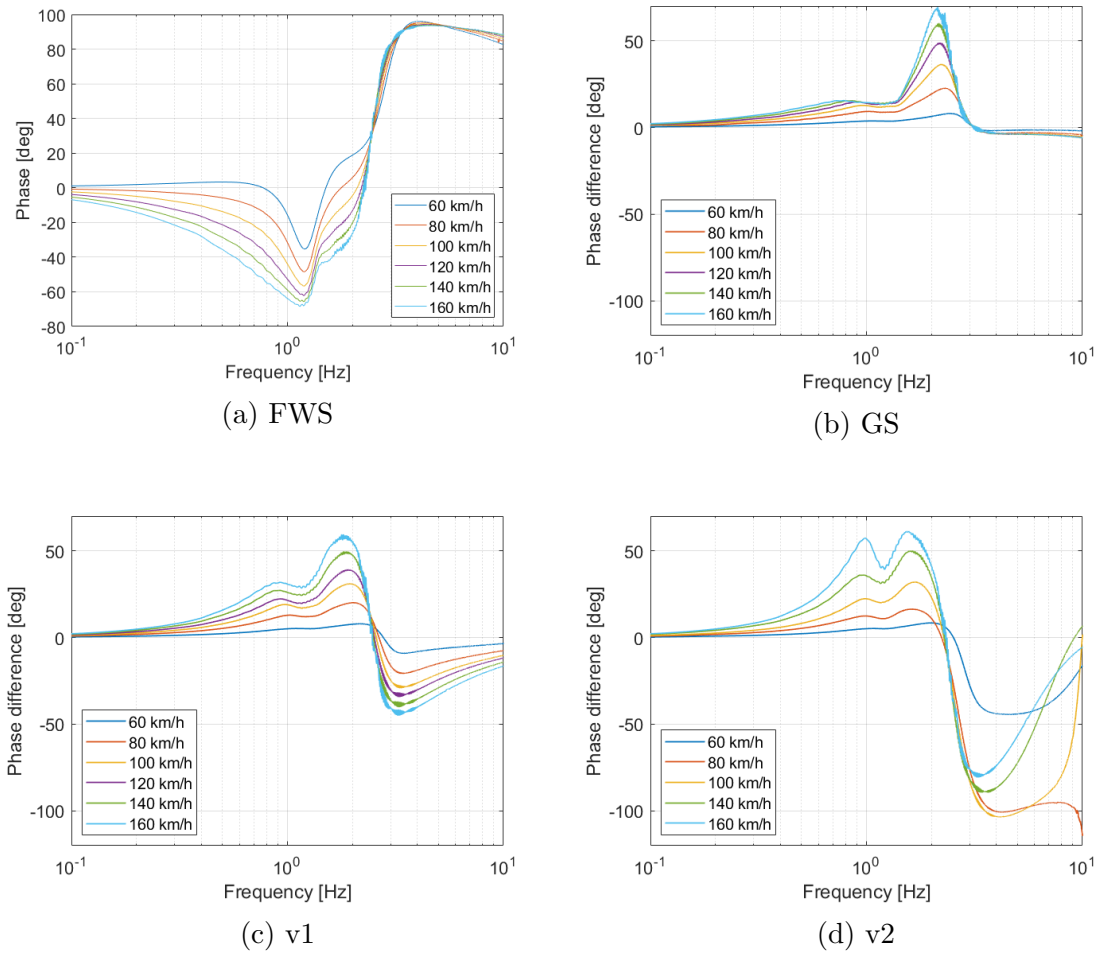

(a) FWS

(b) GS

(c) v1

(d) v2

Figure 7.20: Comparison of the phase differences between AWS vehicles (controlled with a gain scheduling (b), v1 (c), v2 (d) methods) and the phase of the FWS vehicle (a) for the FRF from yaw rate to lateral acceleration.

7.5 Subjective assessment with the Dynamic Driving Simulator

Figure 7.21: Dynamic driving simulator DiM 150 at Volvo Cars (Source: Volvo Cars database).

After discussing the simulations results, also a subjective assessment with the Volvo Cars' Dynamic Driving Simulator DiM150 (Figure 7.21) is carried out. Even though the simulator is one of the most advanced on the market, it embeds some limitations compared to a real driving scenario, especially in terms of yaw motion and maximum acceleration in the horizontal plane.

The goal of this subjective assessment is to check whether an average driver, like the authors, is able to individuate any improvement between a FWS vehicle and an AWS vehicle controlled with gain scheduling, method $v1$ and method $v2$. In order to avoid any bias, the assessment is blind, meaning that the drivers are not aware of what kind of vehicle or control logic they are driving.

The assessment focuses on stability, for velocities above $70\,km/h$. The simulations are carried out on the digital reconstruction of the handling track of the proving ground of Volvo Cars, and on an infinite straight highway to simulate emergency manoeuvres.

The result is that it is easy to individuate the FWS vehicle, since all the controlled vehicles exhibit a higher damping, less oscillations and a slightly higher steering angle request. When controlled, the vehicle feels much safer to drive.

An interesting consideration is done after the assessment. Figure 7.22 shows the yaw rate FRF of the MBS model for the FWS, $v1$ and $v2$ vehicles. First of all, it is possible to visualise the greater damping of the controlled vehicles, since the magnitude peak at around $1\,Hz$ is reduced. But focusing on the yaw rate magnitude of $v2$, the surface presents some unevenness, especially between 1 and $4\,Hz$. When this surface was obtained, its unevenness was source of doubts, wondering whether it would be negatively perceived by the driver. The answer is: probably yes; indeed,

despite the controller $v2$ shows a better performance according to the previous simulations results, the preferred controller resulted to be the $v1$, probably because of its smoother surface. One possible explanation is that since the steering wheel input has a certain frequency content, a smoother surface provides a more predictable response of the vehicle. Indeed, the predictability of the vehicle is increased by the phase too. Figure 7.16d clearly shows that up to frequencies of $1\,Hz$ the phase of $v1$ is constant with respect to velocity.

Furthermore, according to the authors, a slightly higher steering angle request or, equally, a slightly lower yaw rate gain (with respect to the steering wheel input) can be beneficial. When driving at high velocity the driver usually has to control the vehicle in a narrow range of steering wheel angles; a small increase of this range might make it easier for the driver to follow the desired trajectory or to correct it.

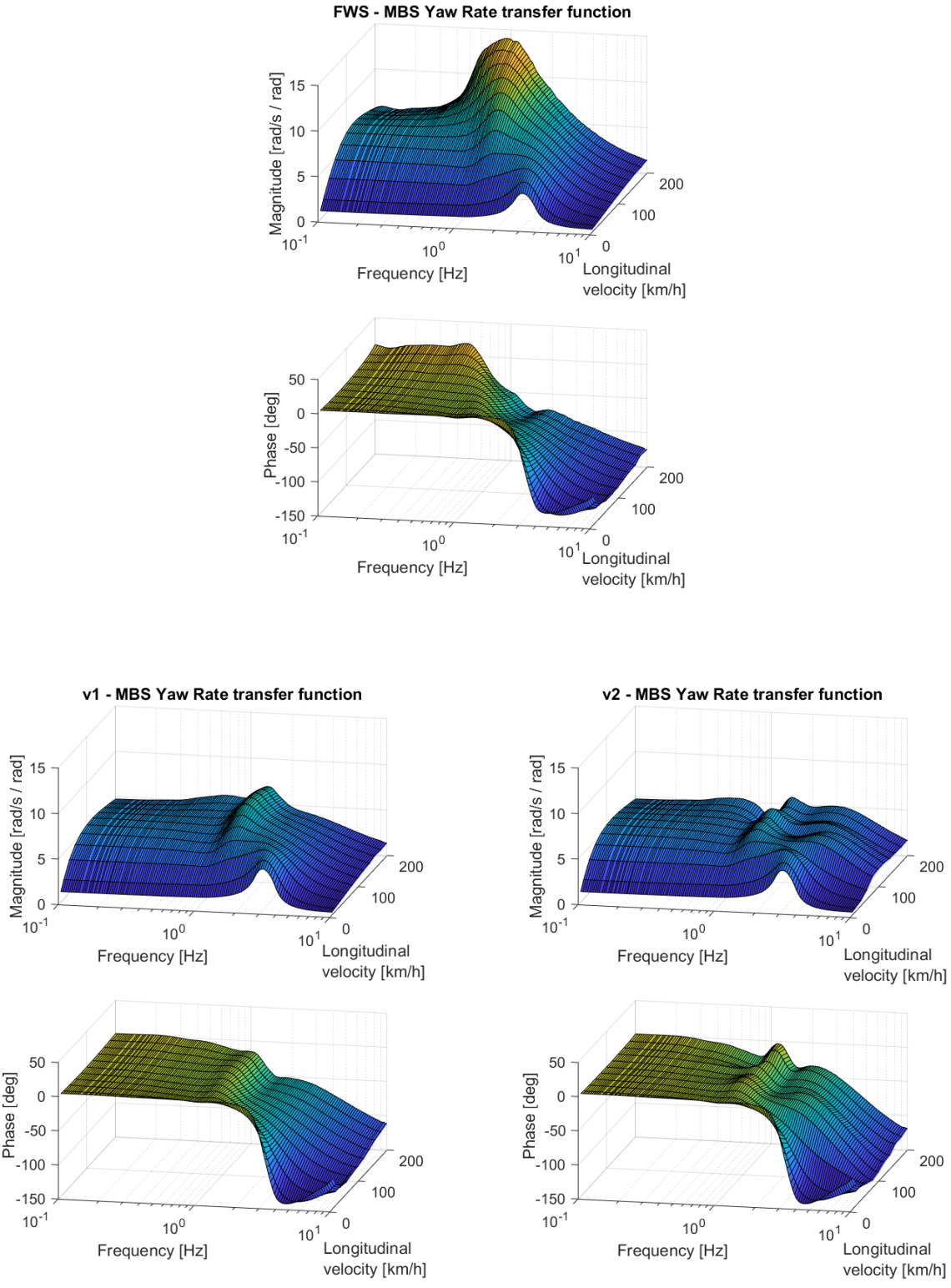

Figure 7.22: Comparison of the yaw rate transfer functions obtained from the MBS model, between a FWS and AWS vehicle controlled with methods $v1$ and $v2$.

Chapter 8

Conclusions

This chapter summarises the conclusions that can be drawn from the simulations results, in terms of manoeuvrability, stability and agility.

8.1 Manoeuvrability

Manoeuvrability is assessed in terms of minimum turning radius, steering angle request and swept area.

The turning radius is reduced by 19 %, with a front steer angle of 35 deg and a rear steer angle of 9 deg. This reduction depends on the maximum steer angle that the rear wheels can achieve.

The reduction of the turning radius implies that the steering effort, in terms of angle request, is reduced when the rear wheels are turning in the opposite direction of the front wheels, i.e. the driver needs to steer less to drive along the same corner.

At high velocity the opposite is true: since the rear wheels are turning in the same direction as the front wheels, the steering angle request is increased. According to the authors, a slightly higher steering angle request might be beneficial; indeed, with a passive vehicle, the driver usually controls the vehicle in a narrow range of steering wheel angles when driving at high velocity, since the gain from steering wheel input and yaw rate is high. Reducing this gain by a small percentage would allow the driver to control the vehicle in a slightly wider range of steering wheel angles, making it easier to follow or correct the desired trajectory.

Finally, the introduction of rear steer allows to reduce the swept area of the vehicle. Intuitively, the minimum swept area is achieved when the sideslip angle is zero; indeed, Figure 5.1 shows that a nose-in or nose-out configuration would only increase the swept area.

It is thus possible to say that the gain scheduling that sets the sideslip angle to zero has a big advantage, compared to the other controllers, when driving at very low velocity. A reduced swept area would be extremely useful when driving in urban environments or in parking lots, especially on their ramps. Unfortunately, the rear steer angle required to set the sideslip angle to zero is around the same value of the maximum front steer angle (Figure 5.2).

8.2 Stability

Stability is assessed by evaluating the yaw rate overshoot from a step steer and looking at the yaw rate and the sideslip angle from a sine with dwell manoeuvre.

From the step steer, the yaw rate overshoot can be reduced up to 65 % at high velocity and it is concluded that utilising a controller working in the frequency domain brings remarkable benefits. This reduction of overshoot is due to the increase of damping of the vehicle (visible in Figure A.10).

From the sine with dwell, the yaw rate overshoot and the range of the sideslip angle are both decreased. The reduction of the yaw rate overshoot allows the vehicles equipped with active rear steering to execute the manoeuvre with the maximum steering wheel angle prescribed by the manoeuvre, while the passive vehicle fails the manoeuvre at around half of steering wheel angle amplitude. In addition, the reduction of the sideslip angle allows the driver to better control the vehicle.

The results from the sine with dwell manoeuvre are a clear example of the stability advantage that active rear steering would bring. Indeed, this is a manoeuvre close to a real-life driving scenario, compared to the step steer and the frequency response.

8.3 Agility

Agility is evaluated in terms of delay between yaw rate and steering input and delay between lateral acceleration and yaw rate. The evaluation is done by looking at transient behaviour (from step steer manoeuvres) and frequency response functions (from swept-sine steer manoeuvres).

Delay between steering input and yaw rate

The results from the step steer manoeuvres show that only one controller is able to reduce the yaw rate rise time. However, the frequency response analysis shows that all the controllers are able to reduce the phase delay between steering input and yaw rate, especially for input frequencies from $1\,Hz$ and above. For instance, the phase delay can be reduced up to 75% for the input frequency of $1\,Hz$.

Delay between lateral acceleration and yaw rate

The results from the step steer manoeuvres show that for the AWS vehicle, the difference between lateral acceleration and yaw rate rise time is increased meaning a larger delay between the two. However, this result depends on how the rise time is defined (Figure 7.14). Conversely, the frequency response analysis shows that the phase delay between lateral acceleration and yaw rate can be greatly reduced for frequencies up to $2\,Hz$. For instance, the phase delay is reduced by up to 46% for the input frequency of $1\,Hz$.

8.4 Future work and considerations

Different aspects have been left out because of time constraints. In the future, it would be of interest to:

- **include actuation dynamics and limitations in the MBS model.**

  The proposed controllers are idealised meaning that there are no software nor hardware limitations. In reality, the actuation system can strongly limit the controller performance (i.e. maximum power, torque/force, range, bandwidth and velocity). For this reason, it is necessary to include the actuator model in the full vehicle MBS model.

- **further tune the controllers.**

  Additional time can be spent in tuning the controllers to further improve the vehicle response. For instance, it would be of interest to remove the unevenness in the FRFs created by controller $v2$ and check whether it would still have a better performance compared to controller $v1$. Moreover, when considering the actuation limitations, the control logic might require additional tuning too.

- **investigate other control logic.**

  After investigating feedforward control logic, it is of interest to investigate feedback control logic and make a comparison. It would be useful to include also all the relevant control strategies reported in the literature to understand which one is the most suitable according to the company requirements.

- **carry out more extensive tests in the dynamic driving simulator with the help of test drivers.**

  The subjective evaluation of controllers in realistic driving scenarios brings useful insights. It is of interest to make the controllers tested by more people, especially by trained test drivers, to obtain their feedback and consequently adjust the tuning of the controllers.

- **improve the MBS model.**

  The MBS model can be improved and made more adaptable by including different configurations of front and rear suspensions. Since ARS is currently in its prototype stage, the MBS model cannot be validated towards a physical vehicle. Once a development mule will be available, the model could be validated with test data.

  If required, the model could be improved by including flexible bodies.

Appendix A

Appendix

A.1 C6 Control implementation

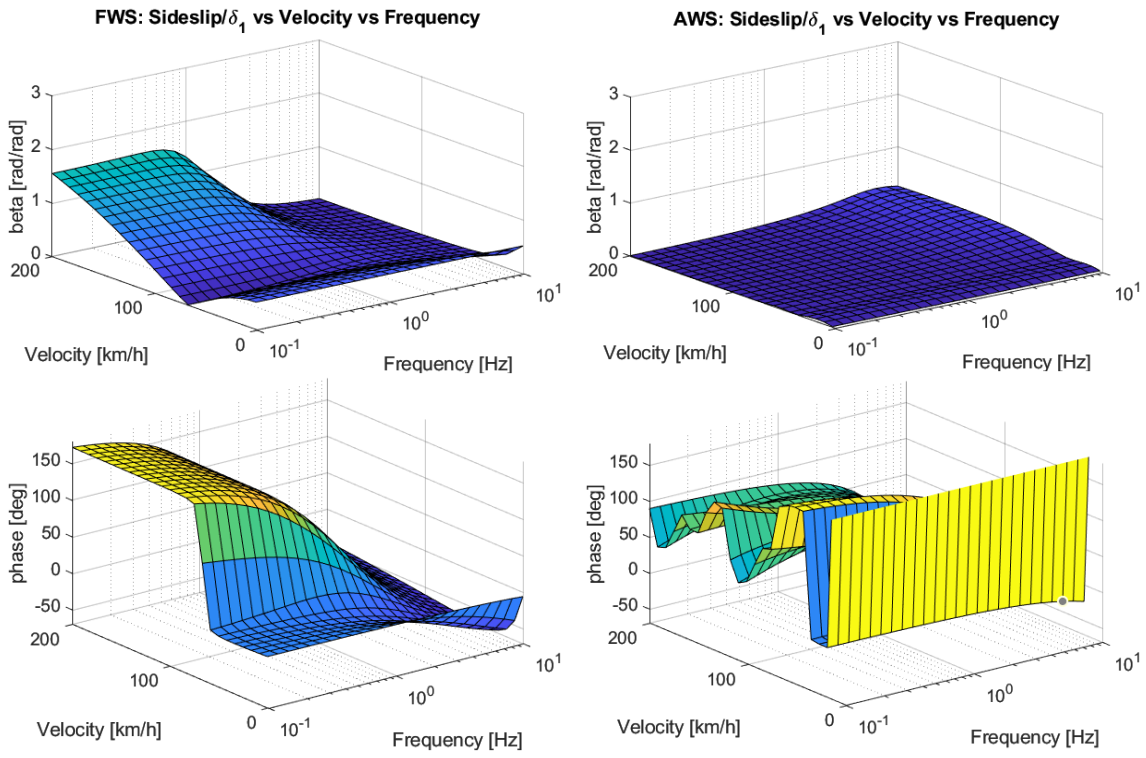

(a) FWS (b) AWS

Figure A.1: Comparison of magnitude (top) and phase (bottom) of the sideslip angle between a FWS and AWS vehicle with a simple gain scheduling. Notice that the phase of the AWS vehicle (bottom-right) has no meaning since the magnitude is zero. Go back to Figure 5.3.

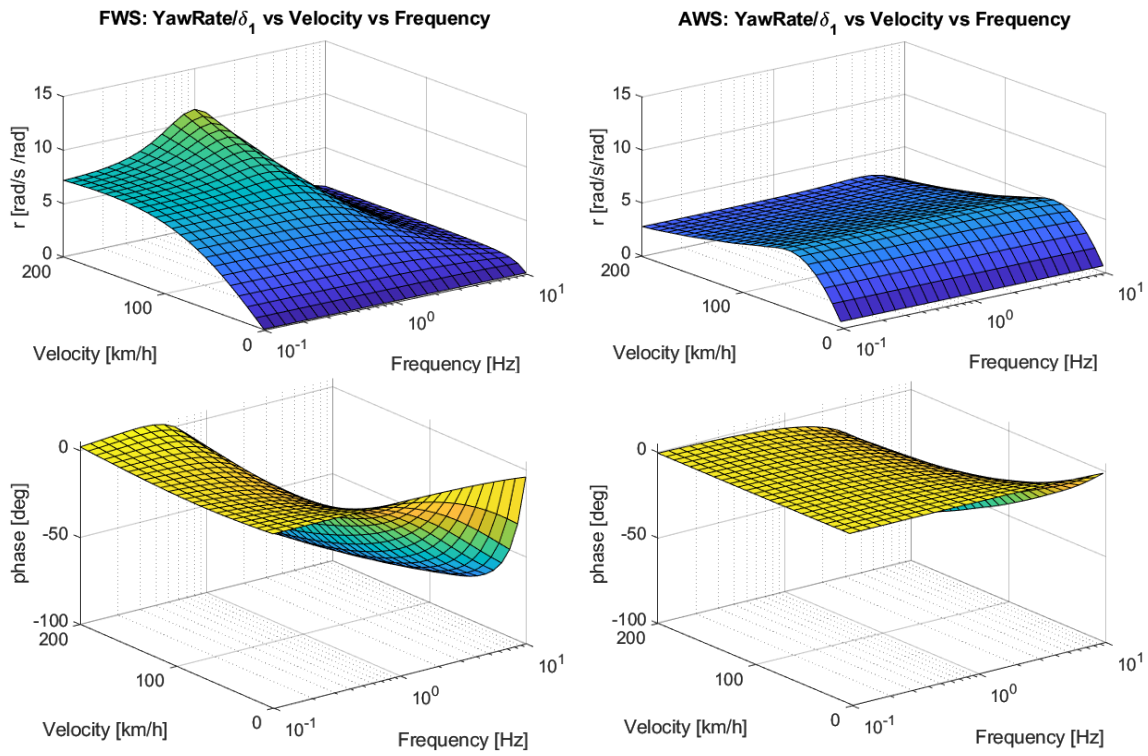

(a) FWS (b) AWS

Figure A.2: Comparison of the yaw rate between a FWS and AWS vehicle with a simple gain scheduling. Go back to Figure 5.4.

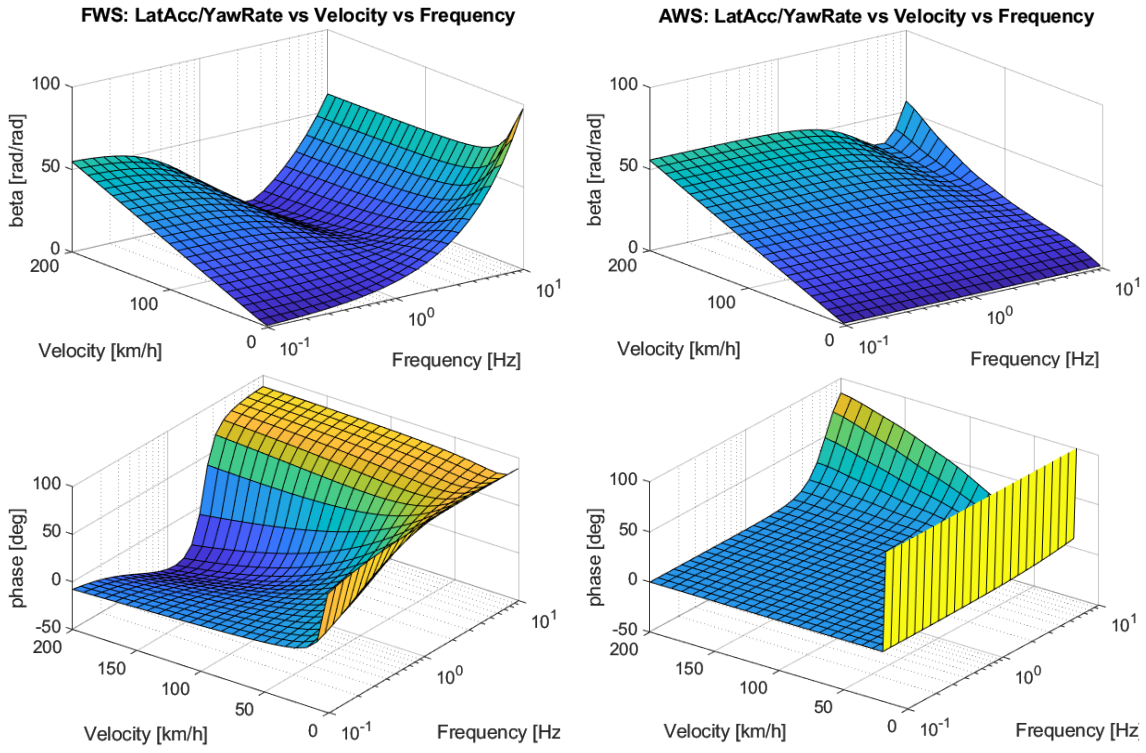

(a) FWS (b) AWS

Figure A.3: Phase and magnitude of lateral acceleration with respect to yaw rate. Go back to Figure 5.6.

A.2 Step steer response

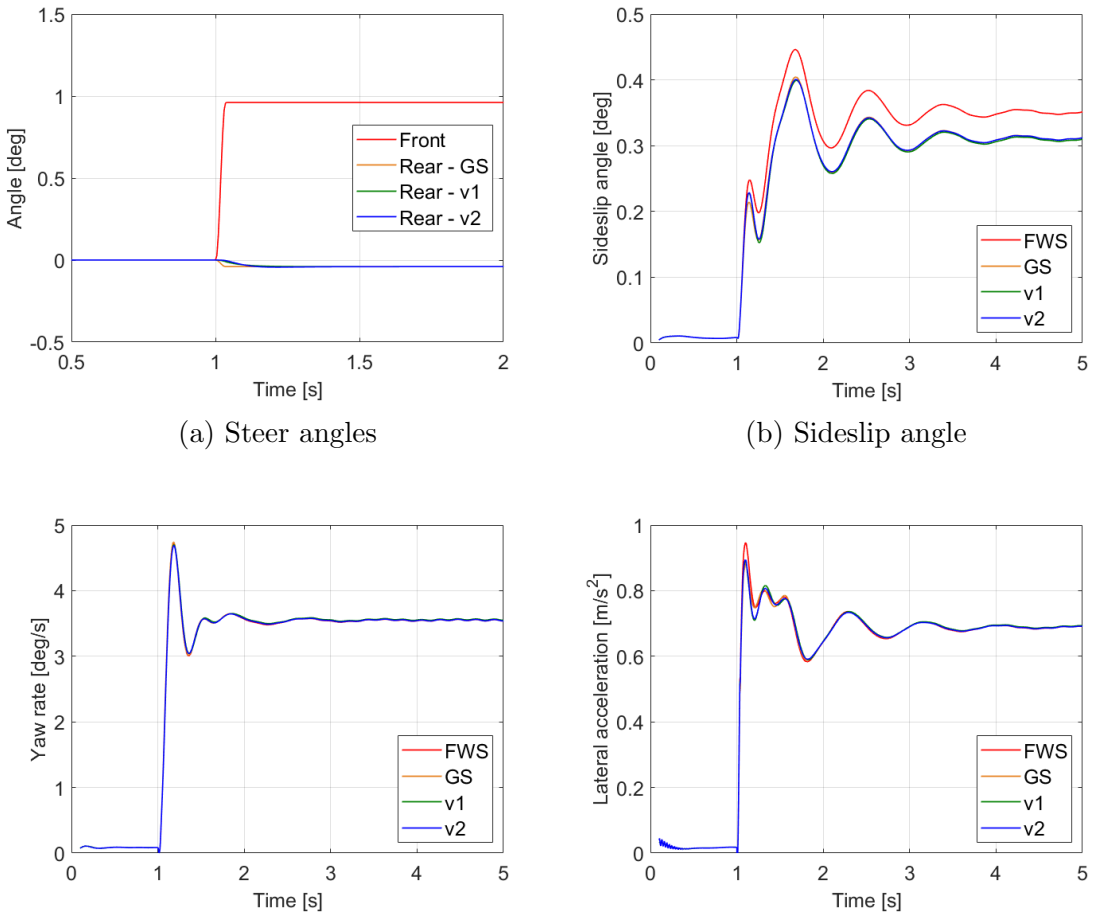

(a) Steer angles

(b) Sideslip angle

(c) Yaw rate

(d) Lateral acceleration

Figure A.4: Step steer at $40\,km/h$. Comparison of the front and rear steer angles (a), sideslip angles (b), yaw rate (c) and lateral acceleration (d) between FWS, gain scheduling, v1 and v2 vehicles.

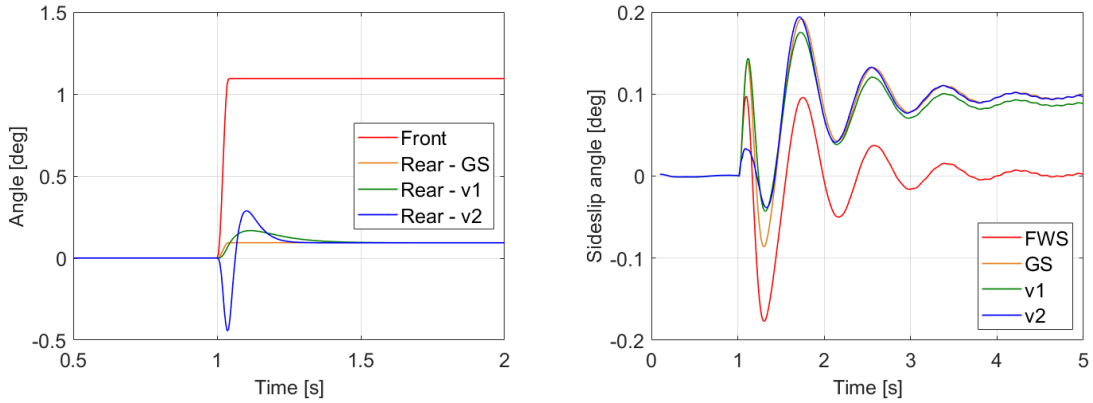

(a) Steer angles

(b) Sideslip angle

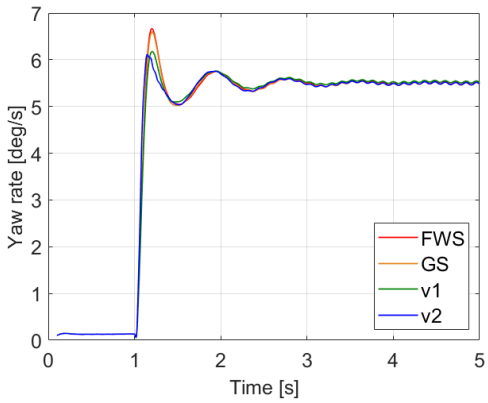

(c) Yaw rate

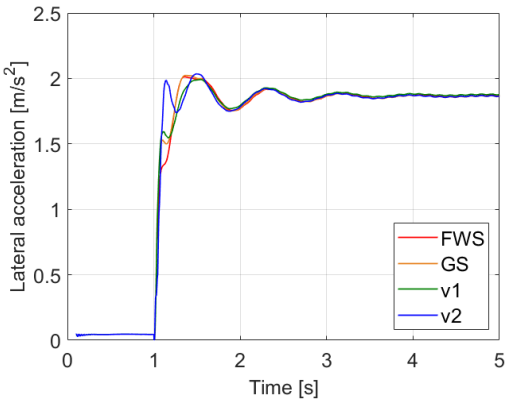

(d) Lateral acceleration

Figure A.5: Step steer at 70 km/h. Comparison of the front and rear steer angles (a), sideslip angles (b), yaw rate (c) and lateral acceleration (d) between FWS, gain scheduling, v1 and v2 vehicles.

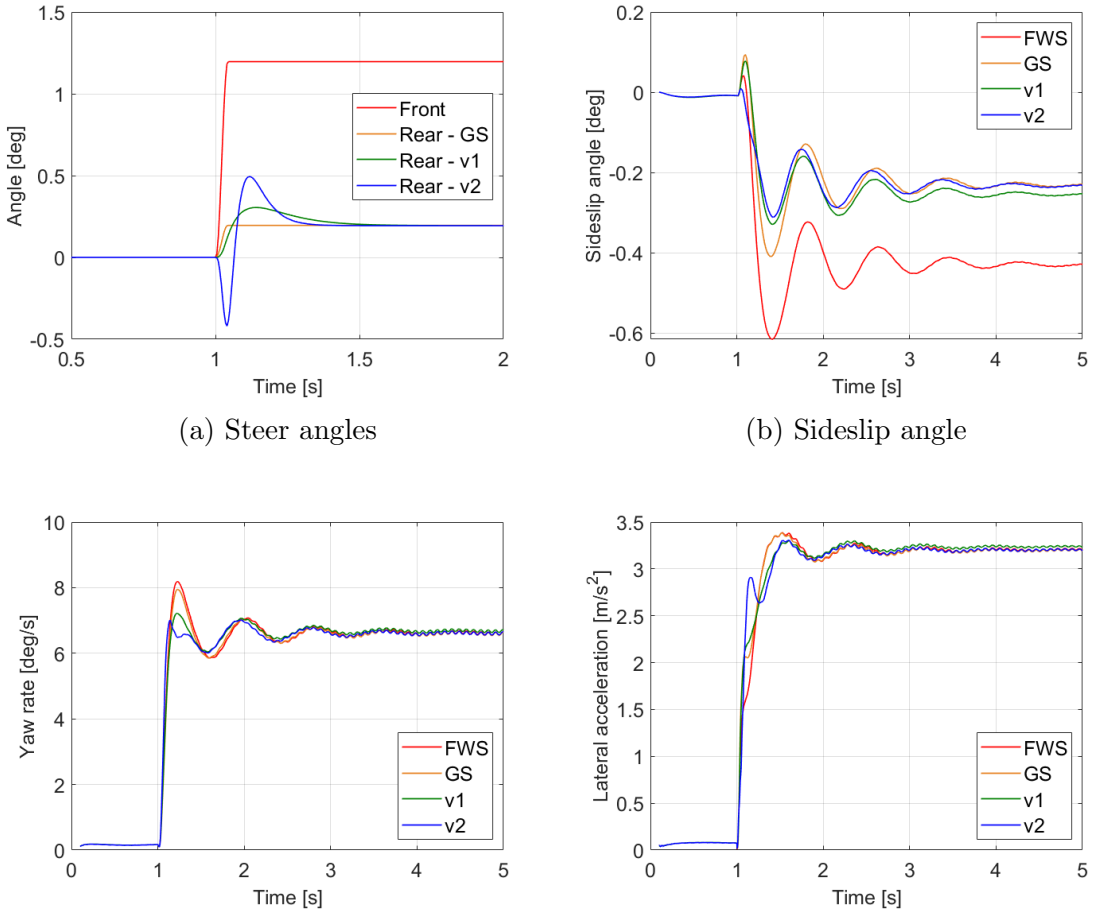

(a) Steer angles

(b) Sideslip angle

(c) Yaw rate

(d) Lateral acceleration

Figure A.6: Step steer at 100 km/h. Comparison of the front and rear steer angles (a), sideslip angles (b), yaw rate (c) and lateral acceleration (d) between FWS, gain scheduling, v1 and v2 vehicles.

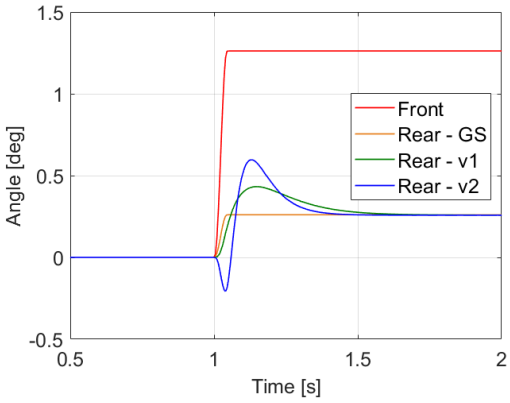

(a) Steer angles

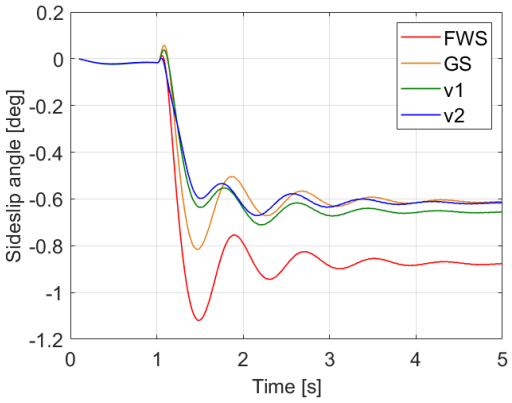

(b) Sideslip angle

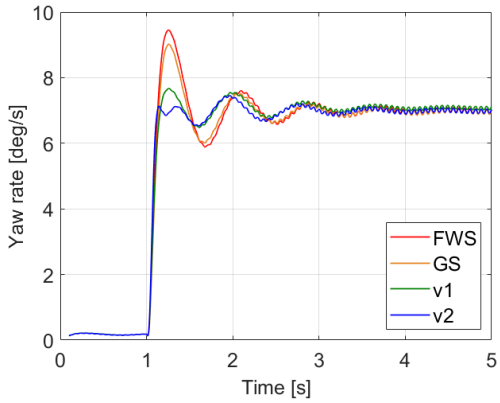

(c) Yaw rate

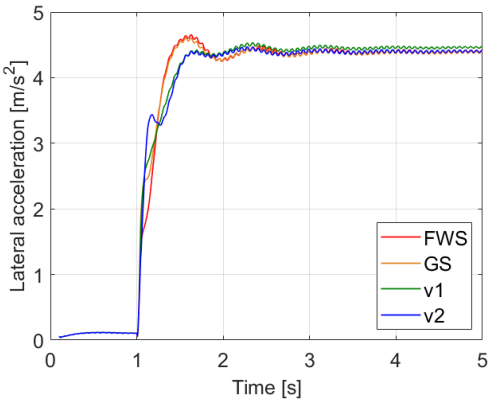

(d) Lateral acceleration

Figure A.7: Step steer at 130 km/h. Comparison of the front and rear steer angles (a), sideslip angles (b), yaw rate (c) and lateral acceleration (d) between FWS, gain scheduling, v1 and v2 vehicles.

A.3 Planar motion assumption

The planar motion assumption reported in equation 2.13 and mentioned in section 7.4.1 is here verified.

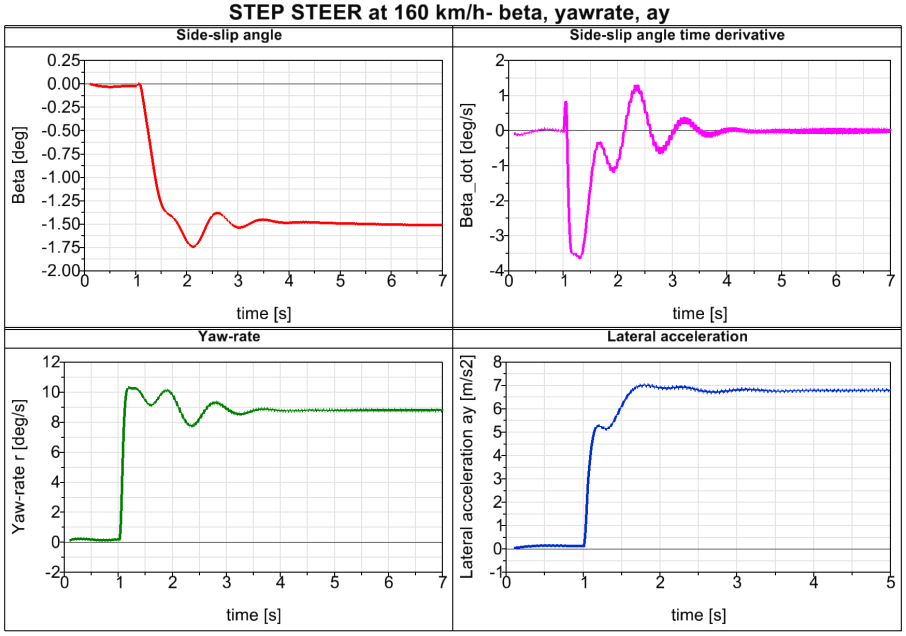

Figure A.8: Vehicle states and lateral acceleration for a step steer manoeuvre at 160 km/h.

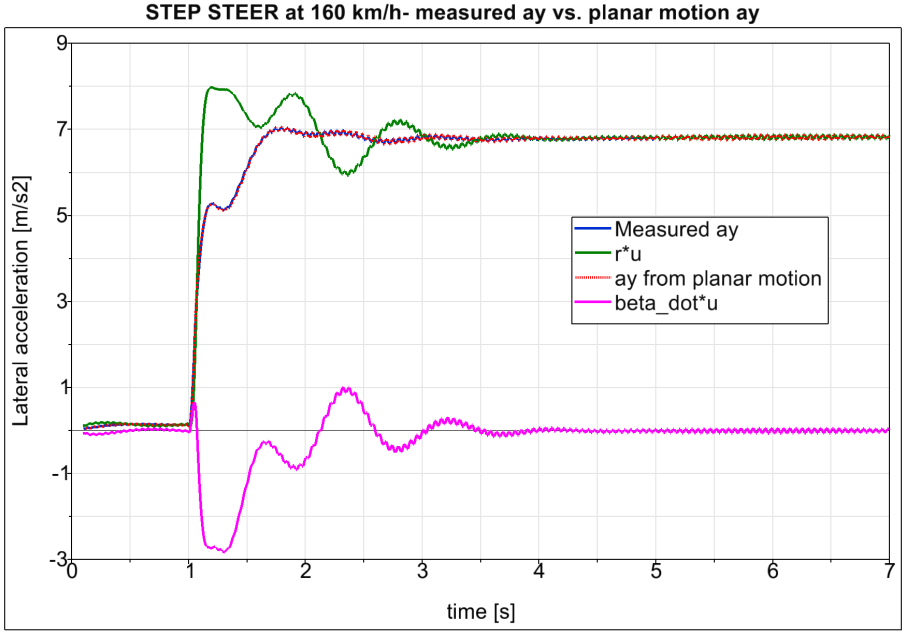

Figure A.9: The lateral acceleration from the planar motion is very similar to the measured lateral acceleration.

A.4 MBS model frequency response functions

This section shows the frequency response functions from the front steer angle to yaw rate, sideslip angle and lateral acceleration obtained from the MBS model, simulating a swept sine from $0.1\,Hz$ to $10\,Hz$ with a steering wheel amplitude of $1.5\,deg$. (Link to go back to the frequency response agility results: chapter A.4).

A.4.1 MBS model yaw rate frequency response functions

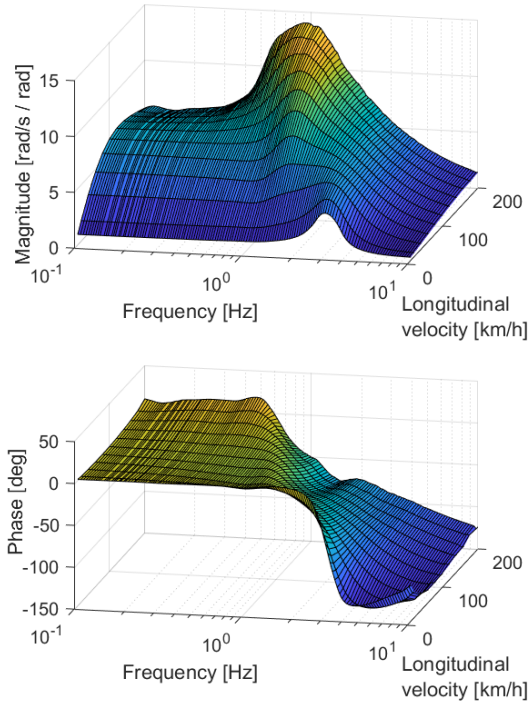

(a) FWS

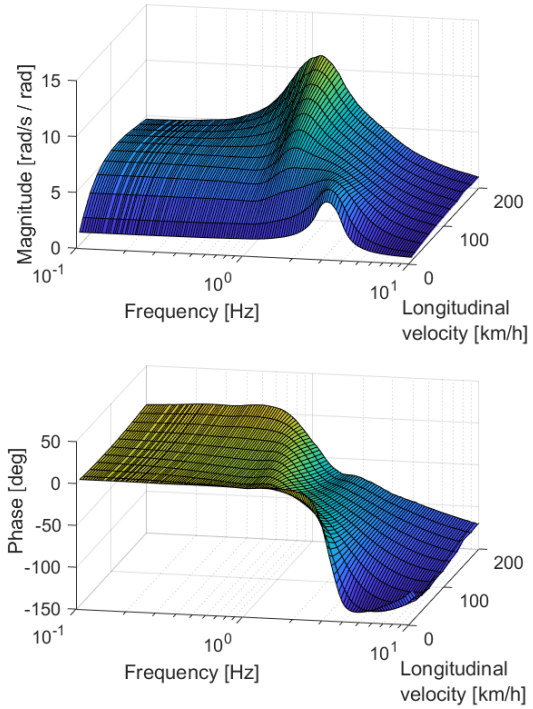

(b) GS

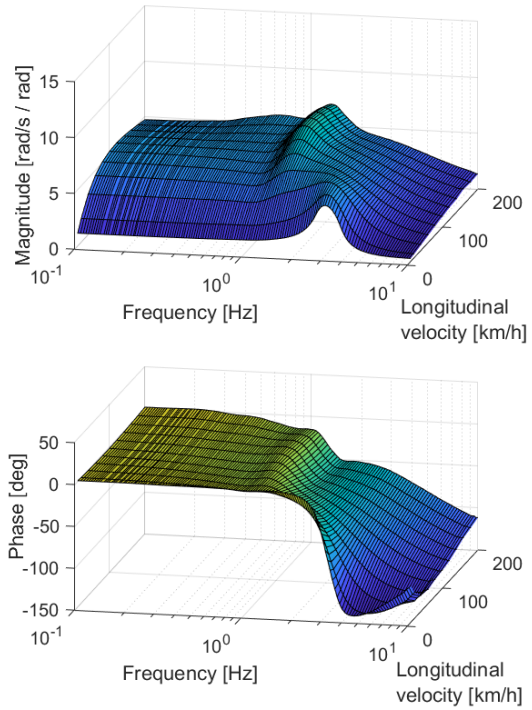

(c) v1

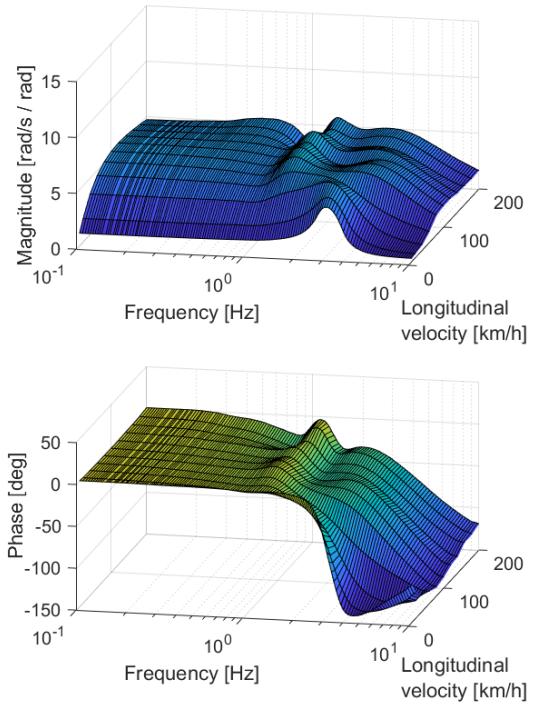

(d) v2

Figure A.10: Comparison of the FRF from front steer angle to yaw rate, obtained from the MBS model. Go back to stability chapter 8.2.

A.4.2 MBS model sideslip angle frequency response functions

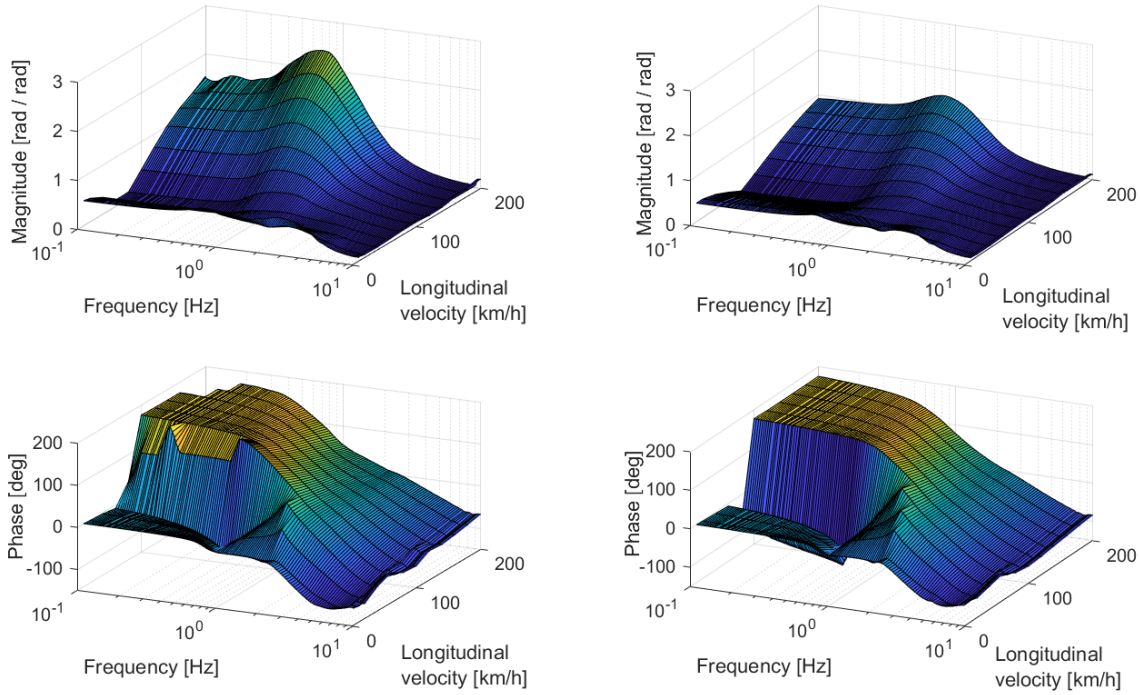

(a) FWS

(b) GS

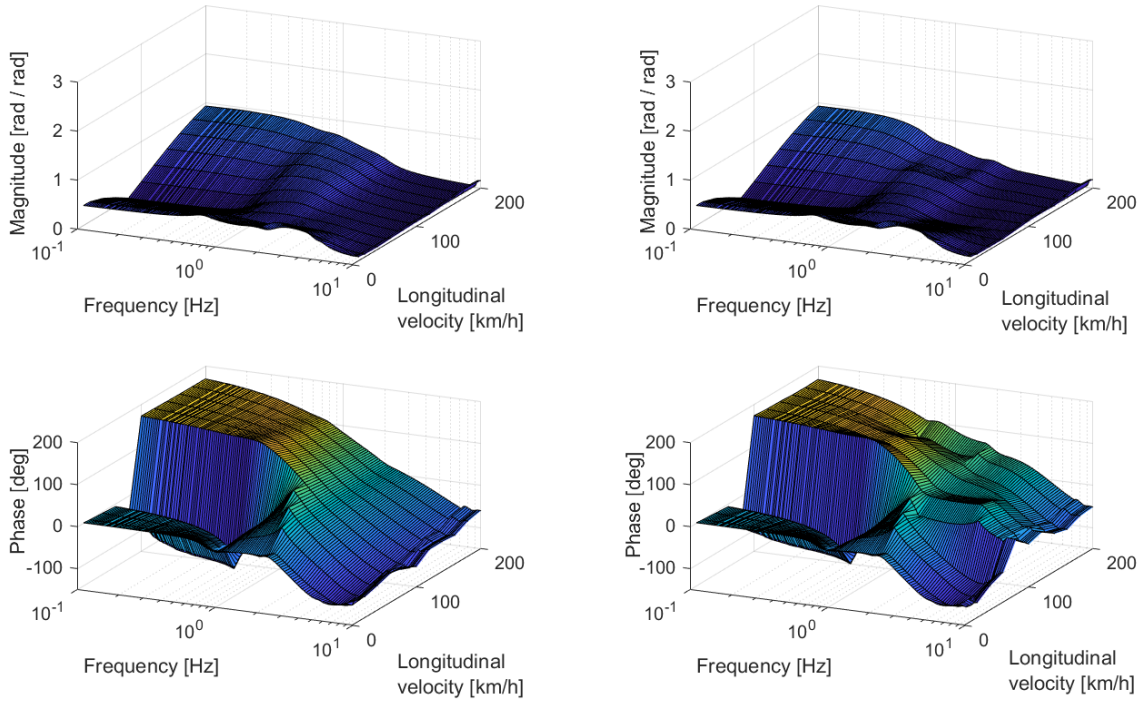

(c) v1

(d) v2

Figure A.11: Comparison of the FRF from front steer angle to sideslip angle, obtained from the MBS model.

A.4.3 MBS model lateral acceleration frequency response functions

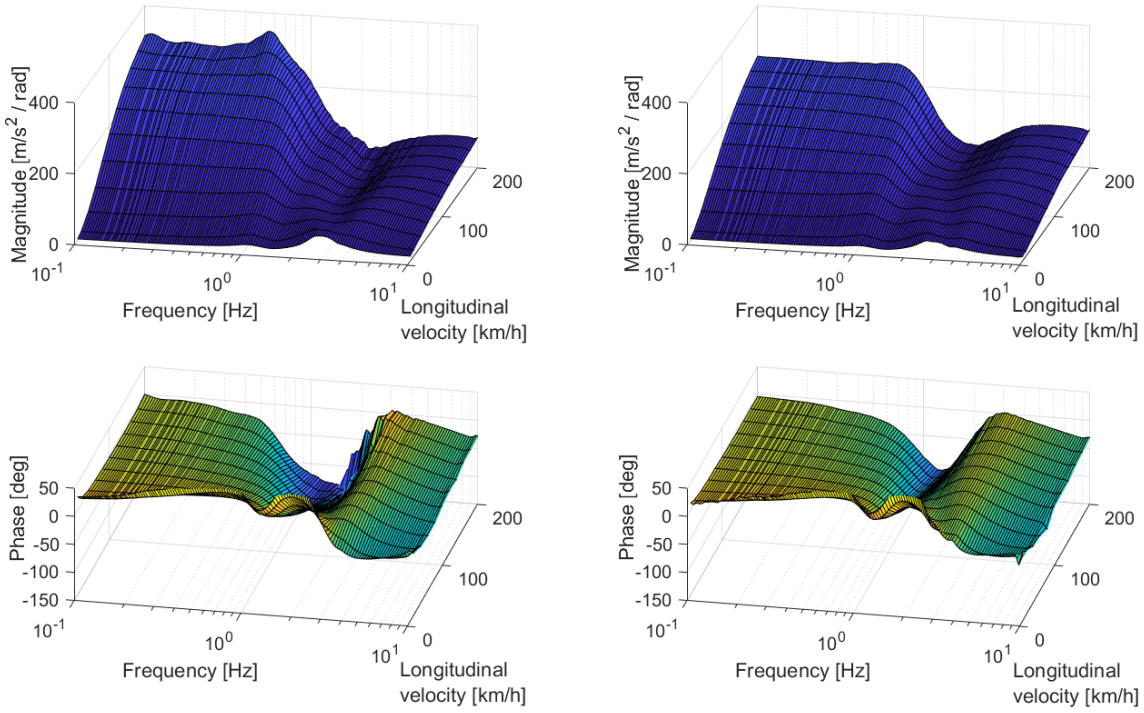

(a) FWS

(b) GS

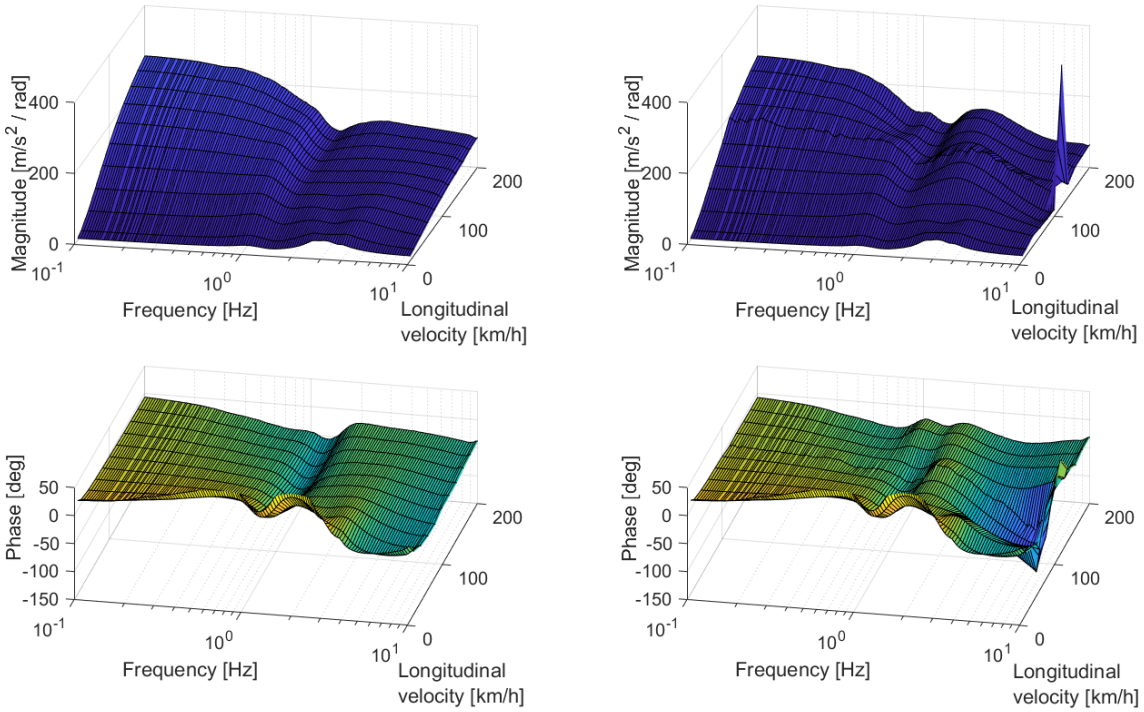

(c) v1

(d) v2

Figure A.12: Comparison of the FRF from front steer angle to lateral acceleration, obtained from the MBS model.

Bibliography

[1] Michael Blundell and Damian Harty. *The Multibody systems approach to vehicle dynamics*. eng. Automotive engineering series. OCLC: 249677935. Amsterdam: Elsevier Butterworth-Heinemann, 2004. ISBN: 9780750651127.

[2] Takaaki Eguchi et al. "Development of "Super Hicas", a New Rear Wheel Steering System with Phasereversal Control". In: Sept. 1989, p. 891978. DOI: 10.4271/891978. URL: https://www.sae.org/content/891978/ (visited on 06/15/2021).

[3] Marlene Kreutz, Martin Horn, and Josef Zehetner. "Improving vehicle dynamics by active rear wheel steering systems". en. In: *Vehicle System Dynamics* 47.12 (Dec. 2009), pp. 1551–1564. ISSN: 0042-3114, 1744-5159. DOI: 10.1080/00423110802691507. URL: https://www.tandfonline.com/doi/full/10.1080/00423110802691507 (visited on 06/15/2021).

[4] R. Subhash L. Bin and F. Ying. "Enhancement of vehicle stability through integration of direct yaw moment and active rear steering". In: *Proceedings of the Institution of Mechanical Engineers, Part D: Journal of Automobile Engineering* 230.6 (2016), pp. 830–840. ISSN: 0954-4070, 2041-2991. DOI: 10.1177/0954407015596255. URL: http://journals.sagepub.com/doi/10.1177/0954407015596255 (visited on 06/16/2021).

[5] H. Nijmeijer I. Besselink T. Veldhuizen. "Improving Yaw Dynamics by Feedforward Rear Wheel Steering". In: *IEEE Intelligent Vehicles Symposium* (2008). URL: http://id.nii.ac.jp/1503/00000058/.

[6] Philip M. Leucht. "Active Four-Wheel-Steering Design for an Advanced Vehicle". In: *1988 American Control Conference*. Atlanta, GA, USA: IEEE, June 1988, pp. 2379–2384. DOI: 10.23919/ACC.1988.4790125. URL: https://ieeexplore.ieee.org/document/4790125/ (visited on 06/15/2021).

[7] S. Kasliwal. "Development of Active Rear Wheel Steering and Evaluation of Steering Feel". Master Thesis. KTH Royal Institute of Technology, 2019.

[8] Jyotishman Ghosh. "State Estimation and Control of Active Systems for High Performance Vehicles". PhD Thesis. Politecnico di Torino, 2017.

[9] Masao Nagai, Yutaka Hirano, and Sachiko Yamanaka. "Integrated Control of Active Rear Wheel Steering and Direct Yaw Moment Control". In: *Vehicle System Dynamics* 27.5-6 (June 1997), pp. 357–370. ISSN: 0042-3114, 1744-5159. DOI: 10.1080/00423119708969336. URL: http://www.tandfonline.com/doi/abs/10.1080/00423119708969336 (visited on 06/19/2021).

[10] J. Joonsang Y. Seungjin Y. Seung-Han, K. Duhyung, and L. Kyo II. "Optimal integration of active 4 wheel steering and direct yaw moment control". In: *IFAC Proceedings Volumes* 39.12 (2006), pp. 603–608. ISSN: 14746670. DOI: 10.3182/20060829-3-NL-2908.00104. URL: https://linkinghub.elsevier.com/retrieve/pii/S1474667015336892 (visited on 06/19/2021).

[11] S. Li L. Wu H. Tang and W. Fang. "Improvement of Vehicle Handling and Stability by Integrated Control of Four Wheel Steering and Direct Yaw Moment". In: *2007 Chinese Control Conference* (2006). DOI: 10.1109/chicc.2006.4347270.

[12] Dieter Schramm, Manfred Hiller, and Roberto Bardini. *Vehicle Dynamics*. en. Berlin, Heidelberg: Springer Berlin Heidelberg, 2018. ISBN: 9783662544839. DOI: 10.1007/978-3-662-54483-9. URL: http://link.springer.com/10.1007/978-3-662-54483-9 (visited on 06/15/2021).

[13] Massimo Guiggiani. *The Science of Vehicle Dynamics: Handling, Braking, and Ride of Road and Race Cars*. en. Cham: Springer International Publishing, 2018. ISBN: 9783319732206. DOI: 10.1007/978-3-319-73220-6. URL: http://link.springer.com/10.1007/978-3-319-73220-6 (visited on 06/11/2021).

[14] William F. Milliken and Douglas L. Milliken. *Race car vehicle dynamics*. Warrendale, PA, U.S.A: SAE International, 1995. ISBN: 9781560915263.

[15] Sondhi Eshwar and Perinciolo Paolo. "Model Based Handling Analyses". Master Thesis. KTH Royal Institute of Technology, 2018.

[16] Marcus Ljungberg et al. "Electric Power Assist Steering System Parameterization and Optimisation Employing Computer-Aided Engineering". In: Apr. 2015, pp. 2015–01–1500. DOI: 10.4271/2015-01-1500. URL: https://www.sae.org/content/2015-01-1500/ (visited on 06/12/2021).

[17] Mechanical Simulation Corporation. *The Sine with Dwell Test*. 2021. URL: https://www.carsim.com/applications/fmvss126/index.php (visited on 06/14/2021).